ALGEBRAIC SPECTRAL MOMENTS BASED MOVING CLUTTER PARAMETER ESTIMATION AND CLUTTER SUPPRESSION

A THESIS SUBMITTED TO
THE GRADUATE SCHOOL OF NATURAL AND APPLIED SCIENCES
OF
MIDDLE EAST TECHNICAL UNIVERSITY

BY

ONUR OKTAR

IN PARTIAL FULFILLMENT OF THE REQUIREMENTS
FOR
THE DEGREE OF MASTER OF SCIENCE
IN
ELECTRICAL AND ELECTRONICS ENGINEERING

JANUARY 2014

Approval of the thesis:

ALGEBRAIC SPECTRAL MOMENTS BASED MOVING CLUTTER PARAMETER ESTIMATION AND CLUTTER SUPPRESSION

submitted by **ONUR OKTAR** in partial fulfillment of the requirements for the degree of **Master of Science in Electrical and Electronics Engineering Department, Middle East Technical University** by,

Prof. Dr. Canan Özgen _____
Dean, Graduate School of **Natural and Applied Sciences**

Prof. Dr. Gönül Turhan Sayan _____
Head of Department, **Electrical and Electronics Engineering**

Prof. Dr. Yalçın Tanık _____
Supervisor, **Electrical and Electronics Eng. Dept., METU**

Examining Committee Members:

Prof. Dr. Sencer Koç _____
Electrical and Electronics Engineering Dept., METU

Prof. Dr. Yalçın Tanık _____
Electrical and Electronics Engineering Dept., METU

Assoc. Prof. Dr. Ali Özgür Yılmaz _____
Electrical and Electronics Engineering Dept., METU

Assoc. Prof. Dr. Çağatay Candan _____
Electrical and Electronics Engineering Dept., METU

Dr. Ülkü Doyuran _____
Radar System Engineering Division, ASELSAN

Date: _____

I hereby declare that all information in this document has been obtained and presented in accordance with academic rules and ethical conduct. I also declare that, as required by these rules and conduct, I have fully cited and referenced all material and results that are not original to this work.

Name, Last Name : ONUR OKTAR

Signature :

ABSTRACT

ALGEBRAIC SPECTRAL MOMENTS BASED MOVING CLUTTER PARAMETER ESTIMATION AND CLUTTER SUPPRESSION

Oktar, Onur
M.Sc., Department of Electrical & Electronics Engineering
Supervisor : Prof. Dr. Yalçın Tanık

January 2014, 150 Pages

In many modern radar systems, it is desired to detect the presence of targets in the interference which includes clutter and noise. Various signal processing techniques are proposed to effectively suppress the clutter and increase the signal to interference ratio. To achieve optimum suppression, radar system must know clutter characteristics and process the radar echoes based on these characteristics. For ground radars, the clutter environment characteristics are relatively stable and predictable. These characteristics can be stored in radars memory and optimum clutter suppression can be achieved. However, for maritime radars, dealing with sea clutter is a rather big problem since its characteristics changes over time according to change in velocity vector of wind, grazing angle etc. In such a case, a radar needs to adapt itself to changing clutter environment to achieve good clutter suppression. The bigger problem arises when both the rain clutter and the sea clutter coexists since they are differently affected by environmental conditions and radar parameters. In these environments, adaptive estimation of both clutter characteristics to suppress the interference becomes obligatory if high-performance target detection is needed. In this study, parametric clutter parameter estimation techniques are considered and the performance of algebraic spectral moments based moving clutter parameter estimation technique is investigated for different conditions. To compare the clutter suppression of the algebraic spectral moments based moving clutter parameter estimation technique with that of more conventional methods, improvement factor (IF) is used as the figure of merit.

Keywords: K-Distributed Sea Clutter, Rain Clutter, Rain and Sea Clutter Suppression, Parametric Clutter Parameter Estimation, Improvement Factor

ÖZ

CEBİRSEL SPEKTRUM MOMENTLERİ TABANLI HAREKETLİ KARGAŞA PARAMETRELERİ TAHMİNİ VE KARGAŞA BASTIRIMI

Oktar, Onur
Yüksek Lisans, Elektrik & Elektronik Mühendisliği Bölümü
Tez Yöneticisi : Prof. Dr. Yalçın Tanık

Ocak 2014, 150 Sayfa

Modern radarların büyük çoğunluğunda, kargaşa ve gürültünün dahil olduğu enterferans içinde hedef tespiti gerçekleştirilmeye çalışılmaktadır. Kargaşanın bastırılması ve sinyal ile enterferans oranının arttırtması için birçok sinyal işleme teknikleri önerilmiştir. Optimum kargaşa bastırımı için radarın kargaşa parametrelerini bilmesi ve bu parametrelere göre radar yansısını işlemesi gerekmektedir. Kara radarları için, kargaşa ortamı parametreleri tahmin edilebilir ve büyük oranda kararlıdır. Bu parametreler radar hafızasında saklanabilir ve optimum kargaşa bastırımı sağlanabilmektedir. Fakat deniz radarlarında deniz kargaşasının karakteristiği rüzgar, sıyırma açısı v.b. etkenlere göre zaman içinde değiştiği için bastırılması daha güç bir iştir. Bu durumlarda etkin bastırma sağlayabilmek için radar değişken çevreye uyum sağlamalıdır. Hem deniz hem de yağmur kargaşasının bulunduğu ortamlarda ise, iki kargaşa da çevresel faktörlerden ve radar parametrelerinden farklı etkilendiği için kargaşa bastırımı daha güç olmaktadır. Bu tür ortamlarda, iki kargaşanın da karakteristiğinin uyarlamalı şekilde tahmini ve kargaşa bastırımı, yüksek performansta hedef tespiti için zorunlu olmaktadır. Bu çalışmada parametrik kargaşa parametreleri tahmin metotları sunulmuş ve cebirsel spektrum momentleri tabanlı hareketli kargaşa parametreleri tahmini metodunun performansı farklı durumlarda incelenmiştir. Cebirsel spektrum momentleri tabanlı hareketli kargaşa parametreleri tahmini metodunun ve klasik yöntemlerin kargaşa bastırımı etkinliğinin karşılaştırılması için iyileştirme faktörleri hesaplanmıştır.

Anahtar Kelimeler: K-Dağılımlı Deniz Kargaşası, Yağmur Kargaşası, Yağmur ve Deniz Kargaşası Bastırımı, Parametrik Kargaşa Parametreleri Tahmini, İyileştirme Faktörü

To My Family

ACKNOWLEDGMENTS

I have completed my thesis with assistance of various people who helped me during my studies. I would like to take this opportunity to acknowledge their help.

Firstly, I wish to express my deepest gratitude to my supervisor Prof. Dr. Yalçın Tanık for his guidance, advice, criticism and insight throughout this research.

Secondly, I would like to thank Yasemin Hicran Özdemir for her assistance in my personal life which enabled me to focus on my thesis work.

I am also grateful to ASELSAN Inc. for her opportunities and supports during the completion of this thesis.

Special appreciation and gratitude are also for my family for their constant care and understanding, encouragement and endless love throughout my life.

This thesis was supported by TÜBİTAK Scholarship for MS Students.

TABLE OF CONTENTS

LIST OF TABLES

TABLES

LIST OF FIGURES

FIGURES

LIST OF ABBREVIATIONS

AMTI : Airborne Moving Target Indication

ASR : Airport Surveillance Radar

CNR : Clutter to Noise Ratio

CPI : Coherent Processing Interval

DFT : Discrete Fourier Transform

DOA : Direction of Arrival

FI : Fisher Information

GIT : Georgia Institute of Technology

IF : Improvement Factor

ML : Maximum-Likelihood

MM : Method of Moments

MTD : Moving Target Detection

MTI : Moving Target Indicator

MUSIC : Multiple Signal Classification

PDF : Probability Density Function

PRF : Pulse Repetition Frequency

PRI : Pulse Repetition Interval

RADAR : RAdio Detection And Ranging

RCS : Radar Cross Section

RMS : Root Mean Square

SCR : Signal to Clutter Ratio

SIR : Signal to Interference Ratio

SIRP : Spherically Invariant Random Process

SMI : Sample Matrix Inversion

TSC : Technology Service Corporation

WPSF : Weighted Pseudosubspace Fitting

ZMNL : Zero Memory Nonlinear

CHAPTER 1

INTRODUCTION

1.1 Radar Definition

RADAR (RAdio Detection And Ranging) is a detection system which determines range, angle and velocity of distant objects by analyzing electromagnetic waves reflected from their surfaces. The radar antenna transmits high energy radio waves and the radar receiver measures the amplitude, the direction of arrival and the round-trip time of the radar pulse to get to the target and return.

It can be used to detect and track aircraft, spacecraft, ships, missiles and weather formations such as clouds, rain, snow, hail.

1.2 Interference Definition

Interference in radar terminology can be defined as an unwanted signal that may originate from internal and external sources and obstructs the detection of intended targets. There are mainly three types of interference: noise, jammer and clutter.

There are two sources of noise: Thermal noise and external noise. Thermal noise originates mainly from electronics equipment of radar and caused by random fluctuations in the electric signals. It is the major reason that limits a radar's detection performance. It depends mainly on noise figure of the radar receiver and

system temperature. Another source of noise, external noise, is caused by the natural thermal radiation of the background surrounding the target of interest. Using high energy radar pulses, matched filtering and Doppler processing are ways to overcome noise.

Jammers are manmade sources that are used to mask target presences intentionally by transmitting parasite signals in the frequency band of radar. Jamming is the most challenging problem for a radar since target signal travels two-way before entering the radar receiver while jammer signal travels one-way.

Clutter is defined as the nuisance radar echoes reflected from the environment or scene around the interested target. These radar echoes can originate from any natural objects like ground, buildings, sea, precipitation (such as rain, snow or hail), insects and even atmosphere itself. The nuisance radar echoes originated from non-moving environments with respect to radar can be classified as stationary clutter like ground, building etc.; while sea, precipitation, insects, atmosphere can be classified as moving clutter. Clutter is a common problem that must be solved for many types of radars.

1.3 Optimum Interference Suppression Filtering and Moving Target Indicator (MTI) and Moving Target Detection (MTD) Algorithms

To increase the signal to clutter ratio (SCR), in other words, to suppress the clutter, Moving Target Indicator (MTI) and Moving Target Detection (MTD) are two old but still valid methods. The MTI method uses the stationary property of the clutter and it is used to separate moving targets from stationary clutter such as buildings, hills, trees and sea. The phase of the radar echo from a moving target changes from pulse to pulse since the relative distance between the radar and the target differs while the clutter echoes reach the radar antenna at the same phase shift. The MTI algorithm uses this difference and it is mostly implemented as a Single Delay Line Canceler or

a Double Delay Line Canceler in time domain in early radars. Figure 1-1 shows these implementation techniques for MTI. In Figure 1-1, $x(t)$, $y(t)$ and T shows input signal, output signal and pulse repetition interval, respectively.

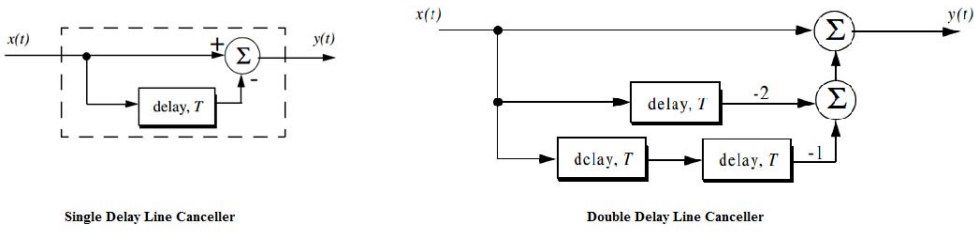

Figure 1-1: Implementation Techniques for MTI [1].

Frequency responses of a single delay line canceler and a double delay line canceler are given in Figure 1-2.

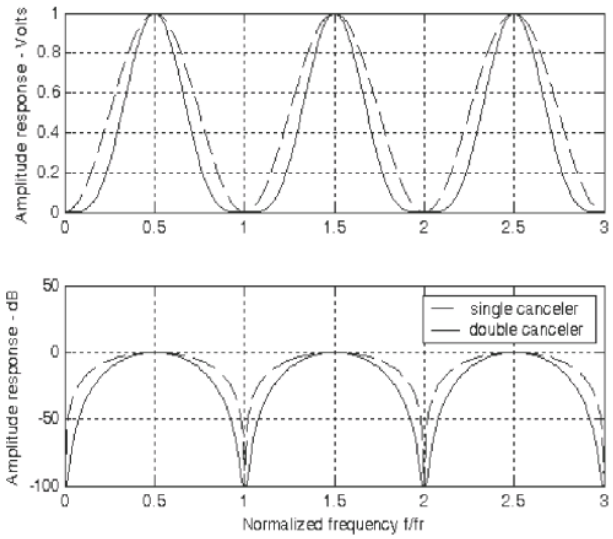

Figure 1-2: Normalized Frequency Responses for Single and Double Cancellers [1].

Although MTI is a very efficient algorithm to suppress the stationary clutter, it has some deficiencies [2]:

- Low detection probability in the presence of precipitation clutter since the mean velocity of the rain clutter may not be centered at zero radial velocity and the rain clutter can leak out of the MTI filter. This results in critical degradation in a radar's performance especially in the case that the radar antenna is looking along the wind direction.
- High false alarm rate for systems having a rotating antenna in the presence of ground clutter (Antenna rotation causes Doppler spread in even stationary clutter and some of its power leaks through the MTI filter causing false alarms and decrease in the target detection performance).

- Wide notch around zero and blind speeds limits the detection of the targets with nearly zero radial velocity or the targets with radial velocity near blind speeds.

With these needs, a next generation algorithm, MTD, which offers better sub-optimum filters, was developed and proposed by Lincoln Laboratory to overcome the limitations of the moving target indicator (MTI) systems [2]. Before addressing the sub-optimum filters offered by the MTD, it is useful to mention the optimum clutter suppression filter.

Consider a complex signal Mx1 column vector

$$\boldsymbol{y} = \begin{bmatrix} y(M-1) & y(M-2) & \dots & y(0) \end{bmatrix}^T \tag{1.1}$$

which represents the radar echoes from a range cell including the target, the clutter and the noise sampled with sampling period T_s and a filter defined by an Mx1 column vector

$$\boldsymbol{h} = \begin{bmatrix} h(M-1) & h(M-2) & \dots & h(0) \end{bmatrix}^T \tag{1.2}$$

where $(\square)^T$ designates transpose operation.

The received signal vector $\boldsymbol{y}$ is composed of the target signal vector $\boldsymbol{t}$ and the interference vector $\boldsymbol{w}$:

$$\boldsymbol{y} = \boldsymbol{t} + \boldsymbol{w}\,. \tag{1.3}$$

Then, the filtered target signal becomes $\boldsymbol{h}^T\boldsymbol{t}$ with power $\boldsymbol{h}^H\boldsymbol{t}^*\boldsymbol{t}^T\boldsymbol{h}$ and the filtered interference becomes $\boldsymbol{h}^T\boldsymbol{w}$ with power $\boldsymbol{h}^H\boldsymbol{w}^*\boldsymbol{w}^T\boldsymbol{h}$ where $(\square)^H$ designates Hermitian transpose operation and $(\square)^*$ designates conjugate operation.

The signal to interference ratio (SIR) at the output of the filter is

$$SIR = \frac{\boldsymbol{h}^H \boldsymbol{t}^* \boldsymbol{t}^T \boldsymbol{h}}{\boldsymbol{h}^H \boldsymbol{S}_I \boldsymbol{h}} \tag{1.4}$$

where the interference covariance matrix $\boldsymbol{S}_I$ is

$$\boldsymbol{S}_I = E\left\{\boldsymbol{w}^* \boldsymbol{w}^T\right\}. \tag{1.5}$$

The optimum clutter suppression filter coefficient vector $\boldsymbol{h}_{opt}$ is the filter that maximizes the signal to interference ratio (SIR) at the output [3].

According to Schwarz inequality

$$\boldsymbol{h}^H \boldsymbol{t}^* \boldsymbol{t}^T \boldsymbol{h} \le \|\boldsymbol{A}\boldsymbol{h}\|^2 \left\|\left(\boldsymbol{A}^H\right)^{-1} \boldsymbol{t}^*\right\|^2 = \left(\boldsymbol{h}^H \boldsymbol{S}_I \boldsymbol{h}\right)\left(\boldsymbol{t}^T \left(\boldsymbol{S}_I\right)^{-1} \boldsymbol{t}^*\right) \tag{1.6}$$

where

$$\boldsymbol{S}_I = \boldsymbol{A}^H \boldsymbol{A}. \tag{1.7}$$

After arranging (1.6), the upper bound to the SIR can be expressed as

$$SIR \le \boldsymbol{t}^T \left(\boldsymbol{S}_I\right)^{-1} \boldsymbol{t}^*. \tag{1.8}$$

The optimum clutter suppression filter coefficient vector $\boldsymbol{h}_{opt}$ is the vector satisfies the equality in (1.8):

$$\boldsymbol{h}_{opt} = \left(\boldsymbol{S}_I\right)^{-1} \boldsymbol{t}^*. \tag{1.9}$$

As seen, to design the optimum clutter suppression filter, a priori knowledge of the interference covariance matrix and the desired target signal replica to which the filter is matched is needed.

Since adaptive estimation of the interference covariance matrix needs high processing powers and the target signal is unknown a priori, the MTD algorithm

introduces some approximate approaches that simplify the optimum filtering that leads to a sub-optimum filtering [2]:

- The MTD algorithm uses an assumed $\boldsymbol{S}_I$ of ground clutter and receiver noise which is a function of only CNR and antenna scanning modulation [2]. The CNR can be obtained adaptively by clutter maps and the antenna scanning modulation can be calculated according to antenna rotation speed.
- The target return signal is assumed to be a Swerling-0 target which has unit power and constant velocity

$$\boldsymbol{p} = \begin{bmatrix} 1 & e^{-j2\pi f_t T_s} & e^{-j2\pi f_t 2T_s} & \ldots & e^{-j2\pi f_t (M-1)T_s} \end{bmatrix}. \tag{1.10}$$

  where f_t represents the target Doppler frequency, T_s represents the PRI and M represents the number of pulses in CPI.

  Parallel Doppler filters tuned to different target velocities covering whole Doppler Spectra are designed.

An example of frequency responses of the sub-optimum clutter suppression filters used by the MTD algorithm can be seen from Figure 1-3.

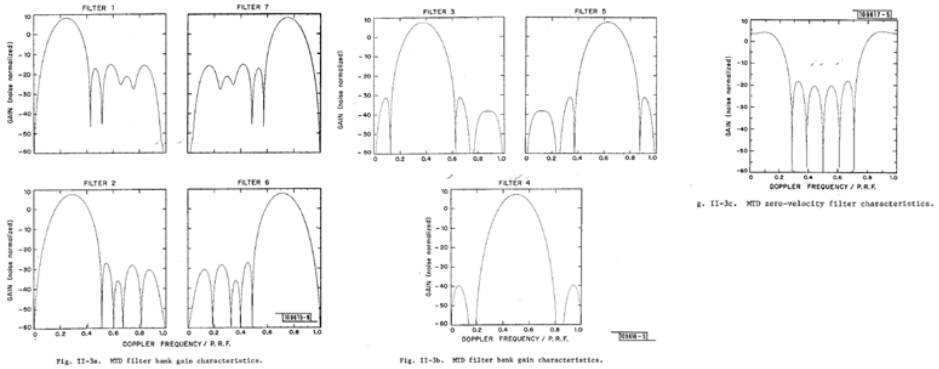

Fig. II-3a. MTD filter bank gain characteristics.

Fig. II-3b. MTD filter bank gain characteristics.

g. II-3c. MTD zero-velocity filter characteristics.

Figure 1-3: MTD-2 Doppler Filter Characteristics (5-bit coefficients) [2].

The MTD algorithm uses basic principles of the MTI; however it enhances its linear dynamic range by adding the parallel Doppler filters followed by constant false alarm rate detectors.

Principle features of the MTD processor presented in Figure 1-4 includes [2]

- Use of digital Doppler filters to separate the target returns from the clutter; the MTD solved this problem by near-optimum filtering. Near-optimum filtering of the rain clutter can be done as in the case of the ground clutter but the mean velocity of rain (can be different from zero) should be considered. The mean velocity of the rain clutter can be measured but it was decided not to do so because measuring the mean velocity of the rain clutter would bring complexity to hardware.
- Adaptive clutter maps to detect targets having no radial velocity vectors with respect to radar,
- Block-staggered ("multiple PRF") pulse repetition frequencies to unmask aircraft masked by precipitation echoes (PRF agility from CPI to CPI assures that if the radial velocity of aircraft is different from rain, high speed aircraft falls in to different Doppler filters on different PRF's),
- Pulse to pulse micro-staggered pulse repetition frequency coupled with the use of a coherent microwave transmitter to eliminate second trip echoes,
- A constant false alarm rate thresholding algorithm testing the output of each range-azimuth-Doppler cell for the presence of a target and clutter (Since weather and noise are statistically Rayleigh distributed, classic cell averaging constant false alarm rate algorithms can stabilize false alarm rate in the Doppler bins which the rain clutter falls in.)
- Correlation and centroiding algorithms that generate a single target report from a cluster of range-azimuth-Doppler target reports.

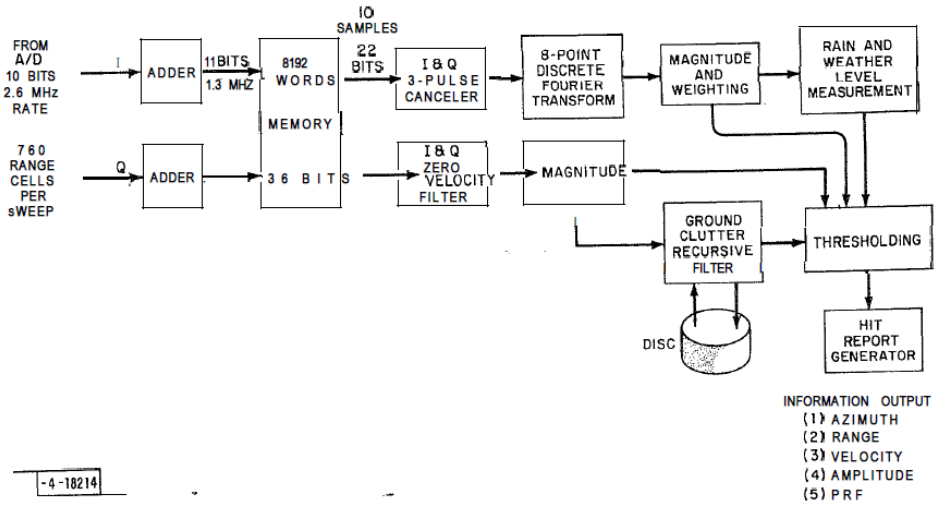

Figure 1-4: MTD-2 (Second Generation MTD) Processor Block Diagram [2]

Superior features of the optimum filters over the pulse cancellers are listed below [2]:

- At zero velocity and blind speeds, improvement factor is zero but there is no worsening as in the case of the 3-pulse canceller.
- Except for the filters tuned to or near the blind speeds, there are very deep nulls at blind speeds.
- Since the width of notch around blind speeds is determined in an optimum way with respect to the antenna rotation speed, the width of the notch increases with the increasing antenna rotation speed. Since optimum weights are the function of clutter power, the need to memorize the scan to scan clutter power rises.
- A simple detector can be built. The optimum processor can be broken into two parts; a clutter filter used to multiply the signal by antenna weighting and by the inverse of the interference covariance matrix and a target filter which is Discrete Fourier Transform. To decrease the computation load, the near-

optimum filter can be approximated by a digital filter which approximates as closely as possible the frequency response of clutter filter and the following target filter which is Discrete Fourier Transform (DFT).

1.4 Thesis Motivation

In many modern radar systems, various signal processing techniques have been proposed to effectively suppress the clutter and increase the signal to interference ratio. To achieve optimum suppression, the radar system must know the clutter characteristics and process the radar echoes based on these characteristics. Knowing the clutter covariance matrix is the first step of achieving this goal.

For fixed ground radars, the clutter environment characteristics are relatively stable and predictable. These characteristics can be stored in radars memory and optimum clutter suppression can be achieved. However, for radars on moving platforms, the clutter characteristics become diverse due to the relative velocity between radar platform and clutter. This problem can be solved since the modulation effect of the relative velocity between the radar platform and the clutter can be cancelled by measuring the radar platform velocity and adaptive moving target indication (AMTI) algorithm. The bigger problem arises when both the rain clutter and the ground clutter exist together in the environment since rain characteristics changes over time according to change in the velocity vector of wind or the rainfall rate or the turbulence strength etc. In such a case, the radar needs to adapt itself to changing clutter environment to achieve good clutter suppression. Adaptation requires instantaneous characterization of the environment and gives rise to the need of estimation of clutter parameters adaptively. The MTD algorithm optimizes its clutter suppression filters for only ground clutter because measuring the mean velocity and Doppler characteristics of the rain clutter would require high processing power and bring complexity to hardware.

A more chaotic environment is the one where both the rain clutter and sea clutter coexists since they are differently affected by the environmental conditions and the radar parameters. In these environments, adaptive estimation of the clutter characteristics to suppress the clutter becomes obligatory if high-performance target detection is needed.

Suppression of clutter by estimation of the clutter characteristics can be done by estimating the clutter covariance matrix or estimating the clutter parameters that can describe the clutter covariance matrix. The estimation of the clutter parameters is more preferable if they describe whole covariance matrix since they possess a priori knowledge and reduce the number of unknowns in the estimation process.

The main motivation of the thesis is to investigate performance of recently proposed clutter spectral parameter estimation techniques that lead to the optimum clutter suppression filtering in the environment that includes both sea clutter and rain clutter and compare their main properties.

1.5 Thesis Organization

The main objectives of the thesis can be listed as follows:

- Reviewing the characteristics of K-distributed sea clutter and Rayleigh distributed rain clutter,
- Reviewing methods to simulate synthetic sea clutter and rain clutter,
- Investigating parametric spectral parameter estimation techniques,
- Calculating Cramér-Rao bounds for estimations of the clutter spectral parameters,

- Determining the RMS errors and biases to estimate the spectral parameters that define the spectrum of K-distributed sea clutter and rain clutter using the algebraic spectral moments estimation technique,
- Comparing the clutter suppression performance of the algebraic spectral moments estimation technique with more conventional methods in terms of improvement factor.

There are totally 6 chapters in the thesis. Chapter 1 presents the radar terminology and interference suppression concepts and outlines the work done in the thesis. Chapter 2 reviews the characteristics of K-distributed sea clutter and Rayleigh distributed rain clutter. Chapter 3 covers the parametric spectral estimation techniques. Chapter 4 investigates the performance of clutter parameter estimation technique which uses algebraic spectral moments for different CNRs, Doppler spreads, Doppler separations, the number of observations and shape parameters. Chapter 5 gives comparisons between the clutter suppression performances of the algebraic spectral moment estimation technique with more conventional methods in terms of improvement factor. Finally, Chapter 6 consists of a summary of the work and main conclusions drawn.

CHAPTER 2

BACKGROUND

2.1 Problem Statement

In this thesis, the main problem is to estimate the covariance matrix of radar signals that contain both the K-distributed sea clutter and rain clutter using parametric spectral estimation methods. Then, the estimated clutter covariance matrix is used to design a filter to suppress clutter and thus to increase the SIR (signal-to-interference ratio). To investigate the performance of the estimators, K-distributed sea clutter and rain clutter are simulated. Then, the parametric estimator performances are investigated for different clutter parameters and compared to the Cramér-Rao bounds. The K-distributed sea clutter model, rain clutter model and radar receiver noise model reviewed in this chapter.

2.2 Sea Clutter

Sea clutter is defined as the unwanted radar echoes from the sea surface. It has a relatively low backscatterer coefficient than the land clutter and does not extend as far as the land clutter. It is difficult to form a relationship between sea clutter characteristics and environmental factors that determine sea clutter characteristics [4]. Moreover, it is difficult to adapt sea clutter echoes since the sea surface changes

with time. In other words, the scenario changes with time, while for ground clutter it stays the same.

The nature of sea echo generally depends upon the sea surface. There are two fundamental motions on the sea surface: Wind waves and swell waves. Wind waves, also known as ripples, result in random-appearing height alternation and caused by wind blowing on the sea surface. They are small waves less than 1.73 cm in wavelength and their phase velocity is determined by surface tension of the water [5]. Swell waves are sinusoidal, less random, long-wavelength, low-amplitude waves and occur when wind waves move out of the region where they were originally exited.

2.2.1 Characteristics of Sea Clutter

In this section, the sea clutter characteristic, its dependencies and modeling method are introduced. For this purpose, amplitude distribution, Doppler spectrum properties of sea clutter shall be covered.

2.2.1.1 Amplitude Characteristics

Unlike white Gaussian radar receiver noise, sea clutter returns exhibit properties of correlated non-Gaussian processes [6]. For the high-resolution radars, experimental sea clutter data collected from low grazing angles has significantly higher amplitude variations than those predicted by the Rayleigh Probability Density Function [6]. For this purpose, many sea clutter amplitude distributions are proposed to model sea clutter: Log-Normal, Weibull and K-distribution. In this thesis, K-distribution is used to model sea clutter returns. The arguments of choice of K-distribution model are as follows [6]:

- The statistical investigation of sea clutter returns collected from many experiments provide evidence that K-distribution can serve as a limiting distribution for sea clutter.
- Except for the K-distribution, other non-Rayleigh distributions are not derived from a physical model or scattering mechanism. While other non-Rayleigh distributions are based on fit to the experimental data, the K-distribution model are proposed to describe temporal and spatial characteristics of sea clutter.

According to the compound K distribution model, the pdf of slowly varying component has root gamma distribution which is

$$p(y)=\frac{2b}{\Gamma(v)}(by)^{2v-1}e^{-b^2y^2} \tag{2.1}$$

where v is the shape parameter, b is the scale parameter and $\Gamma(\cdot)$ is the gamma function.

The other component of compound K distribution model, namely the fast varying component, has Rayleigh distribution which is

$$p(x|y)=\frac{\pi x}{2y^2}e^{-\frac{\pi x^2}{4y^2}}. \tag{2.2}$$

K-distribution function is the weighted integral of (2.2) with respect to y:

$$p(x)=\int_0^\infty p(x|y)\,p(y)dy=\frac{2c}{\Gamma(v)}\left(\frac{cx}{2}\right)^v K_{v-1}(cx) \tag{2.3}$$

where K_{v-1} is a modified Bessel function of the second kind of order $v-1$ and c is a scale parameter whose expression is

$$c = \frac{\sqrt{\pi}}{\bar{x}\Gamma(v)}\Gamma\left(v+\frac{1}{2}\right). \tag{2.4}$$

b is related to c through $c = 2b\sqrt{\pi/4}$ and $\bar{x} = E\{x\}$ is the mean value of x.

$$\bar{x} = \frac{\sqrt{\pi}}{c\Gamma(v)}\Gamma\left(v+\frac{1}{2}\right) \tag{2.5}$$

The second moment of x is

$$E\{x^2\} = \frac{4}{c^2\Gamma(v)}\Gamma(v+1) = \frac{4v}{c^2}. \tag{2.6}$$

2.2.1.2 Shape Parameter Model for Sea Clutter

The shape parameter is an important parameter of compound K-distribution model for sea clutter amplitude characteristics since it defines "spikiness" and some of correlation properties of sea clutter. It is the parameter that affects detection and false alarm performance of maritime radars.

The parameterization of shape parameter has been provided by Ward [7] and is given by a simple empirical formula

$$\log_{10}(v) = \frac{2}{3}\log_{10}(\phi_{gr}^{o}) + \frac{5}{8}\log_{10}(A_c) - k_{pol} - \frac{\cos(2\theta_{sw})}{3} \tag{2.7}$$

where v is the shape parameter, ϕ_{gr}^{o} is the grazing angle in degrees ($0.1^{o} \leq \phi_{gr}^{o} \leq 10^{o}$), A_c is the radar resolved area in square meters and θ_{sw} is the aspect angle with respect to the swell direction.

In formula (2.7), k_{pol} represents polarizations dependence:

- 1.39 for vertical polarization and

- 2.09 for horizontal polarization.

2.2.1.3 Mean Clutter Reflectivity (σ_0)

Several mean sea clutter reflectivity models have been developed based on different analytical methods in electromagnetic scattering theory. These models use a lot of simplifying assumptions and can be used for prediction of the mean sea clutter reflectivity for a limited number of possible situations since scattering in microwave frequencies is complex and complicated further when many scattering mechanism of sea surface is taken in consideration [6]. To characterize sea clutter radar returns, instead of using purely analytical considerations, semi-empirical models have been developed. In these models the theoretical relations between model parameters are defined and experimental data is used to model constants. Sittrop [SIT], the Georgia Institute of Technology (GIT), the Technology Service Corporation (TSC) and Dockery (HYB) are examples of these semi-empirical models.

In this thesis the TSC model is used to simulate sea clutter returns since this model can be used over a broad frequency range (0.5-35 GHz) and provides full direction dependence from upwind to downwind. This model is suggested instead of SIT and GIT models when propagation conditions are unknown because it represents Nathanson's data which is the average of all look directions and closely represents average conditions [6].

The TSC model takes grazing angle, radar frequency, look direction with respect to wind direction, sea state and radar polarization as inputs and gives mean sea clutter reflectivity as an output.

2.2.1.4 Doppler Characteristics of Sea Clutter

Sea clutter has generally correlation between pulses reflected from a single resolution cell. The composite model describes the form of correlation between pulses. Over a short period of time, radar echoes from any clutter cell including sea clutter are always Rayleigh-distributed, which point outs that the radar return consists of many scatterers. Moreover, this speckle component has a Chi-square distribution which results in variations in the mean level of amplitude of sea clutter.

Speckle component of sea clutter has a short temporal decorrelation period and becomes fully decorrelated from pulse to pulse by frequency agility [6]. However, the underlying mean level has strong correlation, long decorrelation time and is not affected by frequency agility.

If sea clutter is observed with a coherent processing interval that is much less than decorrelation time of modulation process, the amplitude characteristics of sea clutter in coherent processing interval is mostly constant as proposed by the composite model. Then, the correlation caused by modulation process can be considered as having negligible effect. Correlation is caused by only rapidly varying speckle component of the composite model.

After removing the sample mean level of clutter, the autocorrelation of speckle component of sea clutter can be found by the following formula:

$$ACF_k = \frac{\sum_{n=0}^{N-1} x_k x_{n+k}^*}{\sum_{n=0}^{N-1} x_k x_k^*} \tag{2.8}$$

where $*$ denotes complex conjugate, x_n denotes complex radar return from a resolution cell consisting of sea clutter and N denotes the number of pulses in coherent processing interval. (2.8) is valid only if the duration of CPI is short when compared to the decorrelation time of modulation component.

This autocorrelation function is real and even when sea clutter spectrum is centered at zero Doppler [8] and it is symmetric. If the spectrum has a Doppler shift, the autocorrelation function is product of the autocorrelation function of zero Doppler clutter and complex sinusoid $\exp(j2\pi f_d T)$ where f_d represents the Doppler shift of clutter spectrum and T represents the time lag [8].

The amount of Doppler shift of sea clutter according to wind speed for upwind conditions is given as follows [5]:

$$\begin{aligned} v_{DopplerVV} &= 0.25 + 0.18U \\ v_{DopplerHH} &= 0.25 + 0.2U \end{aligned} \tag{2.9}$$

where $v_{DopplerVV}$ is Doppler shift of vertical polarization in m/s, $v_{DopplerHH}$ is Doppler shift of horizontal polarization in m/s and U is the wind speed in m/s. As seen from (2.9), the Doppler shift of sea clutter is independent of the radar frequency and the grazing angle. Moreover, the constant terms in (2.9) represent the upwind condition and they can be multiplied by cosine function to address the conditions other than the upwind condition [5].

Since sea clutter characteristics varies according to frequency, grazing angle, polarization, sea state, whether the sea is fully developed or not and radar resolution, fitting models to sea clutter data results in evolving of many sea clutter Doppler spectrum models in literature. In this thesis, Barlow's Gaussian spectrum model [9] is used since it is a classical model which has been used in radar system design for many decades.

The Doppler spread model of Barlow's Gaussian spectrum is

$$\begin{aligned} \sigma_{sVV} &= 0.3U \\ \sigma_{sHH} &= 0.15U \end{aligned} \tag{2.10}$$

where σ_{sVV} is the Doppler spread of vertical polarization in m/s, σ_{sHH} is the Doppler spread of horizontal polarization in m/s and U is the wind speed in m/s [5].

2.2.2 Simulation of K-distributed Sea Clutter

Pulse to pulse independent non-Gaussian clutter returns are easy to generate since their probability density functions are product of marginal probability density functions. Also, it is straightforward to control the covariance matrix of Gaussian clutter returns. However, to generate pulse to pulse dependent non-Gaussian sea clutter is a rather difficult problem since it requires generation of random variables that have a joint probability density function and a specific covariance matrix. In the literature, there are two methods proposed to achieve this: Zero memory nonlinear (ZMNL) transformations and spherically invariant random processes (SIRP) [6].

Using zero memory nonlinear (ZMNL) transformations is considered to be not practical for several reasons [6]. In SIRP model, it is possible to control both the amplitude PDF and the correlation properties of sea clutter at the same time.

In this thesis the SIRP method is used to generate the sea clutter returns. As mentioned before the sea clutter returns obey the composite scatterer theory and can be expressed as a product of two independent processes;

$$x(t) = y(t)v(t) \tag{2.11}$$

where $v(t)$ is a zero-mean complex correlated Gaussian random process representing the speckle component and $y(t)$ is a non-negative stationary non-Gaussian random process representing the underlying modulating component.

It is assumed that the decorrelation time of $y(t)$ is much longer than the decorrelation time of $v(t)$ and the coherent processing interval. As a result, in

coherent processing interval, $y(t)$ is modeled by a random variable rather than a process.

Then, the sea clutter returns can be expressed as

$$x(t) = v(t)\,y\,. \tag{2.12}$$

$v(t)$ can be modeled as a complex white Gaussian process $w(t)$ filtered by a linear time-invariant system to achieve the desired time correlation properties.

The PDF of y is Chi-squared [10]:

$$f(y) = \frac{2v^{v}}{\Gamma(v)} y^{2v-1} \exp\left(-vy^{2}\right) \tag{2.13}$$

where v is the shape parameter and $\Gamma(\cdot)$ is the gamma function.

In the SIRP method, K-distributed sea clutter which has a specific covariance matrix $\boldsymbol{R}$ can be generated by the following steps [6]:

1) Generate a random variable y according to the PDF (2.13).

2) Generate two Nx1 sized uncorreletad white zero-mean Gaussian vectors $\boldsymbol{W_1}$ and $\boldsymbol{W_2}$.

3) Perform liner transformation to obtain two spherically invariant random Nx1 sized vector $\boldsymbol{V_1}$ and $\boldsymbol{V_2}$.

$$\begin{aligned} \boldsymbol{V_1} &= \boldsymbol{G}\boldsymbol{W_1} \\ \boldsymbol{V_2} &= \boldsymbol{G}\boldsymbol{W_2} \end{aligned} \tag{2.14}$$

where

$$\boldsymbol{G} = \boldsymbol{E}\boldsymbol{D}^{\frac{1}{2}}\,. \tag{2.15}$$

$\boldsymbol{E}$ is composed of the normalized eigenvectors of the covariance matrix of $\boldsymbol{R}$ and $\boldsymbol{D}$ is the diagonal matrix of eigenvalues of $\boldsymbol{R}$.

4) To generate K-distributed sea clutter which has the covariance matrix $\boldsymbol{R}$, multiply the $\boldsymbol{V}_1 + j\boldsymbol{V}_2$ by y.

2.3 Rain Clutter

Rain, an important meteorological phenomena, has two major effects on radar performance: attenuation of radar signals and unwanted echoes reflected from raindrops which can mask target echoes.

Attenuation and unwanted echoes reflected from raindrops strictly depend on the rainfall rate. The common rainfall descriptors and rainfall levels defined by The National Weather Service is given in Table 2-1 and Table 2-2.

Table 2-1 Common Rainfall Descriptors

Type	**Rainfall rate, r in mm/hr**
Drizzle	0.25
Light Rain	1.0
Moderate Rain	4.0
Heavy Rain	16.0
Excessive Rain	>40

Table 2-2 Rainfall Levels Defined by The National Weather Service

Level 1	1.52-6.09	mm/hr
Level 2	6.09-25.9	mm/hr
Level 3	25.9-53.1	mm/hr
Level 4	53.1-114.3	mm/hr
Level 5	114.3-180.3	mm/hr
Level 6	180.3-	mm/hr

Instantaneous rainfall rate probabilities in Turkey are given in Table 2-3.

Table 2-3 Instantaneous Rainfall Probabilities in Turkey

Rainfall rate, r in mm/hr	**Instantaneous Rainfall Probability in Turkey**
1.0	% 1.5
2.0	% 0.7
4.0	% 0.25
20.0	% 0.01

2.3.1 Rain Clutter Attenuation

Rain attenuation is a function of rainfall rate and drop-size distribution model. Since drop-size distributions differ in different areas of world, a common, approximate model is used in radar design.

Above 2 GHz, the attenuation effect of rain on electromagnetic waves becomes significant when the droplets are small compared to the wavelength, in other words, the size of rain droplets lies in the Rayleigh region [4]. In this region, the rain attenuation coefficient in terms of dB/km can be calculated by [11]

$$k = ar^b \tag{2.16}$$

where k is the attenuation coefficient, r is the rainfall rate in mm/h, a and b are constants that depends on radar frequency, polarization and temperature.

a and b for different radar frequencies given in Table 2-4. a_{hor} and b_{hor} should be used for the horizontal polarization and a_{ver} and b_{ver} should be used for the vertical polarization.

Table 2-4 Rain Attenuation Model Parameters for Different Radar Frequencies [11]

Frequency (GHz)	a_{hor}	a_{ver}	b_{hor}	b_{ver}
1	0.0000387	0.0000352	0.912	0.880
3	0.00065	0.000591	1.121	1.075
10	0.0101	0.00887	1.276	1.264
20	0.0751	0.0691	1.099	1.065
40	0.350	0.310	0.939	0.929

2.3.2 Characteristics of Rain Clutter

2.3.2.1 Amplitude Characteristics

The performance of the constant false alarm rate algorithm does not change when the rain comes into the radar observation area since the statistical distribution of the amplitude of the rain echo is Rayleigh [2].

2.3.2.2 Mean Clutter Reflectivity (σ_0)

Rain reflectivity is denoted with the symbol Z and is called volume reflectivity. It relates rain clutter reflectivity to distribution of rain drop sizes and usually expressed in decibel units.

The relationship between mean rain clutter reflectivity and Z is as follows [11]:

$$\eta = \frac{\pi^5 |K|^2}{\lambda^4} Z \tag{2.17}$$

where η is mean rain clutter reflectivity in m^{-1}, λ is the radar wavelength in m, K depends on the temperature and wavelength, for most weather conditions $|K|^2$ is equal to 0.93 for liquid scatterers and 0.197 for frozen scatterers and Z is in m^6/m^3.

Z values for different rainfall rates are given in Table 2-5.

Table 2-5 Z values for different rainfall rates [11]

Rainfall rate, r in mm/hr	**Z, dBz**
0.25	14
1.0	23
4.0	32
16.0	41

2.3.2.3 Doppler Characteristics

Doppler spectra of radar echoes reflected from rain can be described by four mechanisms when only inter clutter motion is taken into account: wind shear, beam broadening, turbulence and fall velocity distribution [12]. A fifth mechanism can be included if the radar antenna is rotating, namely, antenna rotation effect or antenna scanning modulation.

Assuming these mechanisms are independent, the variance of Doppler velocity spectrum σ_v^2 of rain can be expressed as the sum of the variances from each mechanism:

$$\sigma_v^2 = \sigma_{shear}^2 + \sigma_{beam}^2 + \sigma_{turb}^2 + \sigma_{fall}^2 . \tag{2.18}$$

In fact, these velocity variances are strictly related to the second spectral moment about the mean of Gaussian spectrum model. The power spectral density function of rain clutter can be described by a Gaussian spectrum $G(f)$ [13]

$$G(f) = G_0 e^{\frac{-f^2}{2\sigma_f^2}} \tag{2.19}$$

where G_0 is a constant that depends on the average rain echo power, f is the Doppler frequency and σ_f^2 is the Gaussian spectrum variance.

σ_f^2 and σ_v^2 are related through

$$\sigma_f^2 = \frac{2\sigma_v^2}{\lambda} \tag{2.20}$$

where λ is the radar wavelength.

1. Wind shear: Wind shear effect is caused by the change in wind velocity over the vertical extend of radar beam. Wind velocity changes with altitude and results in a distribution of radial velocities of rain droplets, and this phenomena has great effect on spectrum width when extent of radar beam in vertical direction is large. This mechanism can be the greatest of all mechanisms, especially for ground based radars.

For Gaussian antenna pattern, the effect of wind shear on Doppler spectrum of rain clutter can be related through

$$\sigma_{shear} = 0.42kR\phi_2 \tag{2.21}$$

where k is the velocity gradient in the vertical direction of the beam in m/s/km, R is the slant range to clutter in km and ϕ_2 is the two-way half power antenna elevation beamwidth in radians. For pencil beam radars,

- $k = 4.0$ m/s/km is suggested for averaged over 360º azimuth and
- $k = 5.7$ m/s/km is suggested for along wind direction [14].

2. Beam broadening: The effect of the change of wind speed in vertical direction is covered by the wind shear effect; however, the distribution of radial velocities caused by tangential movement of rain droplets over the radar beam induced by the tangential wind direction is covered by the beam broadening mechanism. In beam broadening mechanism, only the horizontal component is taken into account because the vertical component is negligible when compared to wind shear.

The effect of beam broadening on Doppler spectrum of rain clutter assuming a Gaussian antenna pattern can be found by

$$\sigma_{beam} = 0.42 V_0 \theta_2 \sin\beta \tag{2.22}$$

where V_0 is the wind speed in the beam center in m/s, θ_2 is the two-way half power antenna azimuth beam width in radians and β is the azimuth angle relative to the wind direction at beam center in radians.

3. Wind turbulence: Since wind speed is a stochastic process, fluctuations in the mean wind speed causes variation of speed of rain droplets and broadening of rain clutter spectra. According to a number of experiments, it is found to be independent of height and up to 1.5 km altitude, σ_{turb} can be approximated as 1 m/s and for higher altitudes σ_{turb} can be approximated as 0.6 m/s [14].

4. Fall velocity distribution: A spread in fall velocities of rain droplets due to their different individual sizes causes a spread of velocity components along the radar beam. σ_{fall} is independent from rain intensity and depends on the elevation angle through

$$\sigma_{fall} = 1.0 \sin\psi \tag{2.23}$$

where ψ is the elevation angle.

5. Antenna rotation effect: Antenna scanning also causes spread of rain clutter spectrum caused by the modulation effect of antenna pattern. The resulting antenna rotation modulation effect σ_{arm} in Hz can be calculated by [15]

$$\sigma_{arm} = \frac{f_r \sqrt{\ln 2}}{n\pi} \tag{2.24}$$

where f_r is the pulse repetition frequency and n is the number of hits between the one way 3-dB points of antenna pattern. This effect also added to sea clutter Doppler spread in the same way as rain clutter.

2.3.3 Simulation of Rayleigh-distributed Rain Clutter

The performance of the constant false alarm rate algorithm does not change when the rain comes into the radar observation area since the statistical distribution of the amplitude of the rain echo is Rayleigh [2]. This phenomenon simplifies complexity of rain clutter generation mechanisms when compared to sea clutter.

Since rain clutter has complex Gaussian distribution, generating rain clutter which has a specific covariance matrix $\boldsymbol{R}$ is possible by a simple linear transformation.

Rain clutter can be generated by following steps:

1) Generate two Nx1 sized uncorreletad white zero-mean Gaussian vectors $\boldsymbol{W_1}$ and $\boldsymbol{W_2}$.

2) Perform liner transformation to obtain two spherically invariant random Nx1 sized vector $\boldsymbol{V_1}$ and $\boldsymbol{V_2}$.

$$\begin{aligned} \boldsymbol{V_1} &= \boldsymbol{G}\boldsymbol{W_1} \\ \boldsymbol{V_2} &= \boldsymbol{G}\boldsymbol{W_2} \end{aligned} \tag{2.25}$$

where

$$\boldsymbol{G} = \boldsymbol{E}\boldsymbol{D}^{\frac{1}{2}}. \tag{2.26}$$

$\boldsymbol{E}$ is composed of the normalized eigenvectors of the covariance matrix of $\boldsymbol{R}$ and $\boldsymbol{D}$ is the diagonal matrix of eigenvalues of $\boldsymbol{R}$.

3) The Gaussian distributed rain clutter which has the covariance matrix $\boldsymbol{R}$ is $\boldsymbol{V}_1 + j\boldsymbol{V}_2$.

CHAPTER 3

METHODOLOGY

3.1 Signal Model

It is necessary to define signal models for the sea clutter and the rain clutter and the parameters of them since the methods presented in this thesis are developed to estimate these parameters.

Let $x(t)$ be a signal received from the environment that includes both the sea clutter and the rain clutter. The assumption here is that the radar echoes from sea and rain have Gaussian shaped spectra and are uncorrelated with each other. However, the sea clutter and the rain clutter are related through wind direction and speed. In order to generalize the model, we assume that the mean Dopplers and the spectral widths of the clutters can take any value.

With the assumptions stated above, the power spectrum $P_s(f)$ of $x(t)$ can be written as

$$P_s(f) = \sum_{i=1}^{2} S_i(f) + \sigma_n^2 \tag{3.1}$$

with

$$S_i(f) = \frac{P_i}{\sqrt{2\pi}\sigma_i} \exp\left[-\frac{1}{2}\left(\frac{f - f_i}{\sigma_i} \right)^2 \right] \tag{3.2}$$

where σ_n^2, P_i, f_i and σ_i are the additive white Gaussian circular noise representing the radar receiver noise power spectral density, the mean powers of the clutters, the mean frequencies of the clutters and the standard deviations of the Doppler spectra of the clutters, respectively.

Visualization of an example $P_s(f)$ can be seen in Figure 3-1.

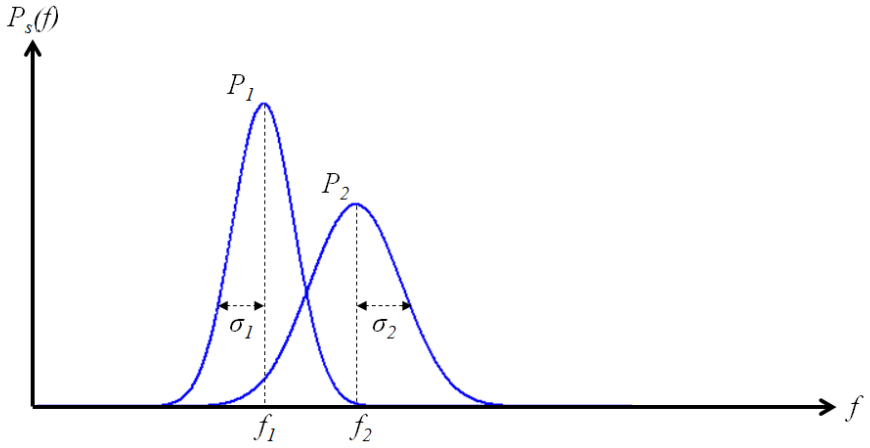

Figure 3-1 Visualization of $P_s(f)$

The autocorrelation function of $x(t)$ is

$$\gamma(t) = \sum_{i=1}^{2} P_i \exp\left[\left(-2\pi^2 \sigma_i^2 t^2 + j2\pi f_i t \right) \right] + \sigma_n^2 \delta(t) \tag{3.3}$$

where $j^2 = -1$ and $\delta(t)$ denotes the Dirac delta function.

Let $\boldsymbol{x}$ be the Mx1 vector representing the time series formed by sampling $x(t)$ with sampling period T_s:

$$\boldsymbol{x} = \left[x(0) \quad x(T_s) \quad \ldots \quad x\left((M-2)T_s\right) \quad x\left((M-1)T_s\right) \right]^T \tag{3.4}$$

where $(\square)^T$ designates the transpose operation.

Defining the Mx1 vector $\boldsymbol{n}$ as the additive white Gaussian noise, $\boldsymbol{x}$ can be written as

$$\boldsymbol{x} = \boldsymbol{y} + \boldsymbol{n} \tag{3.5}$$

where the Mx1 vector $\boldsymbol{y}$ is a stochastic process which is formed by sampling the radar echo whose power spectrum is $\sum_{i=1}^{2} S_i(f)$.

Since $\boldsymbol{n}$ represents the uncorrelated receiver noise, the covariance matrix of $\boldsymbol{n}$ is

$$\boldsymbol{R}_n = \sigma_n^2 I \tag{3.6}$$

where I represents the MxM identity matrix.

The covariance matrix of $\boldsymbol{y}$ can be written as

$$\boldsymbol{R}_y = E\left[\boldsymbol{y}\boldsymbol{y}^* \right] = \sum_{i=1}^{2} \boldsymbol{R}_{yi}\left(P_i, f_i, \sigma_i^2\right) \tag{3.7}$$

with

$$\boldsymbol{R}_{yi}\left(P_i, f_i, \sigma_i^2\right) = P_i \boldsymbol{A}(f_i)\boldsymbol{B}\left(\sigma_i^2\right)\boldsymbol{A}^*(f_i) \tag{3.8}$$

where

$$\boldsymbol{A}(f_i) = diag\left(1 \quad e^{j2\pi f_i T_s} \quad \ldots \quad e^{j2\pi f_i (M-1)T_s}\right) \tag{3.9}$$

is an MxM matrix representing the Doppler shift of clutter and $\boldsymbol{B}\left(\sigma_i^2\right)$ is an MxM matrix representing the Doppler spread of the clutter:

$$\boldsymbol{B}_{k,l}\left(\sigma_i^2\right) = e^{-2\pi^2\sigma_i^2(k-l)^2T_s^2},\ 1 \le k,l \le M\ . \tag{3.10}$$

After combining (3.6) and (3.7), the covariance matrix of $\boldsymbol{x}$ is obtained

$$\boldsymbol{R}_x\left(\boldsymbol{\mu}\right) = \boldsymbol{R}_y\left(\boldsymbol{\mu}\right) + \sigma_n^2\boldsymbol{I} \tag{3.11}$$

where $\boldsymbol{\mu} = \begin{bmatrix} P_1 & f_1 & \sigma_1^2 & P_2 & f_2 & \sigma_2^2 & \sigma_n^2 \end{bmatrix}$ is the parameter vector. If the elements of $\boldsymbol{\mu}$ are known, the power spectrum of the radar echo can be described precisely and the optimum clutter filter which maximizes the output SIR can be designed.

Actually, it is considered that σ_n^2 can be calculated by the instantaneous radar receiver bandwidth, the system temperature and the noise figure of the radar receiver. Then, the parameter vector that defines the power spectrum of the radar echo becomes

$$\boldsymbol{\mu} = \begin{bmatrix} P_1 & f_1 & \sigma_1^2 & P_2 & f_2 & \sigma_2^2 \end{bmatrix}. \tag{3.12}$$

3.2 Simplified Signal Model

The signal model whose parameter vector is defined in (3.12) can be simplified by eliminating the standard deviation of Gaussian spectra, in other words, we can assume that the sea clutter and the rain clutter echoes are target-like echoes which have very narrow Doppler bandwidths.

This assumption can be used to design suboptimum clutter suppression filters that place notches in the Doppler spectrum where the sea clutter and the rain clutter take place, without taking care of the Doppler spreads.

Actually, the narrow-band assumption is used by two-step algorithms which can estimate the parameter vector (3.12). In first step, only P_1, f_1, P_2 and f_2 are estimated with the assumption that the clutters have very narrow bandwidths and, in the second step, solution is generalized to find σ_1^2 and σ_2^2. An example for two-step algorithms can be found in [16].

Under the assumption, the power spectrum $P_s(f)$ of $x(t)$ can be written as

$$P_s(f) = \sum_{i=1}^{2} P_i \delta(f - f_i) + \sigma_n^2 \tag{3.13}$$

where σ_n^2, P_i, f_i and are the additive white Gaussian circular noise representing the radar receiver noise, the mean powers of the clutters and the mean frequencies of the clutters, respectively.

A visualization of an example $P_s(f)$ can be seen from Figure 3-2.

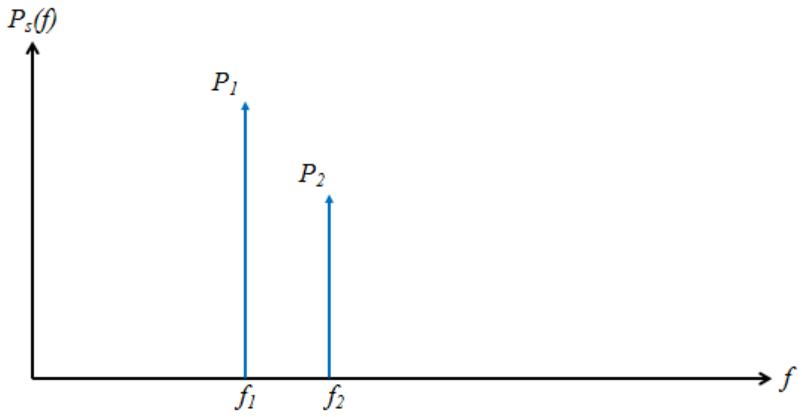

Figure 3-2 Visualization of $P_s(f)$

The corresponding autocorrelation function of $x(t)$ is

$$\gamma(t) = \sum_{i=1}^{2} P_i \exp\left[j2\pi f_i t \right] + \sigma_n^2 \delta(t). \tag{3.14}$$

Following the steps described in Section 3.1, the covariance matrix of $\boldsymbol{x}$ can be found as

$$\boldsymbol{R}_x(\boldsymbol{\mu}) = \sum_{i=1}^{2} P_i \boldsymbol{A}(f_i) \boldsymbol{A}^*(f_i) + \sigma_n^2 \boldsymbol{I} \tag{3.15}$$

where

$$\boldsymbol{A}(f_i) = diag\left(1 \quad e^{j2\pi f_i T_s} \quad \ldots \quad e^{j2\pi f_i (M-1) T_s}\right) \tag{3.16}$$

is an MxM matrix representing the Doppler shift of clutter and $\boldsymbol{\mu} = \left[P_1 \quad f_1 \quad P_2 \quad f_2 \quad \sigma_n^2 \right]$ is the parameter vector. Since σ_n^2 can be calculated by the instantaneous radar receiver bandwidth, the system temperature and the noise figure of the radar receiver, the parameter vector which defines the power spectrum of the radar echo becomes

$$\boldsymbol{\mu} = \left[P_1 \quad f_1 \quad P_2 \quad f_2 \right]. \tag{3.17}$$

3.3 Maximum-Likelihood Estimator

One way to estimate the parameter vector in (3.12) is a standard technique in statistical estimation called the maximum-likelihood (ML) method. In general, this method is useful since it constitutes a basis of comparison when the performance of a new estimation method is studied. In the maximum-likelihood method, unknown parameters which maximize the likelihood function are determined. Negative log-likelihood function for our case is the following [16]:

$$L(\boldsymbol{\mu}) = \log\left(\left| R_x(\boldsymbol{\mu}) \right| \right) + Tr\left\{ R_x^{-1}(\boldsymbol{\mu}) \hat{R}_x \right\} \tag{3.18}$$

where log(.), |.|, and Tr denote the natural logarithm, the matrix determinant and the trace operator, respectively. $\hat{R}_x$ is the sample covariance matrix:

$$\hat{R}_x = \frac{1}{K}\sum_{k=1}^{K} x(k)x(k)^H \tag{3.19}$$

where K is the number of observations.

Maximum-likelihood estimate $\hat{\boldsymbol{\mu}}$ of the parameter vector $\boldsymbol{\mu}$ can be obtained by solving the following minimization problem:

$$\hat{\boldsymbol{\mu}} = arg_{\boldsymbol{\mu}} min\big(L(\boldsymbol{\mu})\big). \tag{3.20}$$

Since analytic solutions to (3.20) do not exist because of its multidimensional nonlinearity, an easy to implement second-order steepest descent algorithm is proposed in [16] to solve (3.20).

In [16], it is shown that the statistical performance of the parametric maximum likelihood estimator fits the Cramér-Rao bound and its optimality is provided. However, in this method, in every step of the second-order steepest descent algorithm, a 6x1 sized gradient vector and a 6x6 sized Hessian matrix must be calculated and these calculations require high computational power. Different suboptimum methods having lesser computational loads are presented in Section 3.4 and 3.5.

The maximum-likelihood estimator described in this section can be also used to estimate the parameter vector of the simplified signal model. The only difference is that the minimization problem defined in (3.20) should be done according to parameter vector (3.17).

3.4 Subspace-Based Methods

When investigating the problem of finding the mean powers, the mean Doppler frequencies and the Doppler spreads of more than one interference signal such as the sea clutter and the rain clutter, high-resolution subspace-based methods like MUSIC (Multiple Signal Classification) can be used for their good statistical performances if the interference signals are assumed to have very narrow spectral widths [17]. They are also low-cost and suboptimal alternatives to the maximum-likelihood method when computational resources are important. However, when large Doppler dispersions of the interference signals are taken into account, DSPE [18] and DISPARSE [19] algorithms outperform MUSIC. In [20], WPSF (weighted pseudosubspace fitting) algorithm is developed and it is claimed that it provides better estimates than the DSPE and the DISPARSE algorithms.

In [20], the solution to the problem of finding the parameter vector $\boldsymbol{\mu}=\begin{bmatrix} P_1 & \omega_1 & \sigma_1^2 & P_2 & \omega_2 & \sigma_2^2 & \sigma_n^2 \end{bmatrix}$ starts with the assumption that interference signals have very narrow spectral widths (σ_1^2 and σ_2^2 are assumed to be 0) and then the solution is generalized to find all the elements of the parameter vector. In other words, in the first step, the radar echo is assumed to be in the form of the simplified signal model and a solution is found and in the second step, the solution found in first step is extended to the non-simplified signal model.

The estimation performance of the WPSF method is presented in [16] and it is shown that it fails when compared to the performance of the parametric maximum likelihood estimator described in Section 3.3. The performance of WPSF method is not investigated in this thesis; however, the WPSF method is mentioned for the sake of completeness and it is just noted that it is a recently developed subspace based parametric clutter parameter estimation method.

Consider the signal $x(t)$ corresponding to echo regarding the radar range cell where the rain and the sea clutter coexists. We assume that the clutter signals are complex-valued sinusoids (very narrow band signals) corrupted by additive white Gaussian complex noise $n(t)$:

$$x(t) = \sum_{i=1}^{2} \alpha_i \exp\left[j\omega_i t + \varphi_i \right] + n(t) = \sum_{i=1}^{2} z_k \exp\left[j\omega_i t \right] + n(t), \qquad z_k = \alpha_i \exp\left[\varphi_i\right] \tag{3.21}$$

where $\alpha_i \exp[\varphi_i]$ and ω_i are representing the complex amplitude and the mean Doppler frequencies of the clutters, respectively. The complex amplitudes of the clutters are assumed constant in the CPI and independent from one CPI to another.

As mentioned before, the Mx1 sized vectors $\boldsymbol{x}$ and $\boldsymbol{n}$ are obtained by sampling $x(t)$ and $n(t)$ M times with sampling period T_s and can be written as

$$\boldsymbol{x} = \boldsymbol{G}(\omega)\boldsymbol{z} + \boldsymbol{n} \tag{3.22}$$

where $\boldsymbol{G}(\omega)$ is an Mx2 matrix which is defined as

$$\boldsymbol{G}(\omega) = \left(\boldsymbol{g}(\omega_1) \quad \boldsymbol{g}(\omega_2) \right); \qquad \boldsymbol{g}(\omega) = \left(1 \quad e^{j\omega T_s} \quad \ldots \quad e^{j\omega(M-1)T_s} \right)^T \tag{3.23}$$

and where $\boldsymbol{z}$ equals the complex amplitudes of the clutter components in a CPI of the radar,

$$\boldsymbol{z} = \left(z_1 \quad z_2 \right)^T . \tag{3.24}$$

The covariance function of $\boldsymbol{x}$ is

$$\boldsymbol{R}_x = E\left[\boldsymbol{x}\boldsymbol{x}^* \right] = \boldsymbol{G}\boldsymbol{R}_z\boldsymbol{G}^* + \sigma_n^2\boldsymbol{I} = \boldsymbol{R}_y + \sigma_n^2\boldsymbol{I} \tag{3.25}$$

where $\boldsymbol{R}_z$ is the covariance matrix of $\boldsymbol{z}$, σ_n^2 is the noise power and $\boldsymbol{R}_y$ is the covariance matrix of noise free signals.

Assuming ω_1 and ω_2 are not equal to each other and are separate enough, the clutter signals lie in the 2-D plane spanned by the linearly independent columns of $\boldsymbol{G}$ and denoted by $span\{\boldsymbol{G}\}$. This 2-D plane is termed *the signal space* and contains the largest two eigenvalues of $\boldsymbol{R}_x$ (Since $\boldsymbol{x}$ contains two sinusoidal interference signals, the rank of $\boldsymbol{R}_x$ is two).

The eigendecomposition of $\boldsymbol{R}_x$ is as follows:

$$\boldsymbol{R}_x = \sum_{i=1}^{2} \lambda_i \boldsymbol{e}_i \boldsymbol{e}_i^* = \boldsymbol{E}_s \Lambda_s \boldsymbol{E}_s^* + \boldsymbol{E}_n \Lambda_n \boldsymbol{E}_n^* \tag{3.26}$$

where $\Lambda_n = \sigma_n^2 \boldsymbol{I} = diag\left(\begin{bmatrix} \lambda_3 & \lambda_4 & \cdots & \lambda_M \end{bmatrix}\right)$, $\Lambda_s = diag\left(\begin{bmatrix} \lambda_1 & \lambda_2 \end{bmatrix}\right)$ and $\boldsymbol{E}_n$ is termed *the noise subspace* and is orthogonal to *the signal space*. The unknown parameters ω_1 and ω_2 can be extracted from $\boldsymbol{E}_s$ since $span\{\boldsymbol{G}\} = span\{\boldsymbol{E}_s\}$.

If the interfering signals have considerable Doppler spread, the rank of $\boldsymbol{R}_x$ increases and extraction of ω_1 and ω_2 becomes difficult. However, if the assumption that most of the power in $x(t)$ belongs to clutter is made, λ_1 and λ_2 are much greater than the rest of the eigenvalues of $\boldsymbol{R}_x$. Then, one can define a *pseudosignal subspace* as the span of eigenvectors corresponding to λ_1 and λ_2 and a *pseudonoise subspace* as the span of eigenvectors corresponding to the rest of the eigenvalues.

The eigendecomposition of $\hat{\boldsymbol{R}}_x$ is then:

$$\hat{\boldsymbol{R}}_x = \sum_{i=1}^{2} \hat{\lambda}_i \hat{\boldsymbol{e}}_i \hat{\boldsymbol{e}}_i^* = \hat{\boldsymbol{E}}_s \hat{\Lambda}_s \hat{\boldsymbol{E}}_s^* + \hat{\boldsymbol{E}}_n \hat{\Lambda}_n \hat{\boldsymbol{E}}_n^*. \tag{3.27}$$

In the WPSF algorithm, the key idea is finding $\hat{\boldsymbol{\mu}}$ which makes $\hat{\boldsymbol{E}}_s$ as orthogonal as possible to $\hat{\boldsymbol{E}}_n$:

$$\hat{\boldsymbol{\mu}} = \arg_{\boldsymbol{\mu}} \min \boldsymbol{\rho}^*(\boldsymbol{\mu}) \boldsymbol{W} \boldsymbol{\rho}(\boldsymbol{\mu}) \tag{3.28}$$

where

$$\boldsymbol{\rho}(\boldsymbol{\mu}) = vec\left[\boldsymbol{E}_n(\boldsymbol{\mu}) \hat{\boldsymbol{E}}_s \right] \tag{3.29}$$

where $vec[\boldsymbol{A}]$ is the column vector obtained by stacking the columns of $\boldsymbol{A}$, and where $\boldsymbol{W}$ is a $2(M-2)x2(M-2)$ sized Hermitian positive definite matrix. The choice of $\boldsymbol{W}$ takes place in [20] and a second-order steepest descent algorithm which optimizes the criterion in (3.28) is proposed in [16].

The WPSF algorithm can estimate the parameter vector

$$\boldsymbol{\mu} = \left[\omega_1 \quad \sigma_1^2 \quad \omega_2 \quad \sigma_2^2 \right], \tag{3.30}$$

but it cannot find P_i and σ_n^2 because these parameters have no effect on orthogonality between $\hat{\boldsymbol{E}}_s$ and $\hat{\boldsymbol{E}}_n$.

From (3.27) an estimate of σ_n^2 can be obtained from [16]

$$\hat{\sigma}_n^2 = \frac{1}{M-2} \sum_{i=3}^{M} \hat{\lambda}_i . \tag{3.31}$$

The solution to the estimation problem for P_i is also proposed in [16]. The autocorrelation of sequence of $\boldsymbol{x}$ can be written

$$\boldsymbol{\gamma} = \boldsymbol{C}(\omega, \sigma) \boldsymbol{P} + \boldsymbol{n}_{\gamma} \tag{3.32}$$

where

$$\boldsymbol{P} = \begin{bmatrix} P_1 & P_2 \end{bmatrix}^T,$$

$$\boldsymbol{C}(\omega,\sigma) = \begin{bmatrix} \boldsymbol{c}(\omega_1,\sigma_1) & \boldsymbol{c}(\omega_2,\sigma_2) \end{bmatrix},$$

$$\boldsymbol{c}(\omega_i,\sigma_i) = \begin{bmatrix} 1 & \alpha_i(T_s)e^{j\omega_i T_s} & \ldots & \alpha_i\big((M-1)T_s\big)e^{j\omega_i(M-1)T_s} \end{bmatrix}^T, \tag{3.33}$$

$$\boldsymbol{n}_\gamma = \begin{bmatrix} \sigma_n^2 & 0 & \ldots & 0 \end{bmatrix}^T \text{ and}$$

$$\alpha_i(t) = \exp\left(-2\pi^2\sigma_i^2 t^2\right).$$

The estimates of P_i's can then be found as

$$\hat{\boldsymbol{P}} = \begin{bmatrix} \hat{P}_1 & \hat{P}_2 \end{bmatrix} = \left[\left(\boldsymbol{C}^*\boldsymbol{C}\right)^{-1}\boldsymbol{C}^*\right]\hat{\boldsymbol{\gamma}}. \tag{3.34}$$

3.5 Algebraic Spectral Moment Based Moving Clutter Parameter Estimation

High-resolution spectral analysis methods are based on trigonometric moment representation of spectral functions. Many estimators are designed to estimate these trigonometric moments to describe the spectral properties like MUSIC, periodogram etc. Algebraic moment representation is another useful way of representing the spectral functions. However the algebraic moment approach is useless without suitable methods for statistical estimation techniques for the algebraic moments. Such methods are recently obtained in [21] and proposed to solve direction of arrival (DOA) problem of more than one interference signals. This algorithm is calibrated in order to estimate the clutter parameters and the estimation performances under different conditions are investigated in this thesis.

The properties and the advantages of this algorithm can be listed as

- It is based on series representation of the covariance matrix [22],
- It does not require a priori knowledge of the radar receiver noise power [22],

- It is a computationally simpler method than the subspace methods [23],
- It is a high-resolution spectral estimation algorithm, in other words, it requires much less number of observations to analyse the spectral properties of an interference [23],
- It eliminates some mathematical difficulties encountered in the maximum-likelihood estimation of the spectral moments [21],
- It is a generalization of the well-known pulse pair algorithms [21].

First of all, the spectral moments of the radar echoes which contain both the sea and the rain clutter are stated based on the signal models that are described in Sections 3.1 and 3.2. Secondly, the algebraic spectral moment estimation method which is proposed in [21] is presented and finally, the clutter parameter calculation method using estimates of the algebraic spectral moments are presented [23].

3.5.1 Spectral Moments of Simplified Narrow Band Interference Signals

With the assumption that the sea and the rain clutter have zero Doppler spread, the spectral moments of the radar echo are functions of parameter vector (3.17). In this section, algebraic spectral moments in terms of parameter vector (3.17) are described.

The spectral moments are defined as

$$\mathrm{M}_q = \int_{-\infty}^{\infty}(f - f_0)^q S(f)df,\ 0 \le q < \infty \tag{3.35}$$

where M_q is the q'th spectral moment and $S(f)$ is the power spectral density of a process. f_0 is an arbitrary Doppler frequency and the spectral moments is found with reference to this frequency. Changing f_0 will change the spectral moments. One can

eliminate f_0 by taking it 0, however, it must be chosen close to the mean clutter Doppler frequencies. The reason shall be explained in Chapter 4.

Using (3.35), first four moments of the process $x(t)$ described in Section 3.2 are calculated and presented in Table 3-1:

Table 3-1 Spectral Moments of Simplified Narrow Band Interference Signals

Spectral Moment	**Spectral Moment in terms of Clutter Parameters**
M_0	$M_0 = \sum_{i=1}^{2} P_i$
M_1	$M_1 = \sum_{i=1}^{2} P_i (f_i - f_0)$
M_2	$M_2 = \sum_{i=1}^{2} P_i (f_i - f_0)^2$
M_3	$M_3 = \sum_{i=1}^{2} P_i (f_i - f_0)^3$

To find the parameter vector shown in Figure 3-1, only the first 4 moments are needed.

3.5.2 Spectral Moments of Wide Band Interference Signals

Using (3.35), the first six moments of the process $x(t)$ described in Section 3.1 are calculated and presented in Table 3-2:

Table 3-2 Spectral Moments of Simplified Wide Band Interference Signals

Spectral Moment	Spectral Moment in terms of Clutter Parameters
M_0	$M_0 = \sum_{i=1}^{2} P_i$
M_1	$M_1 = \sum_{i=1}^{2} P_i \left(f_i - f_0 \right)$
M_2	$M_2 = \sum_{i=1}^{2} P_i \left[\left(f_i - f_0 \right)^2 + \sigma_i^2 \right]$
M_3	$M_3 = \sum_{i=1}^{2} P_i \left[\left(f_i - f_0 \right)^3 + 3 f_i \sigma_i^2 \right]$
M_4	$M_4 = \sum_{i=1}^{2} P_i \left[\left(f_i - f_0 \right)^4 + 6 \left(f_i - f_0 \right)^2 \sigma_i^2 + 3\sigma_i^4 \right]$
M_5	$M_5 = \sum_{i=1}^{2} P_i \left[\left(f_i - f_0 \right)^5 + 10 \left(f_i - f_0 \right)^3 \sigma_i^2 + 15 \left(f_i - f_0 \right) \sigma_i^4 \right]$

To find the parameter vector shown in Figure 3-2, only the first 6 moments are needed.

3.5.3 Estimating Spectral Moments from Estimated Covariance Matrix

Let the radar echo from the clutter be a zero-mean stationary random process $\xi(t)$, with the correlation function $\mathrm{K}(\tau)$, The correlation function and the spectrum are related through Wiener-Khintchine theorem [21]:

$$\mathrm{K}(\tau) = \int_{-\infty}^{\infty} S(f) e^{i2\pi f \tau} df \tag{3.36}$$

where $S(f)$ is the spectral density of the process.

Since $\mathrm{K}(\tau) = \mathrm{K}(-\tau)$, with Taylor series expansion of $e^{-i2\pi f\tau}$ term in (3.36) in the vicinity of an arbitrary frequency f_0, equation (3.36) turns into

$$\mathrm{K}(\tau) = e^{-i2\pi f_0\tau} \sum_{q=0}^{\infty} \frac{[-i2\pi\tau]^q}{q!} \int_{-\infty}^{\infty} (f - f_0)^q S(f) df. \tag{3.37}$$

When we define the spectral moments as

$$\mathrm{M}_q = \int_{-\infty}^{\infty} (f - f_0)^q S(f) df,\ 0 \leq q < \infty \tag{3.38}$$

and

$$a_q(\tau) = e^{-i2\pi f_0\tau} \frac{[-i2\pi\tau]^q}{q!}, \tag{3.39}$$

(3.37) becomes

$$\mathrm{K}(\tau) = \sum_{q=0}^{\infty} M_q a_q(\tau)\,. \tag{3.40}$$

When we observe the process $\xi(t)$ with uniform sampling periods T_s, equation (3.40) turns into

$$\mathrm{k}_m = \sum_{q=0}^{\infty} M_q a_{qm} \tag{3.41}$$

where k_m are the samples of the covariance function at time mT_s and a_{qm} is

$$a_{qm} = a_q(mT_s) = e^{-i2\pi f_0 mT_s} \frac{[-i2\pi mT_s]^q}{q!}. \tag{3.42}$$

According to the method of moments (MM), the estimates of the spectral moments are related to the estimates of the covariance function samples at time mT_s by

$$\widehat{\mathrm{k}_m} = \sum_{q=0}^{\infty} \widehat{M_q} a_{qm} \quad , \quad 0 \le m \le M-1 \tag{3.43}$$

where M is a number of lags in which estimation of the covariance function samples is performed [21]. In our problem M is the number of coherent radar echoes collected in the coherent process interval. The reason of using the method of moments is that the spectral moments are unobservable directly and their weighted sums (the elements of the covariance matrix) are observable. In the method of moments, the covariance matrix elements are expressed as functions of the spectral moments and estimates of the spectral moments can be found by estimating the covariance matrix and using the inverses of these functions.

The matrix form of (3.43) is

$$\hat{\mathbf{k}} = \sum_{q=0}^{\infty} \widehat{M_q} \boldsymbol{a}_q \tag{3.44}$$

where $\hat{\mathbf{k}} = \left(\widehat{k_0}, \widehat{k_1}, \dots, \widehat{k_{M-1}}\right)^T$ and $\mathbf{a}_q = \left(\mathrm{a}_{q0}, \mathrm{a}_{q1}, \dots, \mathrm{a}_{q(M-1)}\right)^T$.

The linear system corresponding to the equation (3.44) is as follows:

$$\hat{\mathbf{k}} = \boldsymbol{A}\widehat{\boldsymbol{M}} \tag{3.45}$$

where $\boldsymbol{A}$ is the matrix whose columns are the vector set $\{\boldsymbol{a}_q\}_{q=0}^{\infty}$ and $\widehat{\boldsymbol{M}} = \{\widehat{M}_q\}_{q=0}^{\infty}$.

The linear system (3.45) does not have a unique solution because the vector set $\{\boldsymbol{a}_q\}_{q=0}^{\infty}$ is not linearly independent. The vector set $\{\boldsymbol{a}_q\}_{q=0}^{\infty}$ consists of two linearly independent subsets [21]. These subsets are vectors with even and odd indexes. Their independence is due to the fact that even vectors are whole real and odd vectors are whole imagine if f_0 is assumed to be 0. Moreover, the number of linearly independent vectors in the set $\{\boldsymbol{a}_{2q}\}_{q=0}^{\infty}$ is M and the number of linearly independent vectors in the set $\{\boldsymbol{a}_{2q+1}\}_{q=0}^{\infty}$ is M-1 [21].

Thus, it is needed to restrict the dimension of the system. If the dimension of the system is restricted to $L \leq 2M - 1$, (3.45) becomes

$$\hat{\mathbf{k}} = \boldsymbol{A}_L \widehat{\boldsymbol{M}} \tag{3.46}$$

where $\boldsymbol{A}_L$ is the matrix whose columns are the vector set $\{\boldsymbol{a}_q\}_{q=0}^{L-1}$.

The system (3.46) can be divided into two independent subsystems:

$$\begin{aligned} Re\{\widehat{\mathbf{k}}\} &= \boldsymbol{A}_{Le} \widehat{\boldsymbol{M}_e} \\ Im\{\widehat{\mathbf{k}}\} &= \boldsymbol{A}_{Lo} \widehat{\boldsymbol{M}_o} \end{aligned} \tag{3.47}$$

where $\boldsymbol{A}_{Le}$ is the matrix whose columns are the vector set $\{\boldsymbol{a}_{2q}\}_{q=0}^{L/2-1}$, $\boldsymbol{A}_{Lo}$ is the matrix whose columns are the vector set $\left\{Im\{\boldsymbol{a}_{2q+1}\}\right\}_{q=0}^{L/2-1}$, $\widehat{\boldsymbol{M}_e} = \{\widehat{M}_{2q}\}_{q=0}^{L/2-1}$ and $\widehat{\boldsymbol{M}_o} = \{\widehat{M}_{2q+1}\}_{q=0}^{L/2-1}$.

The solution to equation (3.46) can be obtained by the least-squares method [21]. Let us define a function

$$Q(\widehat{M}_0, \widehat{M}_1, \widehat{M}_2, \dots, \widehat{M}_{L-1}) = \left\| \sum_{q=0}^{L-1} \widehat{M_q} \boldsymbol{a}_q - \hat{\mathbf{k}} \right\|^2. \tag{3.48}$$

The reason for using the least squares method is that the system is over-determined. The number of independent set of equations is greater than the number of unknowns (the spectral moments). In our case, the number of independent set of equations is $2M$ as can be seen from (3.47) and the number of unknowns is $L \leq 2M - 1$. Thus, overall solution is the one which minimizes the sum of squares of the errors made in the result of every single equation.

The estimates $\widehat{M}_q, q = 0,1,2, \dots, L-1$ will corresponds to the minimum of the functional Q. In this case, the estimates satisfy following equations:

$$\sum_{q=0}^{L-1} \widehat{M_q} Re\{\boldsymbol{a}_q{}^H \cdot \boldsymbol{a}_p\} = Re\{\boldsymbol{a}_q{}^H \cdot \hat{\mathbf{k}}\} \quad , \quad p = 0,1,2,\dots,L-1 \tag{3.49}$$

where $\mathbf{a}_p = \left(\mathrm{a}_{p0}, \mathrm{a}_{p1}, \dots, \mathrm{a}_{p(M-1)}\right)^T$, $(\cdot)$ designates the scalar product and (H) designates the Hermitian transpose.

The matrix form of (3.49) is

$$\boldsymbol{H}_L \widehat{\boldsymbol{M}_L} = \boldsymbol{W}_L \tag{3.50}$$

where $\boldsymbol{H}_L = \left\{Re\{\boldsymbol{a}_q{}^H \cdot \boldsymbol{a}_p\}\right\}_{q,p=0}^{L-1}$ is a finite sized matrix and $\widehat{\boldsymbol{M}_L} = \{M_q\}_{q=0}^{L-1}$ and $\boldsymbol{W}_L = \left\{Re\{\boldsymbol{a}_p{}^H \cdot \widehat{\boldsymbol{k}}\}\right\}_{p=0}^{L-1}$ are finite vectors.

The solution for the spectral moments using (3.50) is as follows [21]:

$$\widehat{\boldsymbol{M}_L} = \boldsymbol{H}_L^{-\mathbf{1}} \boldsymbol{W}_L. \tag{3.51}$$

Open form of (3.51) is

$$\widehat{M_p} = \sum_{q=0}^{L-1} \bar{h}_{pq} Re\{\widehat{\boldsymbol{k}}^H \cdot \boldsymbol{a}_q\} = Re\{\widehat{\boldsymbol{k}}^H \cdot \sum_{q=0}^{L-1} \bar{h}_{pq} \boldsymbol{a}_q\} \quad , \quad p = 0,1,2,\dots,L-1 \tag{3.52}$$

where $\bar{h}_{pq}$ is the (p , q)th element of matrix $\boldsymbol{H}_L^{-\mathbf{1}}$.

If $\boldsymbol{g}_p$ is defined as

$$\boldsymbol{g}_p = \sum_{q=0}^{L-1} \bar{h}_{pq} \boldsymbol{a}_q \quad , \quad p = 0,1,2,\dots,L-1 \tag{3.53}$$

then, the spectral moments can be calculated as scalar products of the vector $\widehat{\boldsymbol{k}}$ and vectors $\boldsymbol{g}_p$, $p = 0,1,2,\dots,L-1$.

$$\widehat{M_p} = Re\{\widehat{\boldsymbol{k}} \cdot \boldsymbol{g}_p{}^H\} \quad , \quad p = 0,1,2,\dots,L-1 \tag{3.54}$$

Vectors $\boldsymbol{g}_p$, $p = 0,1,2,\dots,L-1$ do not depend on the radar echoes and correlation between them. The vectors can be stored in radars and used whenever needed.

3.5.4 Finding Mean Frequencies and Powers of Simplified Narrow Band Interference Signals Using Spectral Moments

According to Table 3-1 and Table 3-2, we can observe that the clutter parameters are nonlinear functions of the spectral moments. There is no analytical solution to find the clutter parameters using the spectral moments.

Fortunately, in [23], a method is proposed to find the directions and the mean powers of a group of N noncoherent signal sources. In this thesis, this method is used to find the mean frequencies and the mean powers of simplified narrow band clutter signals using the spectral moments.

In [23], the performance of this method under wide band interference signals is also investigated and it is concluded that it has comparable results with MUSIC for much less computational load. Therefore, in our problem, we use this method to find the mean frequencies and the mean powers of the sea and the rain clutter.

Because of the narrow band interference signal assumption the spectral moments of the radar return are given by

$$M_p = \sum_{i=1}^{2} P_i \left(f_i - f_0 \right)^p \text{ where } p = 0,1,2,\ldots . \tag{3.55}$$

To find f_i's and P_i's in Table 3-1, a rational function,

$$R(f) = \sum_{p=0}^{\infty} \frac{M_p}{f^{p+1}} \text{ where } |f| > \max_i |f_i| \tag{3.56}$$

is proposed in [23].

We can relate the rational function in (3.56) to the clutter parameters using (3.55):

$$R(f) = \sum_{i=1}^{2} \frac{P_i}{f - f_i} . \tag{3.57}$$

The poles of the function $R(f)$ are f_i's.

Since the function $R(f)$ is rational it is possible to write it in the form of

$$R(f)=\frac{g(f)}{h(f)} \tag{3.58}$$

where

$$\begin{aligned} g(f) &= g_1 f + g_0 \text{ and} \\ h(f) &= f^2 + h_1 f + h_0 \end{aligned} \tag{3.59}$$

are polynomials.

After extending the rational function (3.56) using the definition (3.59), the following equation is obtained:

$$g_1 f + g_0 = \sum_{p=0}^{\infty} M_p \frac{f^2 + h_1 f + h_0}{f^{p+1}} . \tag{3.60}$$

Open form of (3.60) is

$$g_1 f + g_0 = (M_0) f + (M_0 h_1 + M_1) + (M_0 h_0 + M_1 h_1 + M_2)\frac{1}{f} + (M_1 h_0 + M_2 h_1 + M_3)\frac{1}{f^2} + \ldots . \tag{3.61}$$

Then, comparing coefficients with equal powers of the variable f in both parts of (3.61), two mutually connected linear systems can be written as

$$\begin{aligned} M_0 h_0 + M_1 h_1 + M_2 &= 0 \\ M_1 h_0 + M_2 h_1 + M_3 &= 0 \end{aligned} \tag{3.62}$$

and

$$\begin{aligned} M_0 h_1 + M_1 &= g_0 \\ M_0 &= g_1 \end{aligned} . \tag{3.63}$$

To find f_i's and P_i's, first, we need to solve system (3.62) to find h_i's and then solve system (3.63) to find g_i's.

The solution to the equation

$$f^2 + h_1 f + h_0 = 0 \tag{3.64}$$

gives f_i's and the P_i's can be found as

$$P_i = \frac{g_1 f_i + g_0}{2 f_i + h_1}. \tag{3.65}$$

3.5.5 Frequency Domain Spectral Moments Estimation

In this section, an alternative way to the spectral moments estimation method explained in section 3.5.3 is presented.

The spectral moments can be estimated directly from the relation (3.38).

Let $\boldsymbol{x}$ be the Mx1 vector defined in section 3.1. Then, the discrete Fourier transform (DFT) of $\boldsymbol{x}$ is

$$X_k = \sum_{n=0}^{M-1} x_n e^{-i2\pi k\frac{n}{M}},\ k = 0,1,...,\mathrm{M}-1 \tag{3.66}$$

where $x_0, x_1, ..., x_{M-1}$ are elements of the vector $\boldsymbol{x}$.

The relationship between the spectral moments estimates and the DFT based spectral density estimate of the vector $\boldsymbol{x}$ is given as

$$\widehat{\mathrm{M}_q} = \frac{1}{M^3} \sum_{k=0}^{M-1} k \left|\widehat{X_k}\right|^2 \tag{3.67}$$

CHAPTER 4

SIMULATION RESULTS

4.1 Simulations

In this section, the estimation performance of the algebraic spectral moments based method for different clutter parameters is investigated.

In simulations, the clutter parameters are calculated in two steps:

1) In the first step, the mean powers and the mean Doppler frequencies of sea and rain clutter are found by the algebraic spectral moments based moving clutter parameter estimation method.

2) In the second step, using the clutter parameters estimated in the first step, minimization of the negative log-likelihood function of (3.20) is done by fixing the mean powers and the mean Doppler frequencies and changing the Doppler spreads.

The estimation performance of the algebraic spectral moments based method is investigated for different CNR, Doppler separation, Doppler spread, number of observation and the shape parameter values. Performance results are compared with the Cramér-Rao bounds and are presented in five subsections. The derivations for the Cramér-Rao bounds for the clutter parameters are given in Appendix A.

In all simulations, only 8 coherent radar pulses are used and it is assumed that the clutter spectrum can be expressed by 14 spectral moments instead of infinity. Actually, this assumption corresponds to choosing $L=14$ in (3.50) and it is necessary to estimate the spectral moments from the estimated covariance matrix [21]. It is useful to note that the maximum allowable value of L is 15 to find the spectral moments in this case.

In all simulations, two clutters each having a Gaussian power spectrum are simulated to represent sea and rain clutter. Clutter-1 is defined as the one having less mean Doppler frequency. Clutter-1 and clutter-2 are assumed to be uncorrelated with each other.

The number of Monte Carlo runs is 1000 to calculate the standard deviations and the biases of the proposed method. In section 4.1.1, sufficiency of number of Monte Carlo runs is presented in terms of confidence interval of 95% together with the estimation performance of the proposed method. In other sections, only the estimation performance of the proposed method is investigated.

4.1.1 Simulations for Different CNR Values

In this simulation, clutter-1 and clutter-2 are located at -0.1 and 0.1 in the normalized Doppler spectrum, respectively. In other words, the Doppler separation value corresponds to 20% of the PRF.

Both Doppler spreads (the sigma values of the Doppler spectrums) are assumed to be equal to 0.01. With the Gaussian Doppler spectrum assumption, this means that clutter correlations drop to 10% after 34.2 times the PRI.

Amplitude distributions of both clutters are assumed to be Rayleigh.

20 range bins are used for estimation of the clutter covariance matrix using formula (3.19). The clutter returns in these range bins are assumed to be independent.

The mean clutter powers are assumed to be 0.5 and the mean power of the additive white Gaussian noise, which represents the radar receiver noise, is adjusted such that the CNR varies from -10 dB to 30 dB for both clutters.

The rms errors for the estimates of the first four spectral moments as a function of CNR can be observed from Figure 4-1 through Figure 4-4.

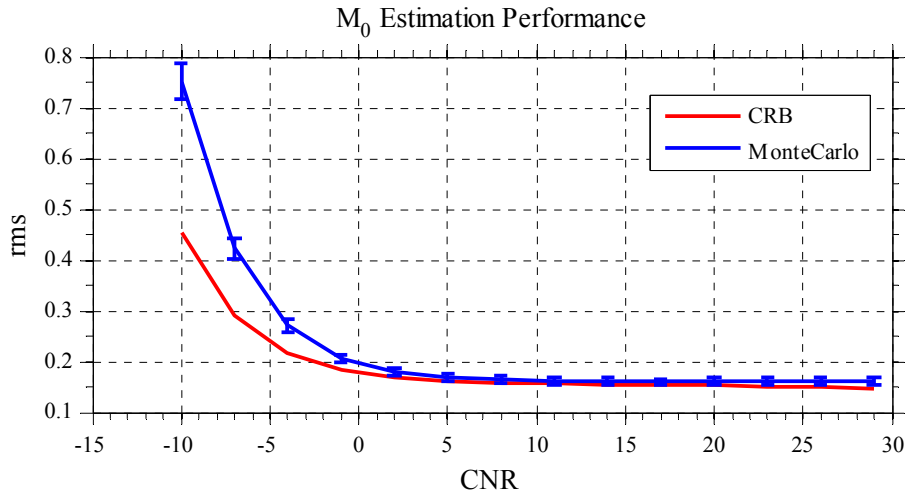

Figure 4-1 M_0 Estimation Performance as a Function of CNR

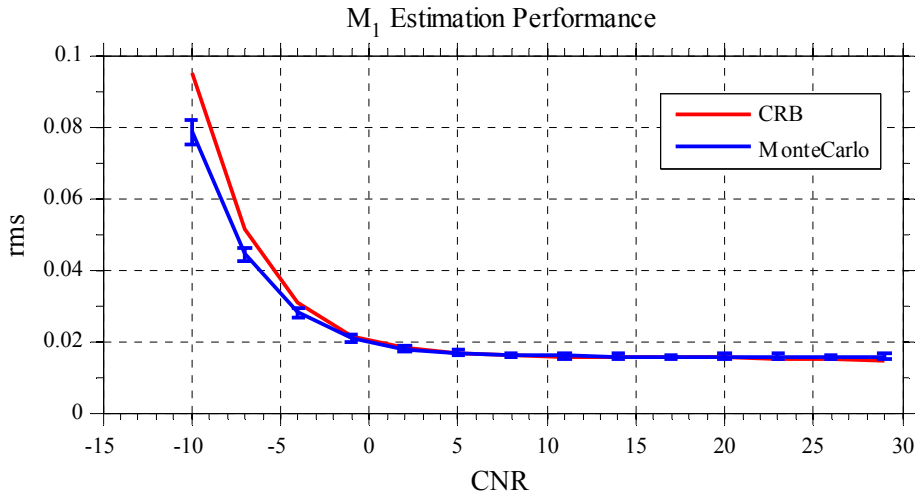

Figure 4-2 M_1 Estimation Performance as a Function of CNR

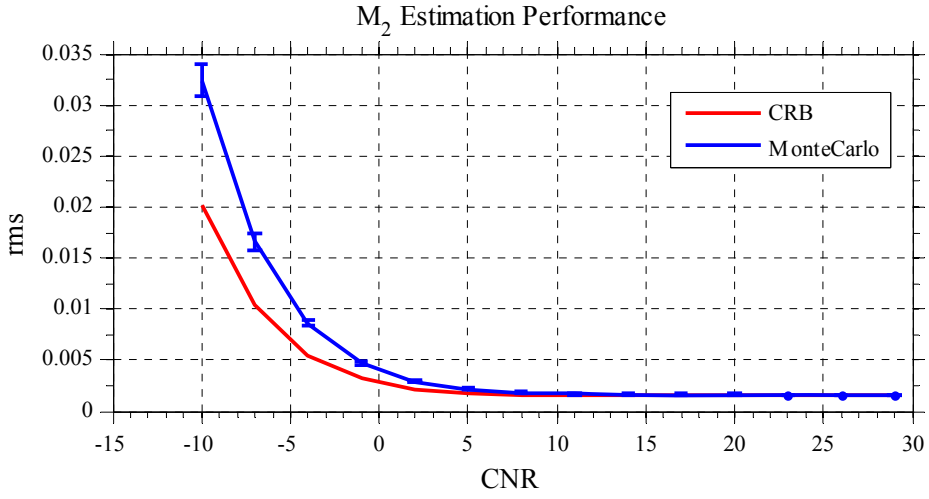

Figure 4-3 M_2 Estimation Performance as a Function of CNR

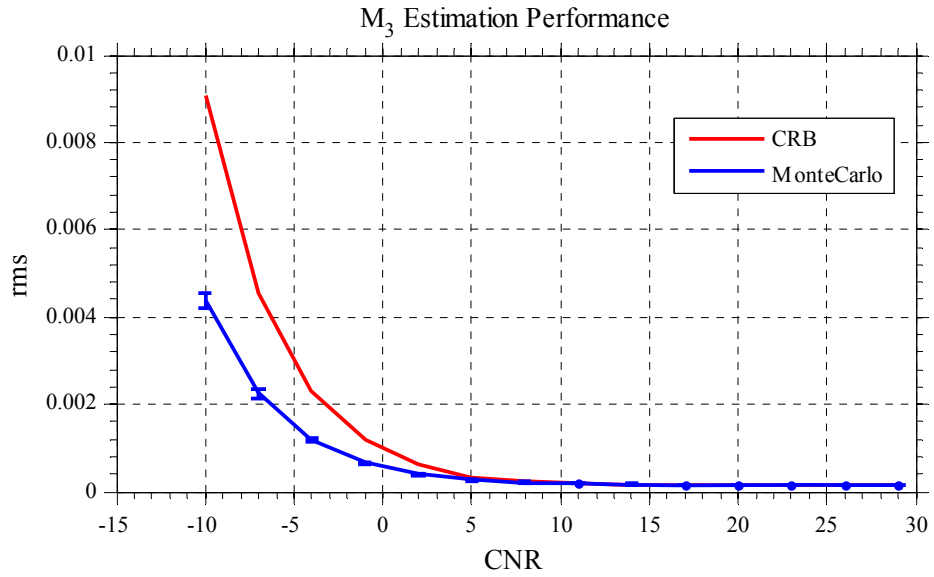

Figure 4-4 M_3 Estimation Performance as a Function of CNR

Figure 4-1, Figure 4-2, Figure 4-3 and Figure 4-4 depict that above 0 dB CNR, the spectral moment estimation performance of the proposed method approaches the Cramér-Rao bound significantly.

In section 3.5.3, we have already mentioned that the spectral moments are estimated from the estimated covariance matrix using the method of moments. Disadvantages of the method of moments when compared with the maximum likelihood method are that it is often not available and it does not have the desirable asymptotic optimality properties of the maximum likelihood method and the least squares estimators, as the CNR or the number of observations increases. Generally, the primary use of the moment estimates is to obtain initial values for the more precise maximum likelihood and least squares estimates. However, as Figure 4-1, Figure 4-2, Figure 4-3 and Figure 4-4 depict, the optimality problem does not show up and we can state that in this configuration, the method of moments can be used for its computational advantages.

Standard deviations for estimates of the clutter parameters as a function of CNR can be observed from Figure 4-5 through Figure 4-7. Since clutter-1 and clutter-2 are located symmetrically in the Doppler spectra and other clutter parameters are the same for both clutters, only the estimation performances for clutter-1 parameters are presented.

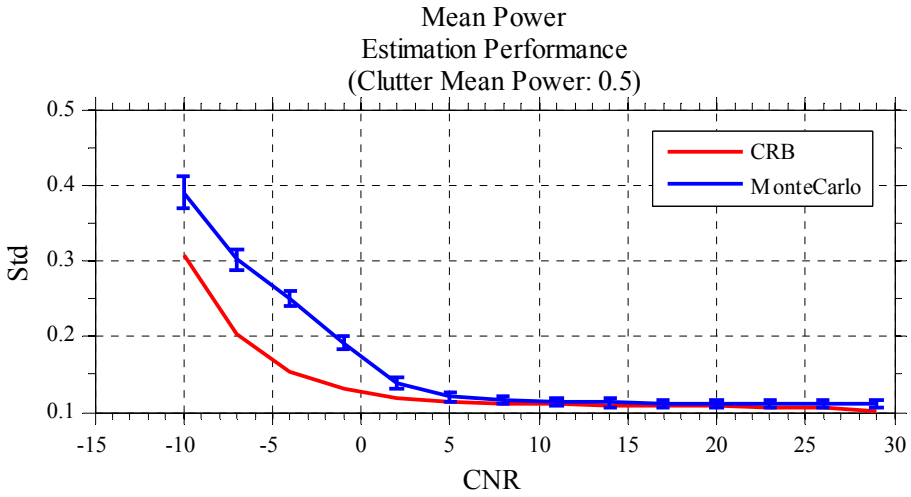

Figure 4-5 Standard deviations for Mean Clutter Power Estimates as a Function of CNR

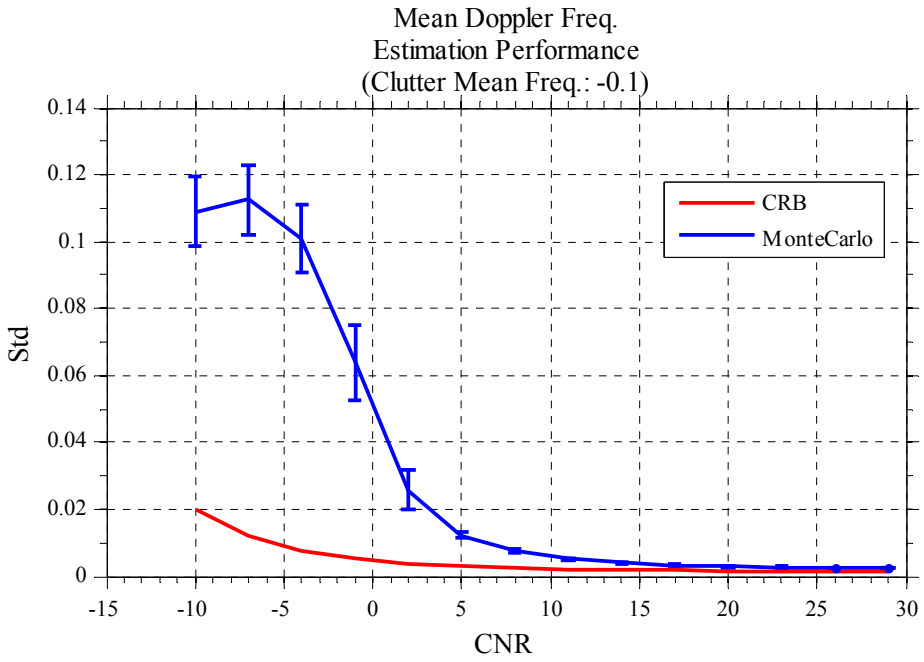

Figure 4-6 Standard deviations for Mean Doppler Frequency Estimates as a Function of CNR

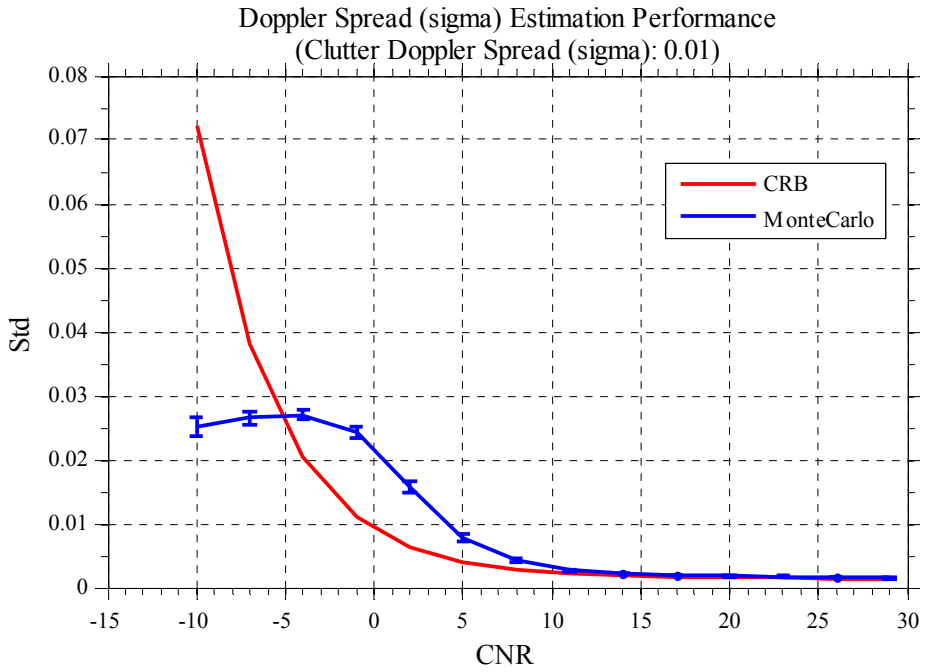

Figure 4-7 Standard deviations for Doppler Spread Estimates as a Function of CNR

Figure 4-5 depicts that the mean power estimation performance approaches the Cramér-Rao bound for CNR values above 5 dB. Figure 4-7 depicts that the Doppler spread estimation performance approaches the Cramér-Rao bound for CNR values above 8 dB.

The estimation performance for the Doppler spread appears to be better than the Cramér-Rao bound for CNR values below -5 dB. This discrepancy is caused by the large biased estimates of algebraic spectral moment estimation method, which can be observed from Figure 4-10.

The mean Doppler frequency estimation performance appears to be increasing with increasing CNR but there is always an offset between Monte Carlo results and the Cramér-Rao bound. The reason shall be explained in detail in section 4.2 (Comments on Simulation Results).

Biases for estimates of the clutter parameters as a function of CNR can be observed from Figure 4-8 through Figure 4-10.

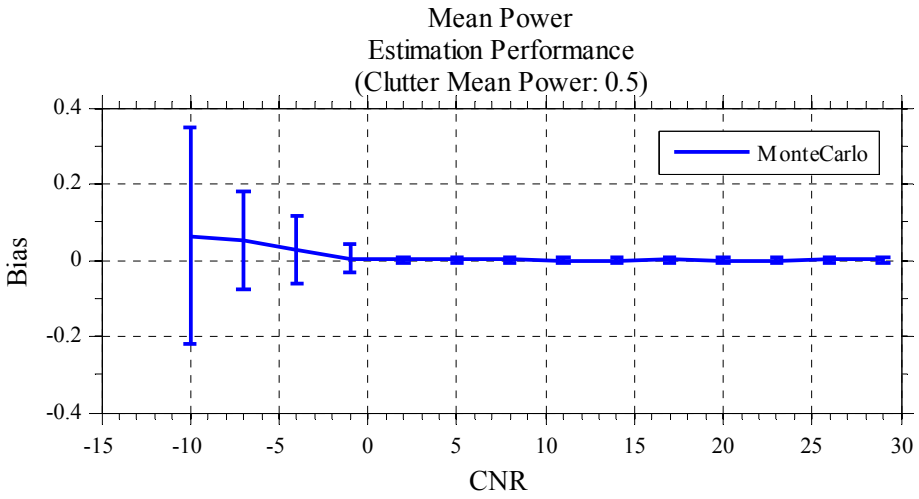

Figure 4-8 Biases for Mean Power Estimates as a Function of CNR

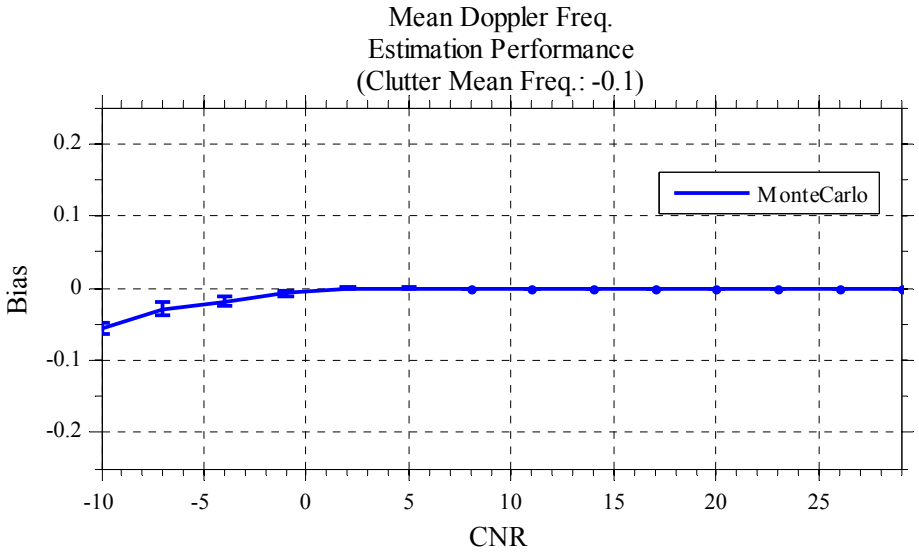

Figure 4-9 Biases for Mean Doppler Frequency Estimates as a Function of CNR

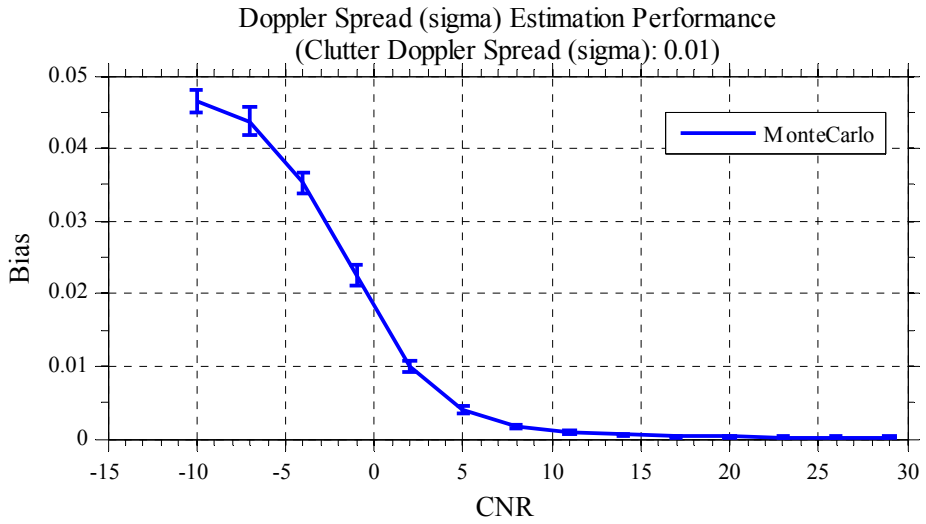

Figure 4-10 Biases for Doppler Spread Estimates as a Function of CNR

Figure 4-8, Figure 4-9 and Figure 4-10 depict that the biases on the mean power and mean Doper frequency estimates vanish for CNR values above 0 dB and the biases on the Doppler spread estimates vanish for CNR values above 10 dB.

It is conjectured that as CNR decreases from 10 dB, the proposed method perceives that the radar receiver noise, which spreads over all the spectra, is a part of clutter and this is why a positive bias is included to the Doppler spread estimates.

4.1.2 Simulations for Different Spectral Separation Values

In this simulation, clutter-1 and clutter-2 are located at the opposite sides of the Doppler spectra and at the same distance from zero Doppler frequency. The Doppler separation value is altered from 0.1 to 0.4.

Both Doppler spreads (the sigma values of the Doppler spectrums) are assumed to be equal to 0.01. With the Gaussian Doppler spectrum assumption, this means that clutter correlations drop to 10% after 34.2 times the PRI.

Amplitude distributions of both clutters are assumed to be Rayleigh.

20 range bins are used for estimation of the clutter covariance matrix using formula (3.19). The clutter returns in these range bins are assumed to be independent.

The mean clutter powers are assumed to be 0.5 and the mean power of the additive white Gaussian noise, which represents the radar receiver noise, is adjusted such that the CNR is equal to 20 dB.

The rms errors for the estimates of the first four spectral moments as a function of Doppler separation can be observed from Figure 4-11.

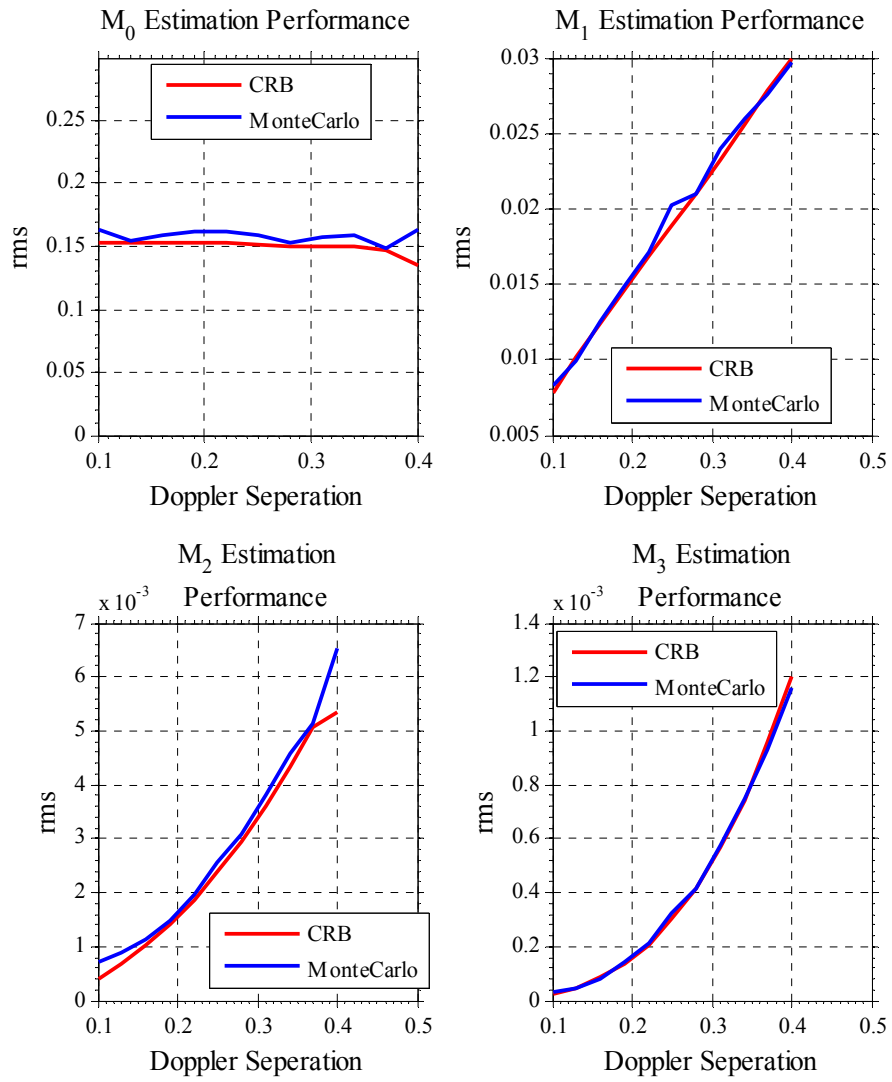

Figure 4-11 Spectral Moment Estimation Performance as a Function of Doppler Separation

Figure 4-11 depicts that for the Doppler separation values from 0.1 to 0.4, the spectral moment estimation performance of the proposed method approaches the Cramér-Rao bound significantly.

Moreover, as Figure 4-11 depicts, the standard deviations for the first, the second and the third moments increase as the Doppler separation increases. The reason for this outcome is that the first, the second and the third moments are functions of the mean Doppler frequencies of clutters as can be observed from Table 3-2. They increase as the mean Doppler frequencies of clutters increase and so do standard deviations.

Standard deviations for estimates of the clutter parameters as a function of Doppler seperation can be observed from Figure 4-12. Since clutter-1 and clutter-2 are located symmetrically in the Doppler spectra and other clutter parameters are the same for both clutters, only the estimation performances for clutter-1 parameters are presented.

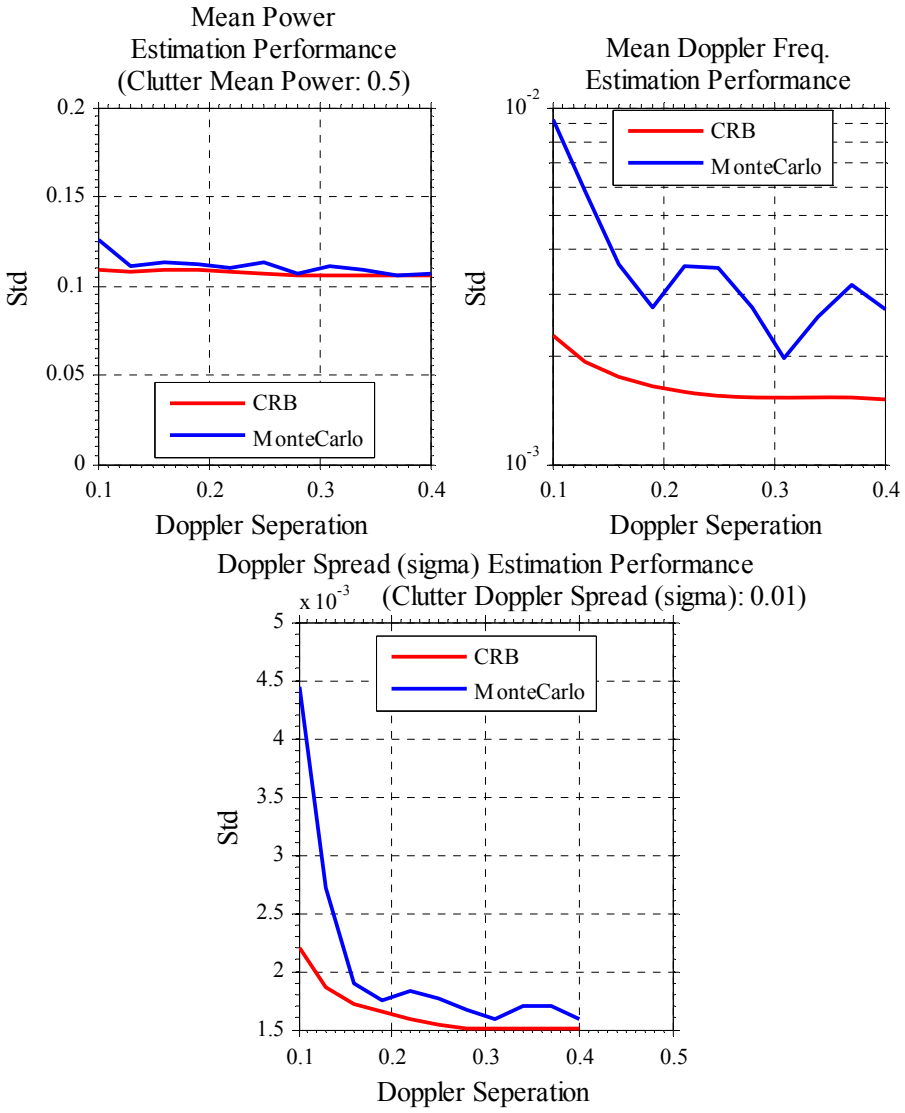

Figure 4-12 Standard deviations for Estimates of Clutter-1 Parameters as a Function of Doppler Separation

As can be observed from Figure 4-12, the mean power estimation performance approaches the Cramér-Rao bound.

For the Doppler separation values below 0.15, the estimation performance of the proposed method drops significantly. This result is related to the Doppler resolution of this method while using 8 coherent radar pulses for the clutter parameter estimations.

Moreover, as the Doppler separation increases from 0.1 to 0.4, estimation quality of the mean Doppler frequency and the Doppler spread oscillates. The reason for the oscillations in the Doppler spread is the oscillations in the mean Doppler frequency, since the Doppler spread is calculated in the second step in the proposed algorithm that uses the estimates of mean Doppler frequencies found in the first step. The reason for the oscillations in the mean Doppler frequency shall be explained in detail in section 4.2 (Comments on Simulation Results).

Biases for estimates of the clutter parameters as a function of Doppler spreads can be observed from Figure 4-13.

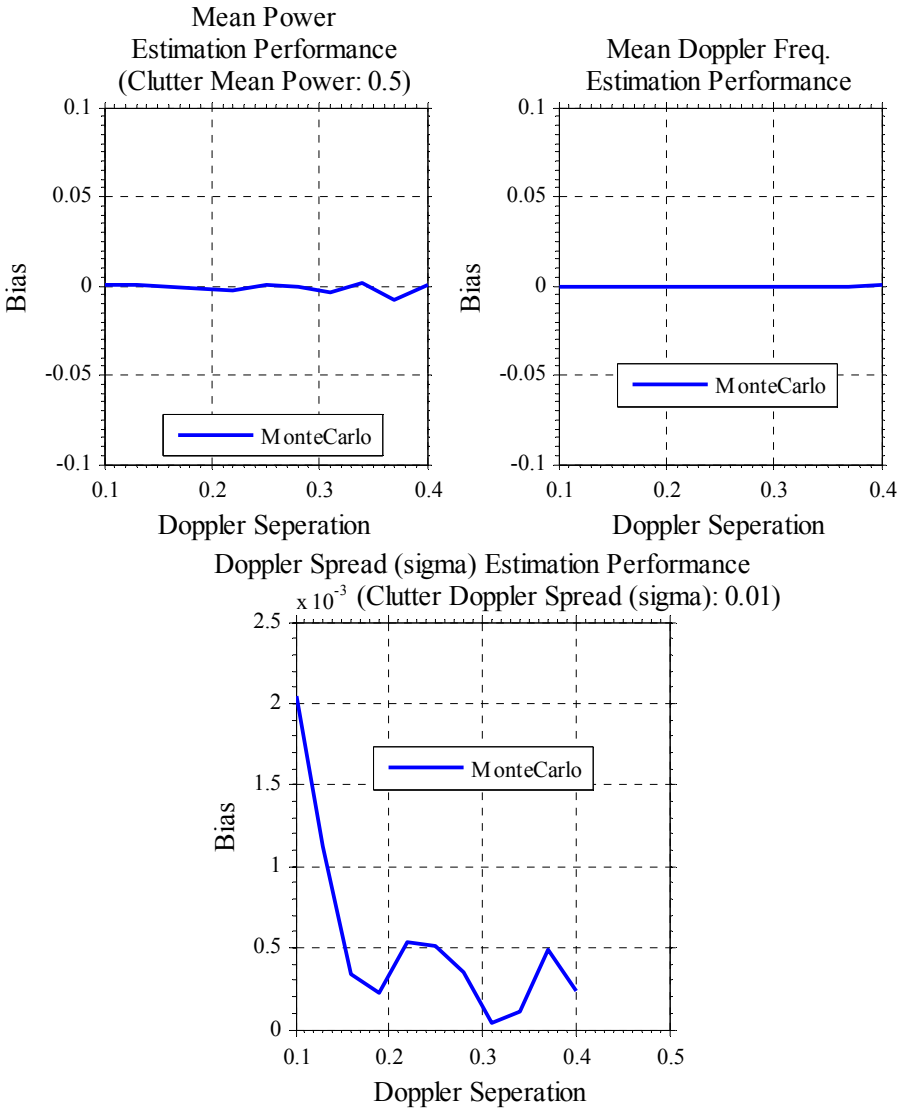

Figure 4-13 Biases for Estimates of Clutter-1 Parameters as a Function of Doppler Separation

Figure 4-13 depicts that although there are negligible biases on the estimates of the mean power and the mean Doppler frequency, there is an oscillation on the biases of the Doppler spread estimates similar to that in standard deviation in Figure 4-12.

4.1.3 Simulations for Different Spectral Spread Values

In this simulation, clutter-1 and clutter-2 are located at -0.15 and 0.15 in the normalized Doppler spectrum, respectively. In other words, the Doppler separation value corresponds to 30% of the PRF.

Both Doppler spreads (the sigma values of the Doppler spectrums) are altered from 0.004 to 0.034.

Amplitude distributions of both clutters are assumed to be Rayleigh.

20 range bins are used for estimation of the clutter covariance matrix using formula (3.19). The clutter returns in these range bins are assumed to be independent.

The mean clutter powers are assumed to be 0.5 and the mean power of the additive white Gaussian noise, which represents the radar receiver noise, is adjusted such that the CNR is equal to 20 dB.

The rms errors for the estimates of the first four spectral moments as a Function of Doppler Spread can be observed from Figure 4-14.

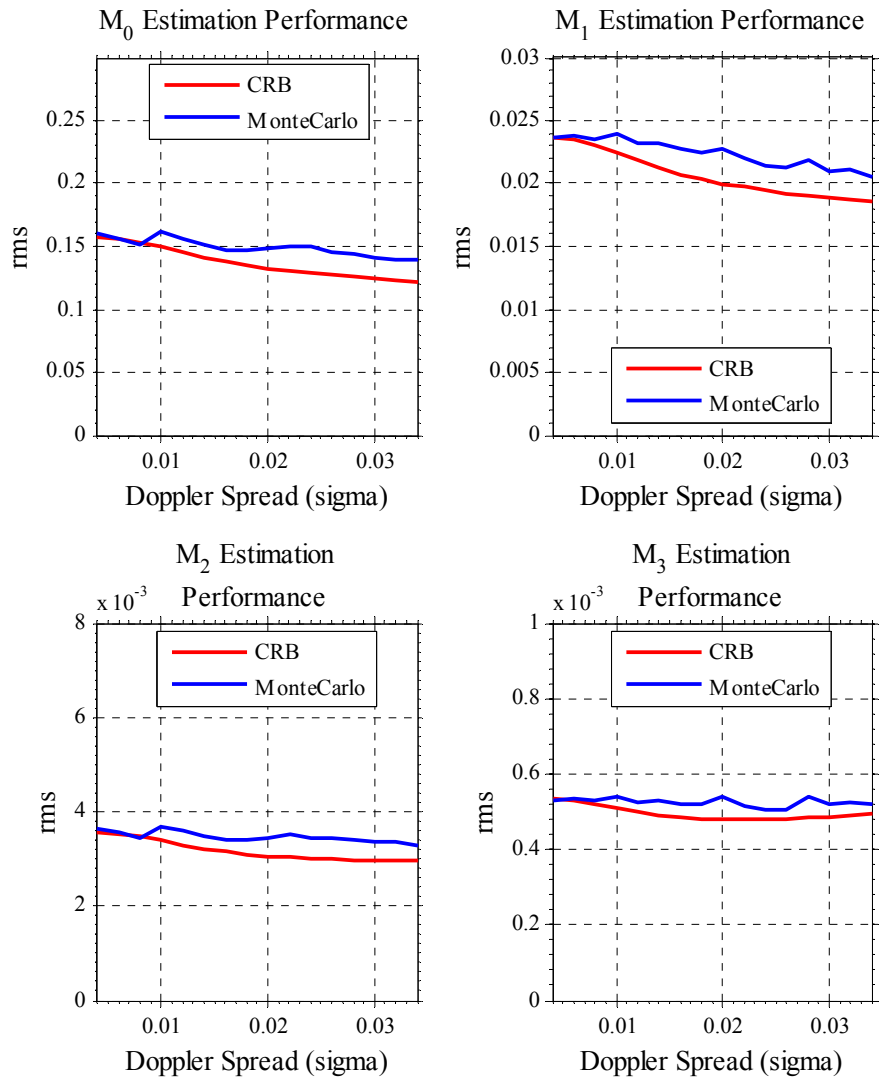

Figure 4-14 Spectral Moment Estimation Performance as a Function of Doppler Spread

Figure 4-14 depicts that for the Doppler spread values from 0.004 to 0.034, the spectral moment estimation performance of the proposed method is very close to the Cramér-Rao bound.

Standard deviations for estimates of the clutter parameters as a function of Doppler spread can be observed from Figure 4-15. Since clutter-1 and clutter-2 are located symmetrically in the Doppler spectra and other clutter parameters are the same for both clutters, only the estimation performances for clutter-1 parameters are presented.

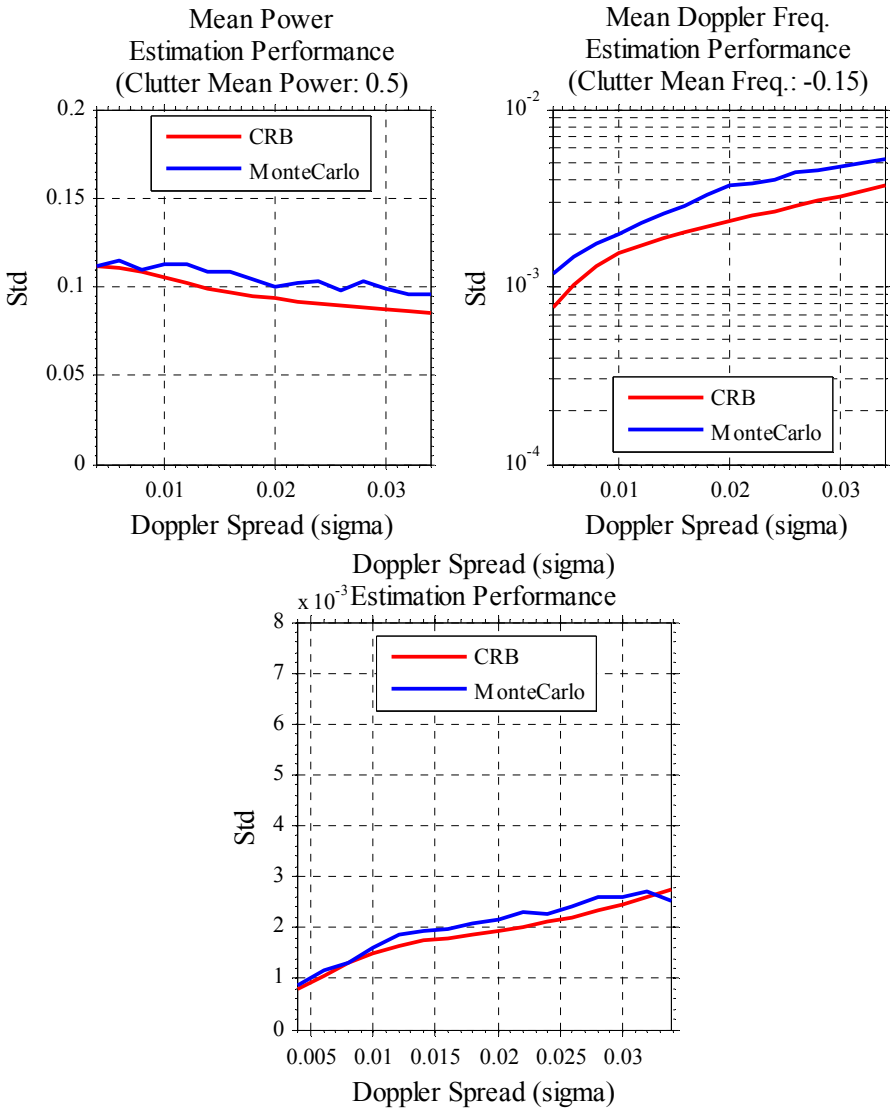

Figure 4-15 Standard deviations for Estimated Clutter-1 Parameters as a Function of Doppler Spread

Figure 4-15 depicts that the mean power and the Doppler spread estimation performances are very close to the Cramér-Rao bound for the Doppler spread values

of interest. The mean Doppler frequency estimation performance appears to be increasing with increasing Doppler spread and there is always an offset between the Monte Carlo results and the Cramér-Rao bound. The reason shall be explained in detail in Section 4.2 (Comments on Simulation Results).

Biases for estimates of the clutter parameters as a function of Doppler spread can be observed from Figure 4-16.

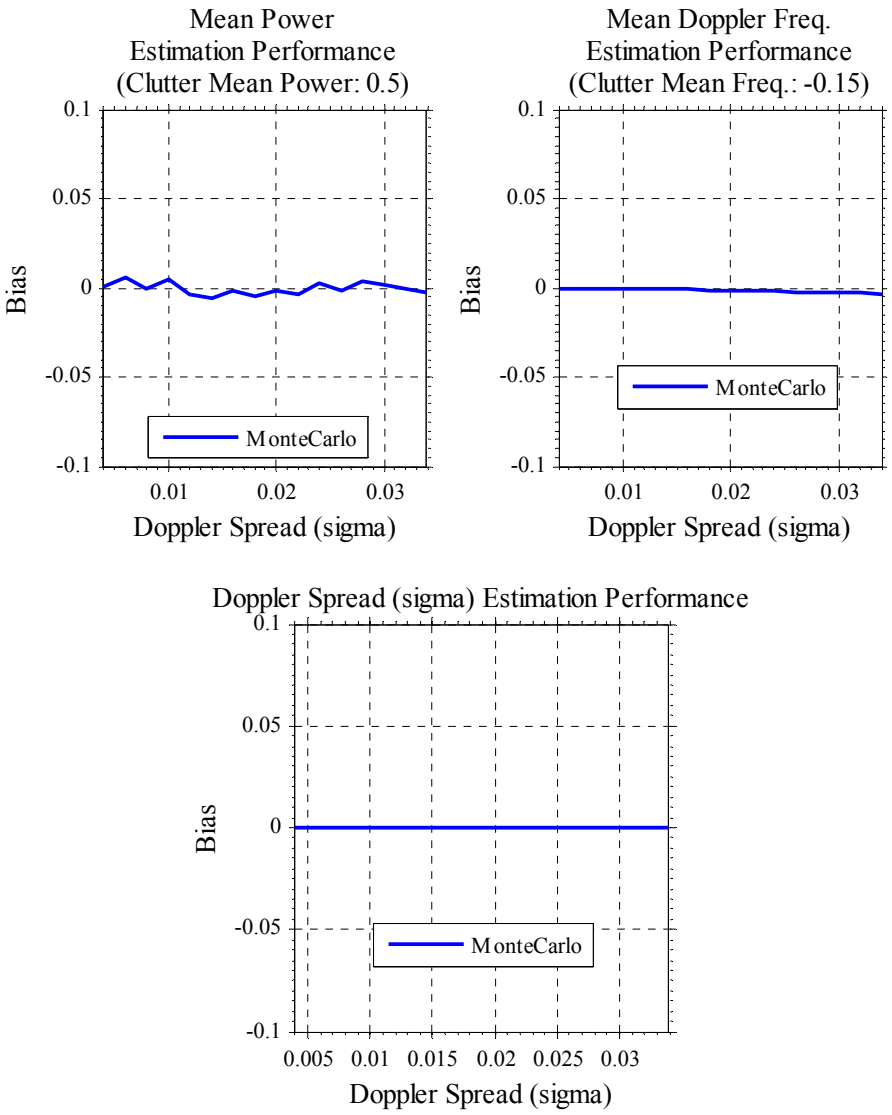

Figure 4-16 Biases for Estimated Clutter-1 Parameters as a Function of Doppler Spread

Figure 4-16 depicts that changing the Doppler Spread values from 0.004 to 0.034 does not introduce a bias on the clutter parameters estimates.

4.1.4 Effect of Number of Observations

In this simulation, clutter-1 and clutter-2 are located at -0.1 and 0.1 in the normalized Doppler spectrum, respectively. In other words, the Doppler separation value corresponds to 20% of the PRF.

Both Doppler spreads (the sigma values of the Doppler spectrums) are assumed to be equal to 0.02. With the Gaussian Doppler spectrum assumption, this means that clutter correlations drop to 10% after 17.1 times the PRI.

Amplitude distributions of both clutters are assumed to be Rayleigh.

The number of range bins that used for estimation of the clutter covariance matrix using formula (3.25) is changed from 8 to 96. The clutter returns in these range bins are assumed to be independent.

The mean clutter powers are assumed to be 0.5 and the mean power of the additive white Gaussian noise, which represents the radar receiver noise, is adjusted such that the CNR is equal to 20 dB.

The rms errors for the estimates of the first four spectral moments as a function of observation number can be observed from Figure 4-17. Standard deviations for estimates of the clutter parameters as a function of observation number can be seen from Figure 4-18. Biases for estimates of the clutter parameters as a function of observation number can be seen from Figure 4-19.

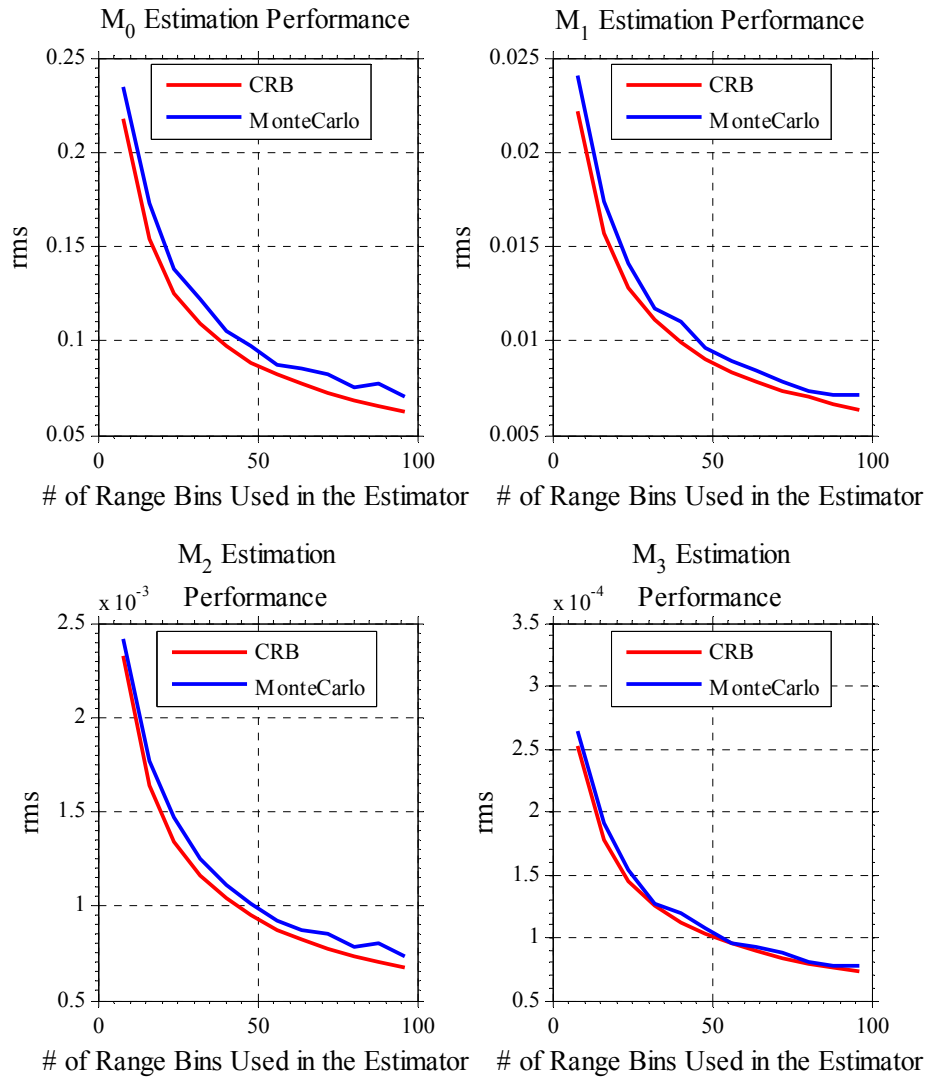

Figure 4-17 Spectral Moment Estimation Performance as a Function of Observation Number

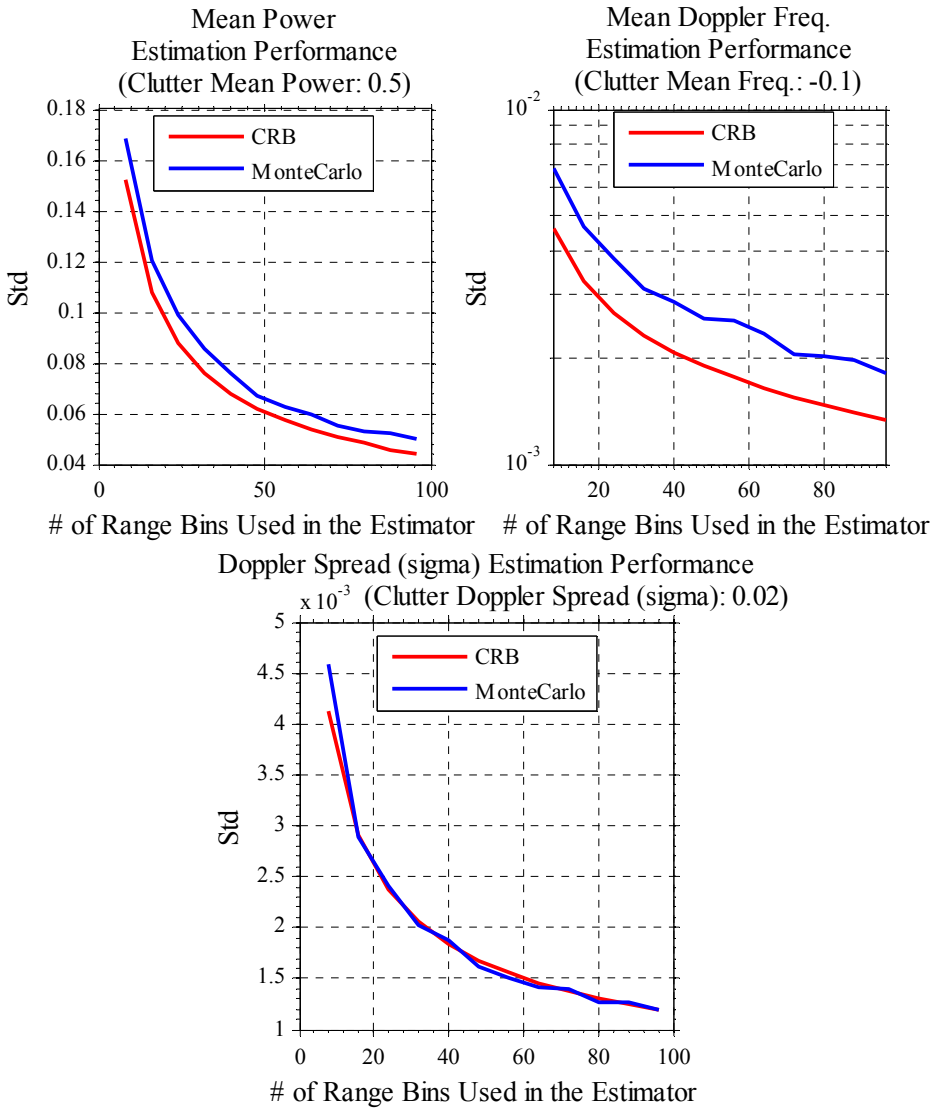

Figure 4-18 Standard deviations for Estimates of Clutter-1 Parameters as a Function of Observation Number

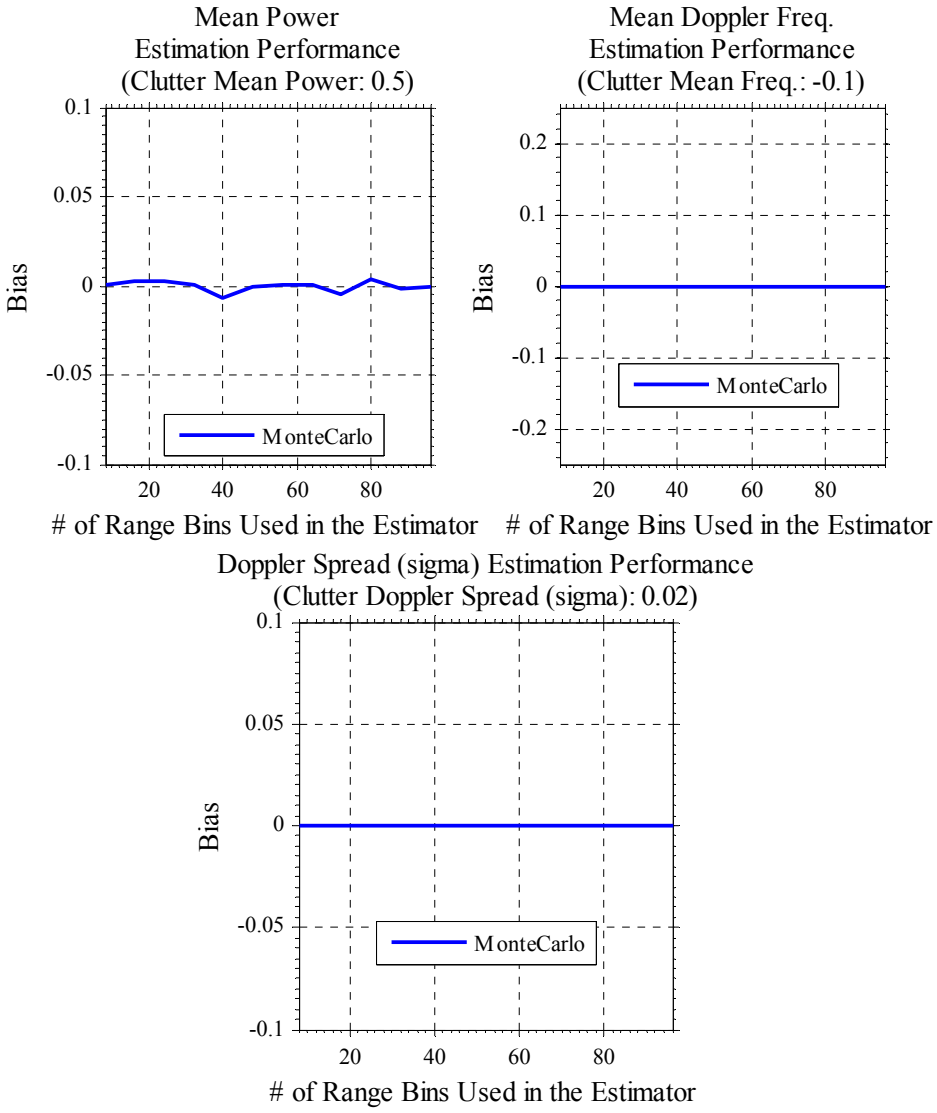

Figure 4-19 Biases for Estimates of Clutter-1 Parameters as a Function of Observation Number

Figure 4-17 and Figure 4-18 depict that as the number of observations increases, estimation quality also increases in consistent with the Cramér-Rao bound for both the spectral moments and the clutter parameters.

Figure 4-19 shows that the number of observations does not affect the bias on the estimates.

4.1.5 Simulations for Different Shape Parameter Values

In this simulation, clutter-1 and clutter-2 are located at -0.1 and 0.1 in the normalized Doppler spectrum, respectively. In other words, the Doppler separation value corresponds to 20% of the PRF.

Both Doppler spreads (the sigma values of the Doppler spectrums) are assumed to be equal to 0.01. With the Gaussian Doppler spectrum assumption, this means that clutter correlations drop to 10% after 34.2 times the PRI.

The amplitude distribution of clutter-1 is assumed to be K-distributed and the amplitude distribution of clutter-2 is assumed to be Rayleigh. The shape parameter of clutter-1 is altered from 0.1 to 15.

20 range bins are used for estimation of clutter the covariance matrix using formula (3.19). The clutter returns in these range bins are assumed to be independent.

The mean clutter powers are assumed to be 0.5 and the mean power of the additive white Gaussian noise, which represents the radar receiver noise, is adjusted such that the CNR is equal to 20 dB.

In section 3.3, we have already mentioned that, in the spectral moment estimation method, we use (3.19) to estimate the clutter covariance matrix. Actually, this estimation method is the maximum likelihood estimation if the interference is Gaussian. For non-Gaussian interference, its performance degrades and different

kind of estimator should be used [24]. We stick to (3.19) since clutter-2 is correlated complex Gaussian clutter.

In this simulation, the Cramér-Rao bounds are calculated according to the correlated complex Gaussian clutter in order to investigate the effect of the shape parameter on the clutter parameter estimations.

In Figure 4-20, some degradation in the estimation performances for the spectral moments can be observed for the shape parameters below 3.

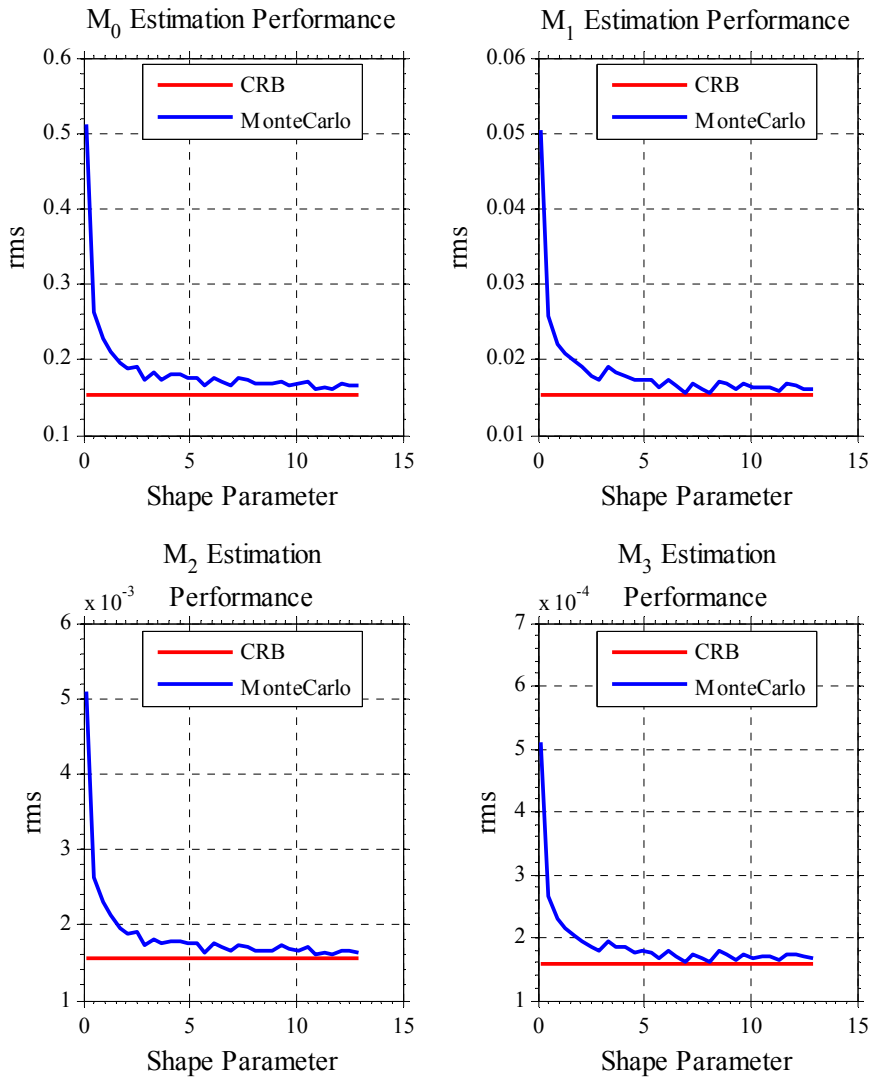

Figure 4-20 Spectral Moment Estimation Performance as a Function of the Shape Parameter

The estimation performance for the clutter-1 parameters in terms of standard deviation can be observed from Figure 4-21.

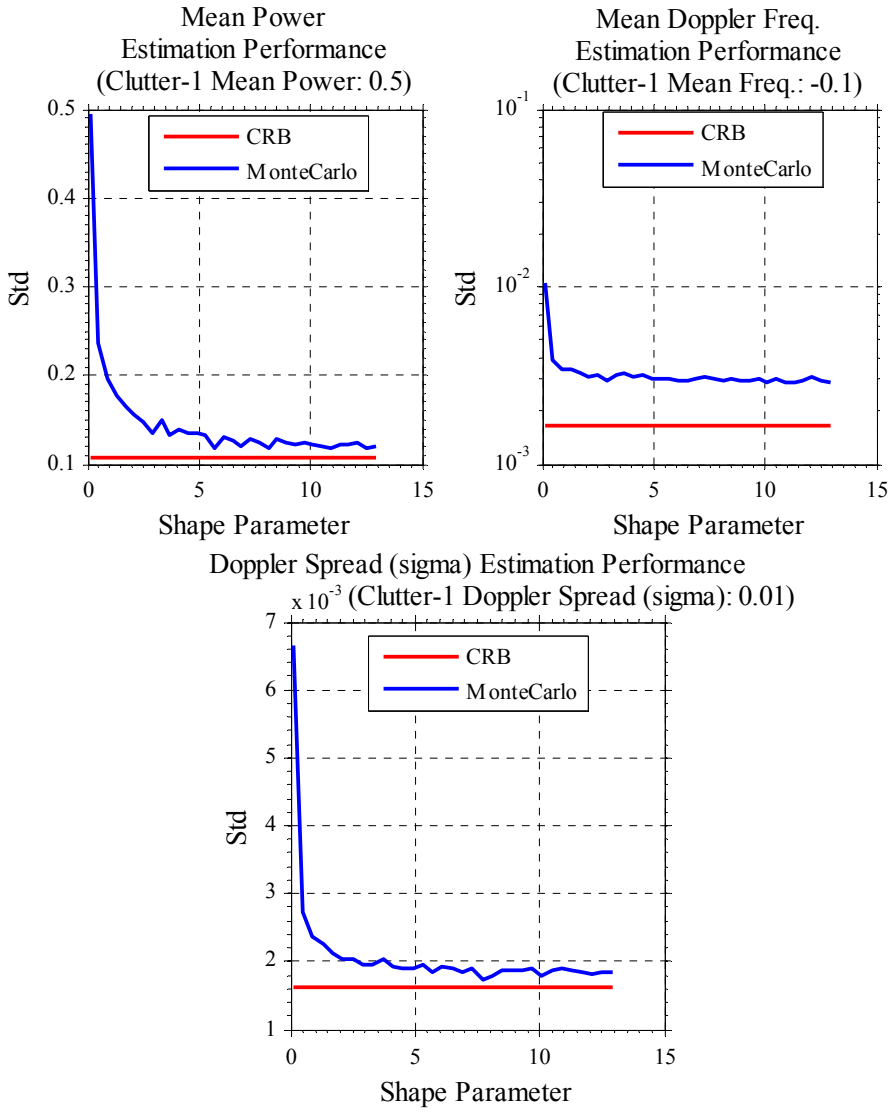

Figure 4-21 Standard deviations for Estimates of Clutter-1 Parameters as a Function of Shape Parameter

The estimation performance for the clutter-2 parameters in terms of standard deviation can be observed from Figure 4-22.

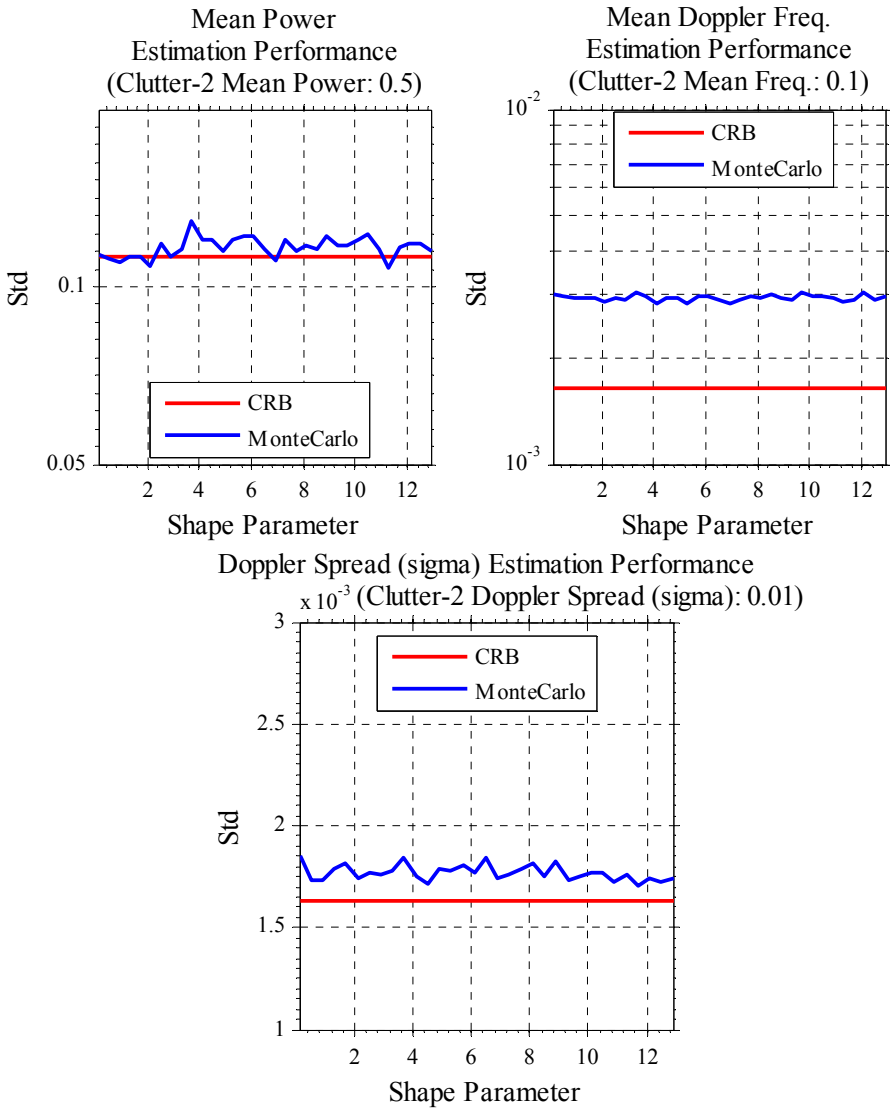

Figure 4-22 Standard deviations for Estimated Clutter-2 Parameters as a Function of Shape Parameter

Figure 4-22 depicts that estimation qualities of clutter-2 parameters are not affected by the shape parameter of clutter-1.

The estimation performance for the clutter-1 parameters in terms of bias can be seen from Figure 4-23.

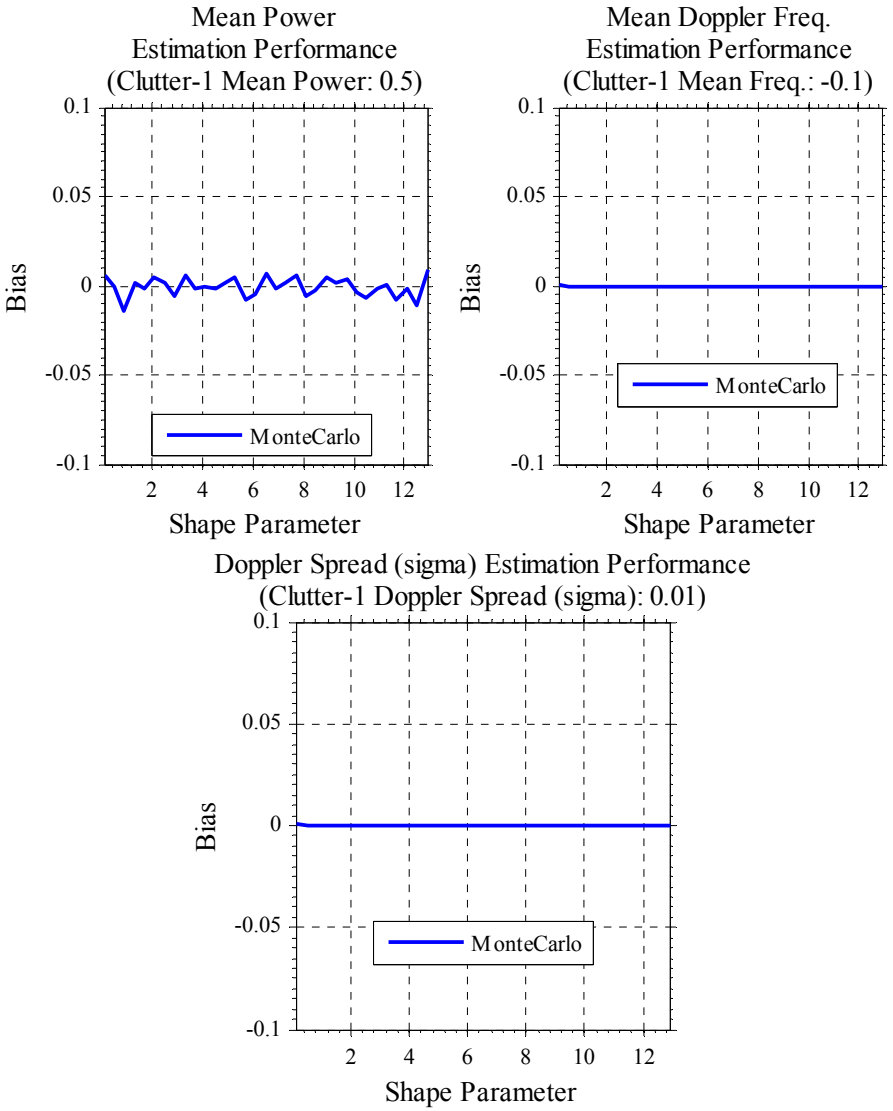

Figure 4-23 Biases for Estimated Clutter-1 Parameters as a Function of Shape Parameter

The estimation performance for the clutter-2 parameters in terms of bias can be seen from Figure 4-24.

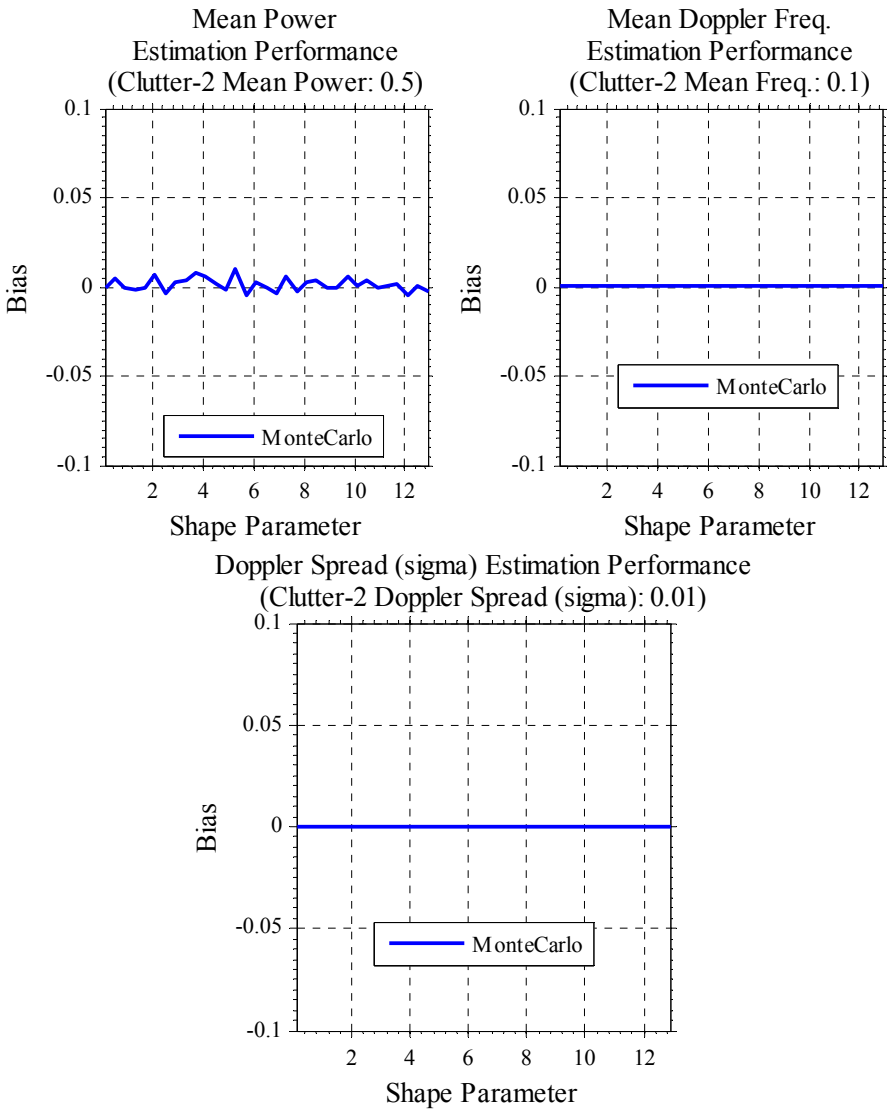

Figure 4-24 Biases for Estimated Clutter-2 Parameters as a Function of Shape Parameter

Figure 4-23 and Figure 4-24 depict that K-distribution property of clutter-1 does not introduce a bias on the estimates of the parameters of both clutters.

4.2 Comments on Simulation Results

There are four possible reasons that may explain the difference between the Cramér-Rao bounds and Monte Carlo analysis of estimation performance of the clutter powers, the mean Doppler frequencies and the Doppler spreads:

1) Sub-optimum estimations of the spectral moments (M_0, M_1, M_2, …) ,

2) Zero Doppler spread assumption while estimating the clutter powers and the mean Doppler frequencies,

3) Errors carried from the estimations of the spectral moments to the estimations of the clutter powers and the mean Doppler frequencies,

4) Errors carried from the estimations of the clutter powers and the mean Doppler frequencies to the Doppler spreads.

1) Sub-optimum estimations of the spectral moments: The power spectrum of a clutter is described completely by infinitely many spectral moments. However, the method proposed assumes the power spectrum of a clutter can be described by a finite number of spectral moments. This is the major reason that explains the difference between the Cramér-Rao bounds and the Monte Carlo analysis of the estimation performance of the spectral moments and why it is a sub-optimum approach. As mentioned before, the number of these finite spectral moments is defined as system order L and the best way to understand the effect of the system order L to the estimation performance is through moment estimator pattern functions [22].

The p th moment estimator pattern function $H_p(f, L)$ is defined as the mean value of the estimate $\widehat{M_p}$ when a deterministic unit power target at Doppler frequency f with zero Doppler spread is observed when the system order is L.

It is useful to note that

$$H_p(f, \infty) = f^p . \tag{4.1}$$

In Figure 4-25, the moment estimator pattern functions for $p = 0,1,2,3$ and $L = 6,10,14,\infty$ are plotted.

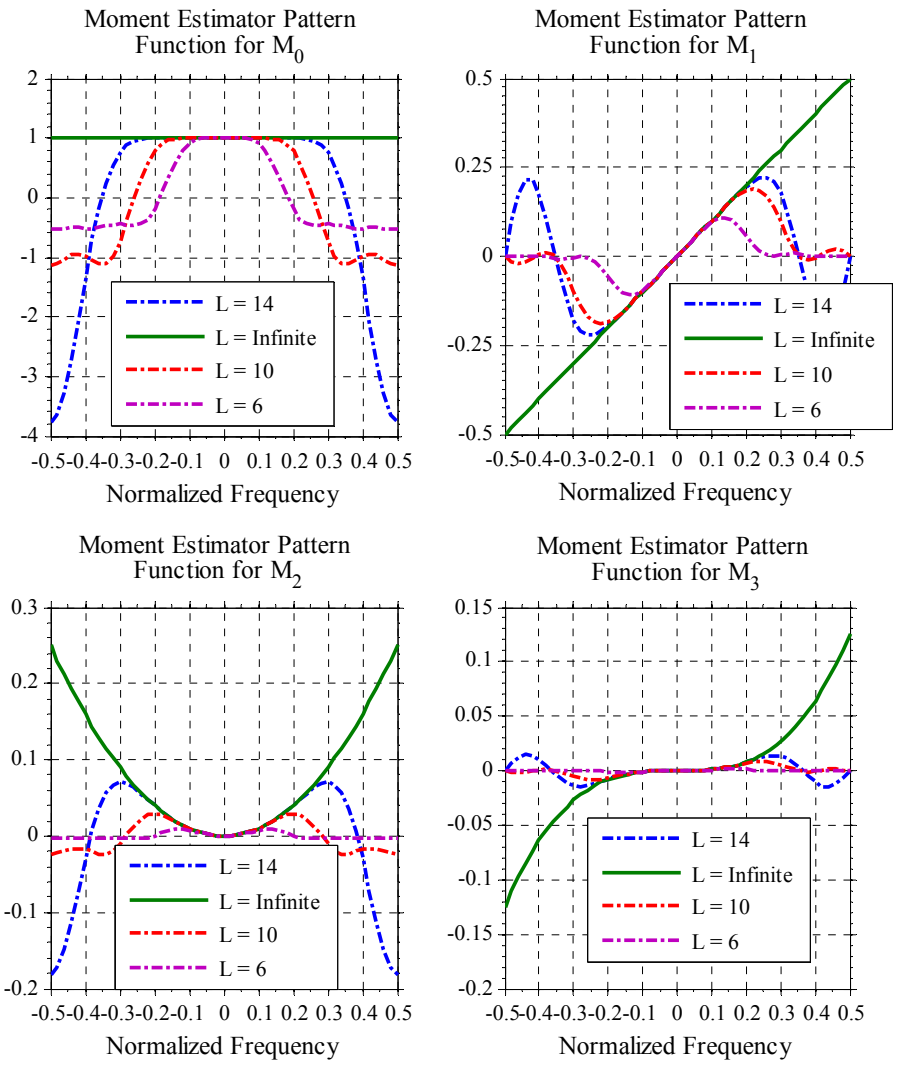

Figure 4-25 Moment Estimator Pattern Functions

In Figure 4-25, the regions where $H_p(f,L) = H_p(f,\infty)$ are the regions that the estimation of the spectral moments holds true. For $L = 6$, $L = 10$, $L = 14$ and $L = \infty$, true estimation of the spectral moments can be done if the clutter Doppler spectrum lies between ±0.06 , ±0.1, ±0.25 and ±0.5 normalized frequencies, respectively.

Since the Doppler separation of clutter power spectrums cannot exceed 0.5 normalized frequency because of spectrum folding, it cannot be counted as a limiting factor.

It is also helpful to note that the valid region of the spectral moment estimation can be shifted towards any Doppler frequency by simply changing the point f_0 about which the Taylor expansion is made. Thus, in order to use this clutter parameter estimating method effectively, it is necessary to calibrate its moment generating functions according to data using coarse location of the clutter Doppler spectrum in the spectra. An example of shifted moment generating functions is plotted in Figure 4-26.

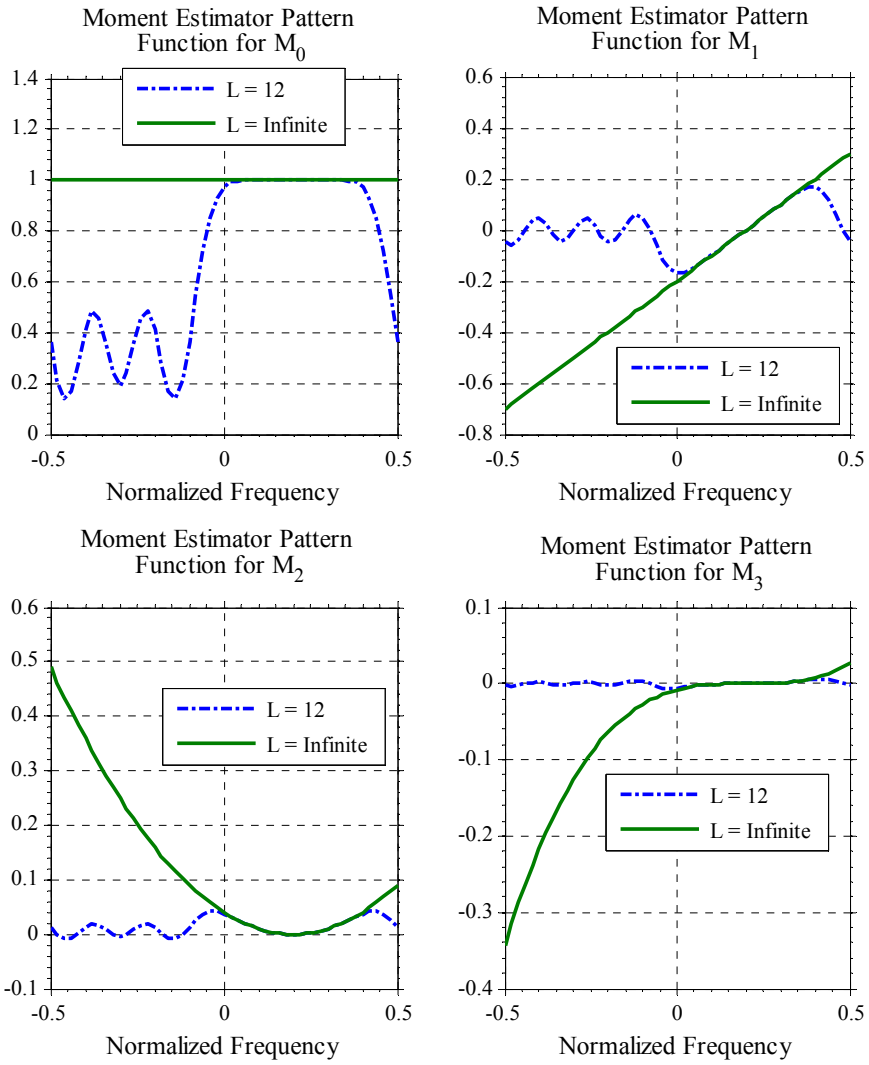

Figure 4-26 Shifted Moment Generating Functions to 0.2 Normalized Frequency

There are four major consequences that can be deduced by examining the moment estimator pattern functions [22]:

- Outside the valid regions, the estimates of spectral moments are less than their actual values and as a result, biases occur. To efficiently run the spectral

moment estimation method without any biases, L is chosen as 14 to cover all clutter spectra in simulations.

- The width of region where good estimation of the spectral moments can be achieved increases with the system order L.
- Outside the region where true estimation of the spectral moments can be done, the spectral moments are estimated less than their actual values and the "proportional" participant of noise increases and biases occur [22]. This leads to an increase in the standard deviations of the spectral moment estimates. As the mean frequency of clutter recedes from zero Doppler, increase in standard deviations of spectral moment estimates occurs. This explains why the standard deviations of the spectral moment estimates increase when the Doppler separation of clutters grows. In addition, if the Doppler spread increases, the tails of power spectrum starts to leak out from the valid region and this leads to receding of the estimation performance of the spectral moments from the Cramér-Rao bound.
- If the clutter spectra width is less than the region where true estimation of the spectral moments can be done, excess noise participates in the estimations and there is always a difference between the standard deviations of the mean frequencies estimates and the Cramér-Rao bound. If the width of the valid region is calibrated according to the clutter spectra, it is expected that the estimation performance approaches the Cramér-Rao bound.

As can be seen from Figure 4-12, the estimation performance (both the bias and the standard deviation) oscillates as the Doppler separation changes. This case is also explained by the moment estimator pattern functions. In this case the pth moment estimator pattern function is modified as $H_p(f_1, f_2, L)$ which is an observation of two deterministic unit power targets at Doppler frequencies f_1 and f_2 with zero Doppler spread. The modified estimator pattern function is plotted for different Doppler

spreads in Figure 4-27. The spectral moment estimation differs from the true value in a periodic way as the Doppler separation increases. This leads to the oscillations in the estimation performance of the clutter parameters.

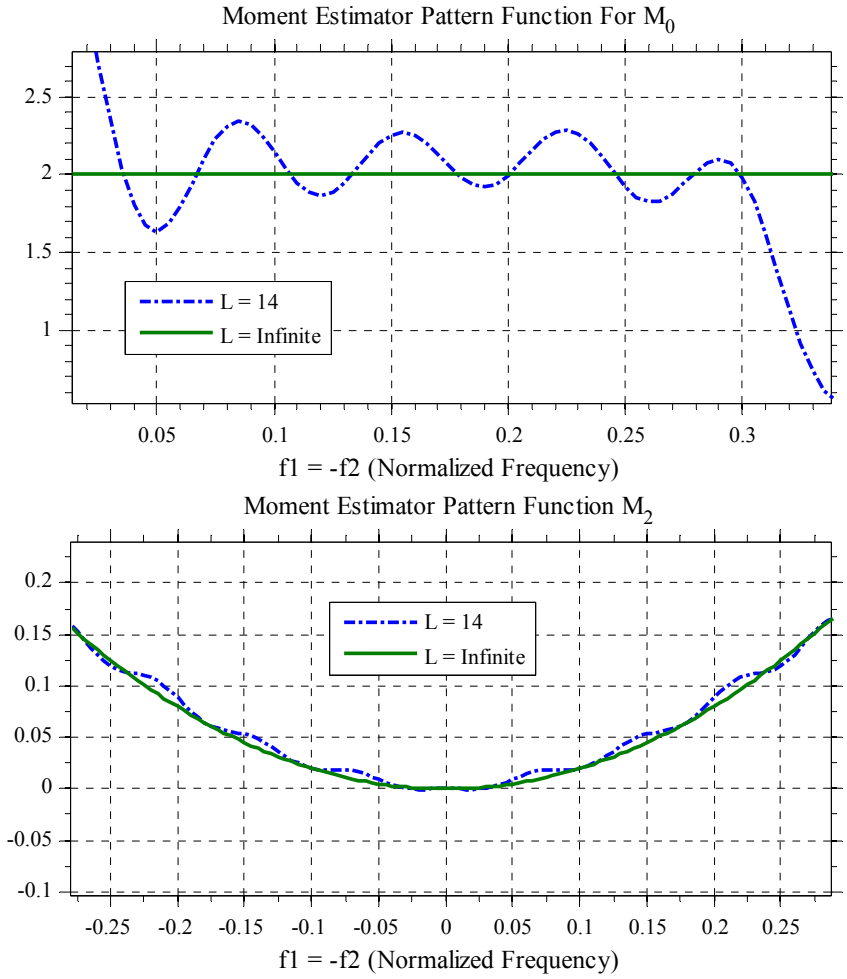

Figure 4-27 Modified Estimator Pattern Function

2) Zero Doppler spread estimation approach while estimating the clutter powers and the mean Doppler frequencies: Since the Doppler spreads of interest are approximately ten times lower than the mean Doppler frequencies, their contribution to spectral moments is relatively low when compared to the mean Doppler frequencies. Thus, it is assumed that the effect of Zero Doppler spread estimation approach has negligible effect on the clutter parameter estimations.

3) Errors carried from the estimations of the spectral moments to the estimations of the clutter powers and the mean Doppler frequencies: Since the mean clutter powers and the mean Doppler frequencies are estimated from the spectral moments, any degradation in the estimation performance of the spectral moments reflects to the estimation performance of the clutter powers and the mean Doppler frequencies.

4) Errors carried from estimations of clutter powers and mean Doppler frequencies to Doppler spreads: Since the Doppler spreads are estimated using the parametric maximum likelihood estimator by fixing the estimated mean clutter powers and the mean Doppler frequencies, any degradation in the estimation performance of the mean clutter powers and the mean Doppler frequencies reflects to the estimation performance of the Doppler spreads.

4.3 Comparison between Spectral Moments Estimation Methods Described in 3.5

The spectral moments estimation methods described in 3.5 is compared in terms of the moment estimator pattern functions for different coherent pulse numbers.

The comparison results can be observed from Figure 4-28, Figure 4-29 and Figure 4-30.

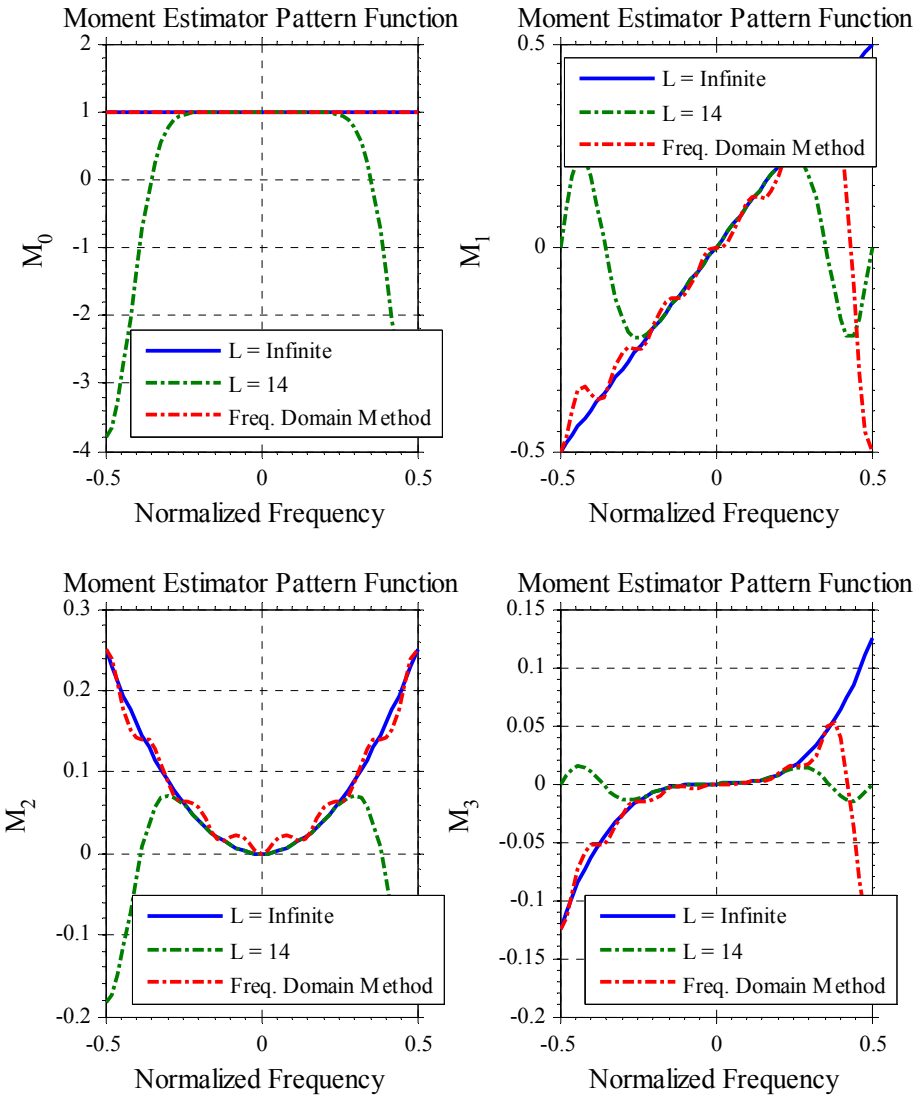

Figure 4-28 Moment Estimator Pattern Functions for 8 Coherent Pulses

According to Figure 4-28, the regions that the estimation of the spectral moments holds true for the frequency domain spectral moments estimation method cover the

whole spectra. However biases occur in the spectral moments estimates. These biases are caused by the DFT process when estimating spectral moments.

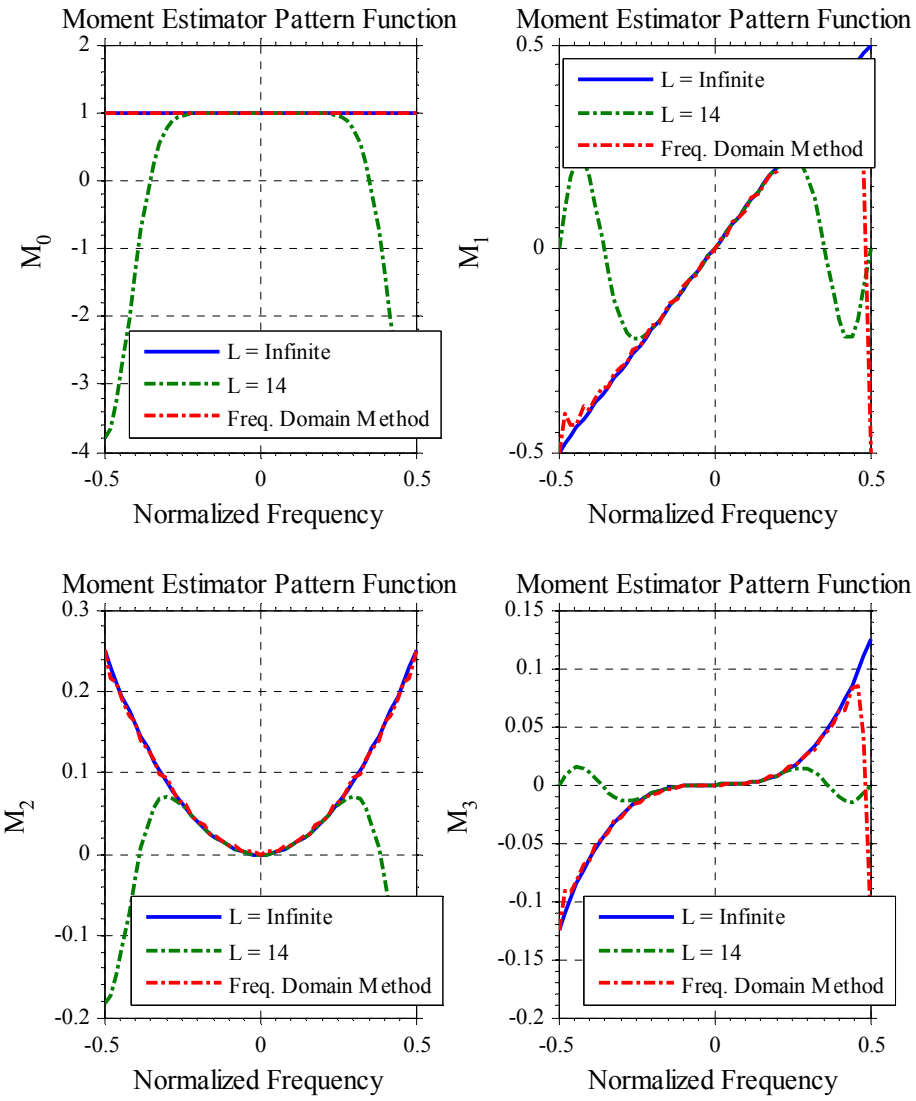

Figure 4-29 Moment Estimator Pattern Functions for 32 Coherent Pulses

According to Figure 4-29, the regions that the estimation of the spectral moments holds true for the frequency domain spectral moments estimation method cover the whole spectra. In this case, the biases are less than 8 coherent pulses case since the resolution of the estimation method is higher due to increasing number of coherent pulses.

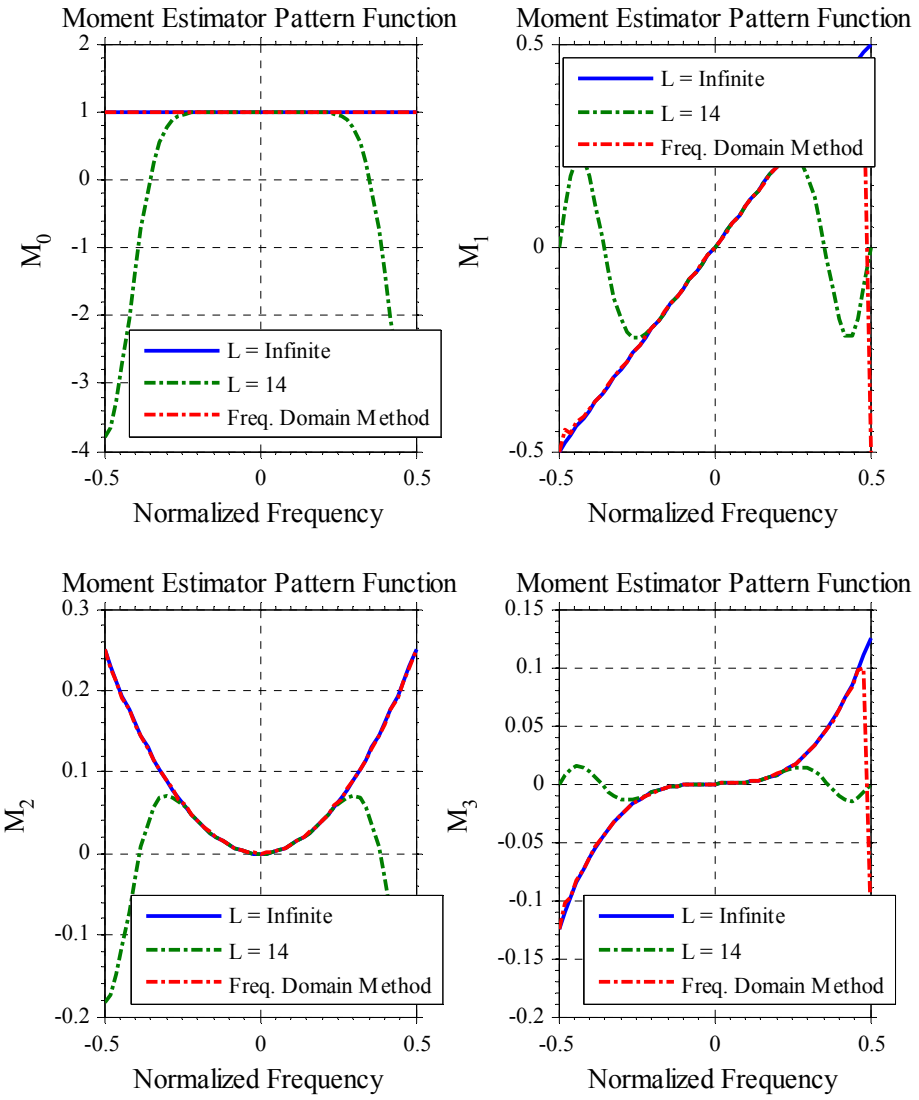

Figure 4-30 Moment Estimator Pattern Functions for 128 Coherent Pulses

According to Figure 4-30, the regions that the estimation of the spectral moments holds true for the frequency domain spectral moments estimation method cover the whole spectra. In this case, the biases are less than Figure 4-28 and Figure 4-29 since

the resolution of the estimation method is higher due to increasing number of coherent pulses.

The spectral moments estimation performances of the methods for different CNR values are also compared and presented in Figure 4-31, Figure 4-32 and Figure 4-33. The clutter parameters are the same as those in Section 4.1.1.

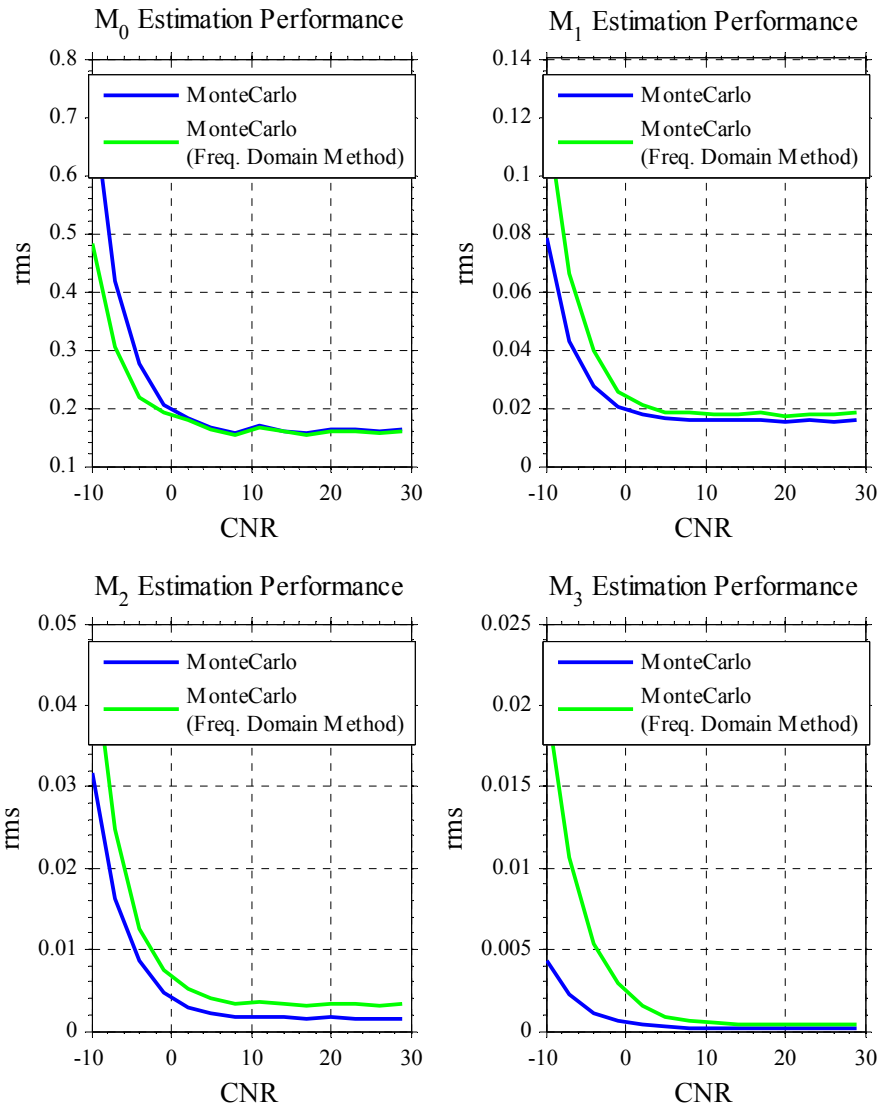

Figure 4-31 Spectral Moment Estimation Performance as a Function of CNR for 8 Coherent Pulses

According to Figure 4-31, there is little difference between the estimation performance of the frequency domain method and the time domain method. The difference is noticeable especially in M_2 estimates.

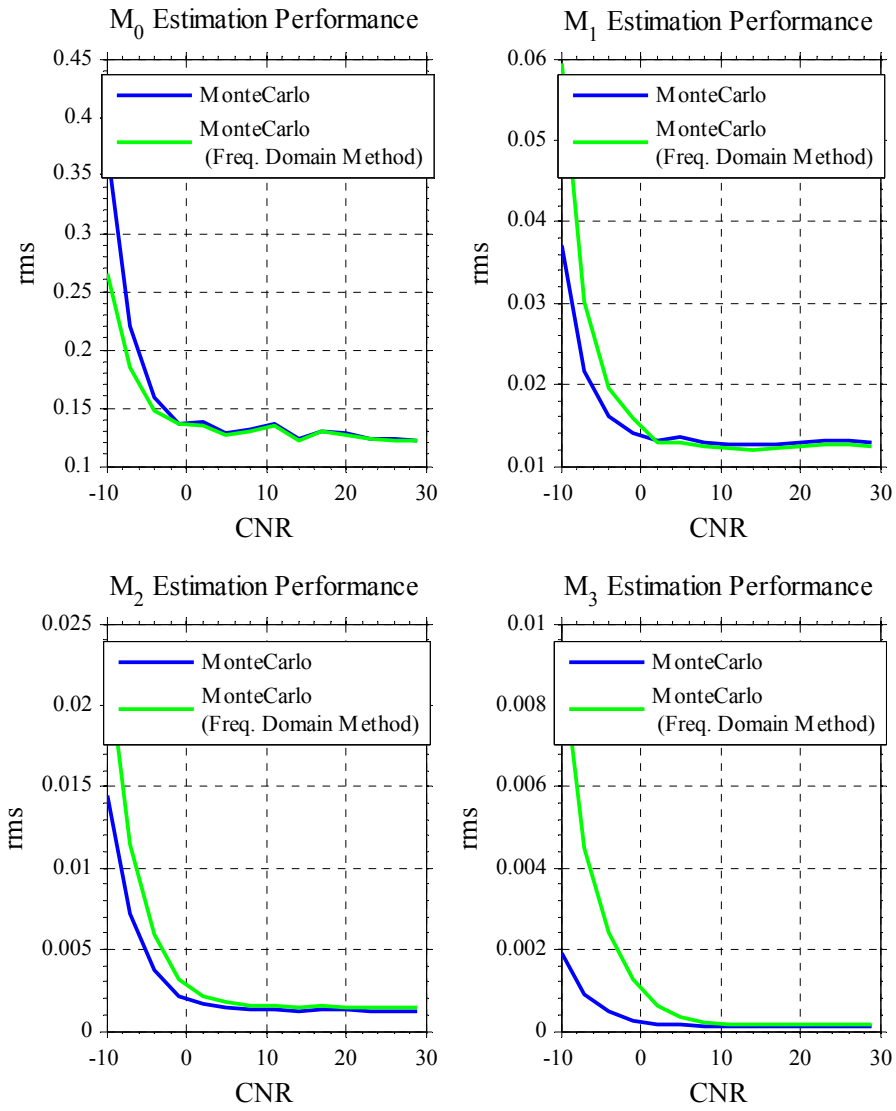

Figure 4-32 Spectral Moment Estimation Performance as a Function of CNR for 32 Coherent Pulses

According to Figure 4-32, the difference between the estimation performances the methods are less than 8 coherent pulses case due to increasing number of coherent pulses.

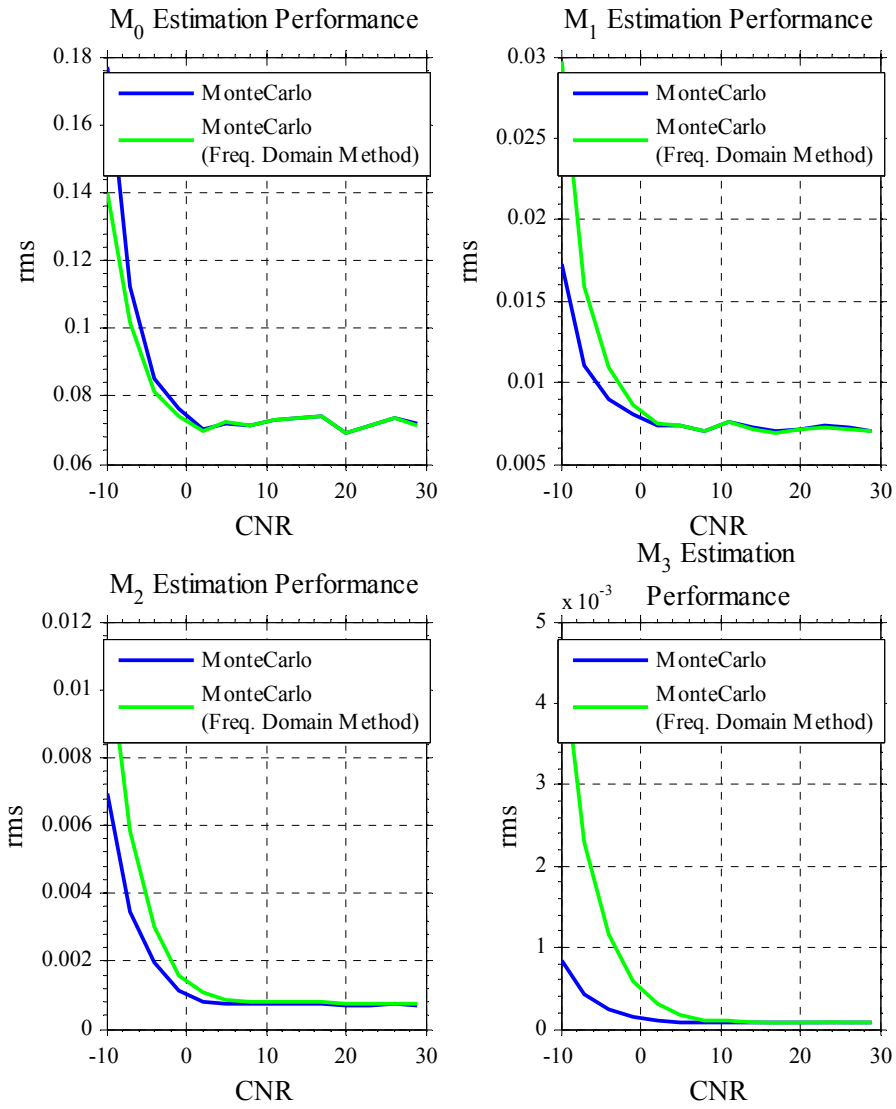

Figure 4-33 Spectral Moment Estimation Performance as a Function of CNR for 128 Coherent Pulses

According to Figure 4-33, the difference between the estimation performances the methods are less than Figure 4-31 and Figure 4-32 due to increasing number of coherent pulses.

CHAPTER 5

PERFORMANCE COMPARISON

5.1 Method of Comparison

In this chapter, the clutter suppression performances of the spectral moment estimation method and more conventional methods are compared in different simulated scenarios. For this purpose, N coherent radar echoes that include the K-distributed sea clutter, the Rayleigh-distributed rain clutter, and the radar receiver noise are simulated. The clutter parameters (the Doppler spreads, the mean Doppler frequencies, and the mean powers) and the radar receiver noise are simulated according to next generation airport surveillance radar (ASR-11) according to predefined wind speed, wind direction and sea state.

N Transversal filter coefficients $\boldsymbol{w} = \begin{pmatrix} w_0 & w_1 & \dots & w_{N-1} \end{pmatrix}^T$ that are calculated according to the algebraic spectral moments based clutter parameter estimation method and more conventional methods are listed below:

- The steered MTI filter for the sea clutter cascaded with the Doppler filter tuned to a known target Doppler frequency,
- The steered MTI filter for the rain clutter cascaded with the Doppler filter tuned to a known target Doppler frequency,

- Cascaded steered MTI filter for the sea clutter and steered MTI filter for the rain clutter and the Doppler filter tuned to a known target Doppler frequency,
- The optimum filter obtained from a known interference covariance matrix and a known target signal,
- The Doppler filter tuned to a known target Doppler frequency,
- The SMI (Sample Matrix Inversion) filter obtained from the estimated covariance matrix that is obtained by the method given in equation (3.19) applied on N radar returns.

The performances of the clutter suppression filters are compared in terms of improvement factor (IF). IF is defined as follows [3]:

$$IF = \frac{(S/I)_{out}}{(S/I)_{in}} = \left(\frac{S_{out}}{S_{in}}\right)\left(\frac{I_{in}}{I_{out}}\right) \tag{5.1}$$

where $(S/I)_{out}$ is the output signal-to-interference ratio, $(S/I)_{in}$ is the input signal-to-interference ratio, S_{out} is the output target power, S_{in} is the input target power, I_{in} is the input interference power and I_{out} is the output interference power.

The target power P_T, the sea clutter power P_S, the rain clutter power P_R and the radar receiver noise P_N are required to determine $(S/I)_{in}$.

$(S/I)_{in}$ can be expressed in terms of P_T, P_S, P_R and P_N as follows:

$$(S/I)_{in} = \frac{P_T}{P_S + P_R + P_N}. \tag{5.2}$$

$(S/I)_{out}$ can also be expressed in terms of the transversal clutter suppression filter coefficients $\boldsymbol{w}$, the Nx1 complex target signal vector $\boldsymbol{s}$ and the interference covariance matrix $\boldsymbol{R}$ [3]:

$$(S/I)_{in} = \frac{\boldsymbol{w}^H \boldsymbol{s}\boldsymbol{s}^H \boldsymbol{w}}{\boldsymbol{w}^H \boldsymbol{R}\boldsymbol{w}} \tag{5.3}$$

The elements of $\boldsymbol{s}$ is in the form of

$$s_i = \sqrt{P_T}\exp\left(-j2\pi(i-1)f_{dt}\right),\ i = 1,2,...,\mathrm{N} \tag{5.4}$$

where f_{dt} is the normalized target Doppler frequency. $\boldsymbol{R}$ is in the form of

$$\boldsymbol{R} = \boldsymbol{R_S} + \boldsymbol{R_R} + P_N \boldsymbol{I} \tag{5.5}$$

where $\boldsymbol{R_S}$ is the sea clutter covariance matrix, $\boldsymbol{R_R}$ is the rain clutter covariance matrix and $P_N \boldsymbol{I}$ is the radar receiver covariance matrix where $\boldsymbol{I}$ is the NxN identity matrix.

5.2 Transversal Filter Coefficients for Processors

Calculations of the transversal filter coefficients are presented in this section.

5.2.1 The steered MTI filter for the sea clutter cascaded with the Doppler filter tuned to a known target Doppler frequency

In this clutter suppression filter, the steered MTI filter for the sea clutter is cascaded with the Doppler filter tuned to a known target Doppler frequency. After denoting the steered MTI filter for the sea clutter as w_{mti_sea} and the Doppler filter tuned to a known target Doppler frequency as w_d, the filter coefficients can be found by

$$w = w_{mti\_sea} \otimes w_d \tag{5.6}$$

where $\otimes$ operator designates the convolution procedure.

w_{mti_sea} is in the form of a steered single delay line canceller:

$$w_{mti\_sea} = \begin{bmatrix} 1 & -\exp\left(j2\pi f_{ds}\right) \end{bmatrix}^T \tag{5.7}$$

where f_{ds} is the normalized mean sea clutter Doppler frequency and the elements of (N-1)x1 vector w_d is in the form of

$$w_d(i) = \exp\left(j2\pi(i-1) f_{dt}\right),\ i = 1,2,...,N-1. \tag{5.8}$$

5.2.2 The steered MTI filter for the rain clutter cascaded with the Doppler filter tuned to a known target Doppler frequency

In this clutter suppression filter, the steered MTI filter for the rain clutter is cascaded with the Doppler filter tuned to a known target Doppler frequency. After denoting the steered MTI filter for the rain clutter as w_{mti_rain}, the filter coefficients can be found by

$$w = w_{mti\_sea} \otimes w_d\ . \tag{5.9}$$

w_{mti_rain} is in the form of a steered single delay line canceller:

$$w_{mti\_rain} = \begin{bmatrix} 1 & -\exp\left(j2\pi f_{dr}\right) \end{bmatrix}^T \tag{5.10}$$

where f_{dr} is the normalized mean rain clutter Doppler frequency and the elements of (N-1)x1 vector w_d is in the form of (5.8).

5.2.3 Cascaded steered MTI filter for the sea clutter and steered MTI filter for the rain clutter and the Doppler filter tuned to a known target Doppler frequency

In this clutter suppression filter, the steered MTI filter for the sea clutter is cascaded with the steered MTI filter for the rain clutter and the Doppler filter tuned to a known target Doppler frequency. The transversal filter coefficients can be found by

$$w = w_{mti\_sea} \otimes w_{mti\_rain} \otimes w_d \,. \tag{5.11}$$

In equation (5.11), the elements of (N-2)x1 vector w_d is in the form of

$$w_d(i) = \exp\left(j2\pi(i-1) f_{dt} \right),\ i = 1,2,...,N-2 \,. \tag{5.12}$$

5.2.4 The optimum filter obtained from a known interference covariance matrix and a known target signal

Although the sea clutter obeys the compound K-distribution model, the interference also includes the Rayleigh distributed rain clutter. Thus, with the assumption of Gaussian interference approach, the optimum filter coefficients can be calculated for perfectly known target signal as follows:

$$w = \boldsymbol{R}^{-1}\boldsymbol{s}^{*} \tag{5.13}$$

where $\boldsymbol{R}^{-1}$ is the inverse of known interference covariance matrix (sum of the sea clutter covariance matrix $\boldsymbol{R_S}$, the rain clutter covariance matrix $\boldsymbol{R_R}$ and the radar receiver covariance matrix $P_N \boldsymbol{I}$) and $\boldsymbol{s}$ is the known Swerling-0 target signal vector which is defined in (5.4).

5.2.5 The Doppler filter tuned to a known target Doppler frequency

The Doppler filter coefficients without any windowing process are defined by

$$w_d(i) = \exp\left(j2\pi(i-1) f_{dt} \right),\ i = 1,2,...,N\ . \tag{5.14}$$

5.2.6 The SMI (Sample Matrix Inversion) filter obtained from the estimated covariance matrix

In this method, the interference clutter covariance matrix is obtained from adjacent range bins. The assumption is that these adjacent range bins include only the sea clutter, the rain clutter and the radar receiver noise.

The covariance matrix $\boldsymbol{R}_{SMI}$ is estimated by equation (3.19) and the filter coefficients are calculated by

$$w_{SMI} = \boldsymbol{R}_{SMI}^{-1} \boldsymbol{s}^* \tag{5.15}$$

where $\boldsymbol{R}_{SMI}^{-1}$ is the inverse of sample estimate of the interference covariance matrix.

5.2.7 The spectral moment estimation method

In this method, the transversal clutter suppression filters are calculated in four steps.

1) In the first step, the mean powers and the mean Doppler frequencies of the sea and rain clutter are estimated by the algebraic spectral moments based clutter parameter estimation method.

2) In the second step, using the clutter parameters estimated in the first step, minimization of the negative log-likelihood function of (3.20) is done by fixing the mean powers and the mean Doppler frequencies and changing the Doppler spreads.

3) In the third step, the interference covariance matrix is calculated using the estimated mean powers, the mean Doppler frequencies and the Doppler spreads of the sea and rain clutter with the Gaussian power spectrum assumption for both sea and rain clutter:

$$\widehat{\boldsymbol{R}} = \widehat{\boldsymbol{R}}_S + \widehat{\boldsymbol{R}}_R + P_N \boldsymbol{I} \tag{5.16}$$

where $\widehat{\boldsymbol{R}}_S$ is the estimated covariance matrix of the sea clutter and $\widehat{\boldsymbol{R}}_R$ is the estimated covariance matrix of the rain clutter.

The estimated covariance matrix of the sea clutter are calculated according to the formula (3.8):

$$\widehat{\boldsymbol{R}}_S\left(\hat{P}_s, \hat{f}_{ds}, \widehat{\sigma_s^2}\right) = \hat{P}_s \boldsymbol{A}\left(\hat{f}_{ds}\right) \boldsymbol{B}\left(\widehat{\sigma_s^2}\right) \boldsymbol{A}\left(\hat{f}_{ds}\right)^H \tag{5.17}$$

where $\hat{P}_s$, $\hat{f}_{ds}$, $\widehat{\sigma_s^2}$ are the estimated mean power, the mean Doppler frequency and the Doppler Spread of the sea clutter, respectively,

$$\boldsymbol{A}\left(\hat{f}_{ds}\right) = diag(1 \quad e^{j2\pi \hat{f}_{ds}} \ldots \quad e^{j2\pi \hat{f}_{ds}(N-1)}) \tag{5.18}$$

and

$$\boldsymbol{B_{kl}}\left(\widehat{\sigma_s^2}\right) = e^{-2\pi^2 \widehat{\sigma_s^2}(k-l)^2}. \tag{5.19}$$

The estimated covariance matrix of the rain clutter is calculated according to the formula (3.8):

$$\widehat{\boldsymbol{R}}_R\left(\hat{P}_R, \hat{f}_{dR}, \widehat{\sigma_R^2}\right) = \hat{P}_R \boldsymbol{A}\left(\hat{f}_{dR}\right) \boldsymbol{B}\left(\widehat{\sigma_R^2}\right) \boldsymbol{A}\left(\hat{f}_{dR}\right)^H \tag{5.20}$$

where $\hat{P}_R, \hat{f}_{dR}, \widehat{\sigma_R^2}$ are the estimated mean power, the mean Doppler frequency and the Doppler Spread of rain clutter, respectively,

$$\boldsymbol{A}(\hat{f}_{dR}) = diag(1 \quad e^{j2\pi\hat{f}_{dR}} \ldots \quad e^{j2\pi\hat{f}_{dR}(N-1)}) \tag{5.21}$$

and

$$\boldsymbol{B_{kl}}\left(\widehat{\sigma_R^2}\right) = e^{-2\pi^2\widehat{\sigma_R^2}(k-l)^2}. \tag{5.22}$$

4) In the final step, the transversal clutter suppression filter is calculated in the following way:

$$\boldsymbol{w} = \widehat{\boldsymbol{R}}^{-1}\boldsymbol{s}^* \tag{5.1}$$

where $\widehat{\boldsymbol{R}}^{-1}$ is the inverse of the estimated interference covariance matrix.

5.3 Results

The improvement factors are calculated for different environmental scenarios and compared to each other. The common assumptions used in the simulations are stated below. Differences between the scenarios take place under related scenario.

- The coherent processing interval (CPI) consists of 8 pulses.
- In a CPI, the PRF remains constant.
- The target Doppler frequency is known and does not change in CPI.
- For the spectral moment estimation method and the sample matrix inversion method, 500 Monte Carlo runs are made and IF is calculated as the average of the results from each Monte Carlo step.
- The radar used in the simulations is ASR-11 and it is assumed that its parameters do not change in a CPI. The technical specifications of ASR-11 are given in Table 5-1 [25].

Table 5-1 ASR technical characteristics

Parameter	ASR-11 Value
Peak transmitter power	25 kW
Transmitter type	solid state
Operational frequency range	2700–2900 MHz
Antenna type	modified parabolic reflector with stacked feed horns
Antenna gain	34 dBi
Typical antenna height above ground	12 m (40 ft)
Antenna beam width	2.3º (horizontal) 5º (vertical)
Antenna polarization	vertical
Antenna sidelobe levels	At least 25 dB below main-beam gain
Antenna beam-scanning protocol	0 º –360 º rotational
Antenna beam-scanning rate	12.5 rpm (4.8 sec/scan)
Transmitted pulse widths	1 us (CW pulse) 89 us (linear FM)
Transmitted pulse modulation	P0N and Q3N (unmodulated CW pulses paired with linear FM pulses)
Transmitted pulse repetition rates	856 pulses/sec (average) in a 4-stagger sequence
Receiver target-processing bandwidth	1.1 MHz
Nominal receiver noise figure	2 dB
Thermal noise level in receiver bandwidth (computed)	-111.6 dBm

5.3.1 Scenario-1 (Both The Sea and Rain Clutter Coexist.)

In this scenario, ASR-11 is located 100 m above mean sea level and its beam is directed parallel to earth surface. A target having 1 m^2 RCS is placed at 40 km range

from the radar. The rainfall rate is 4 mm/hr (moderate rain) and the wind speed is 7.7 m/s towards the radar (corresponds to Sea State 3 according to the TSC model).

The number of coherent pulses and the number of independent range bins used in the spectral moment estimator are 8 and 10, respectively. It is assumed that the clutter power spectrum can be expressed by 14 spectral moments. The spectral moment estimator is using the assumption that there is both rain and sea clutter existing in the radar echoes.

The power and the Doppler Characteristics of the target, the rain clutter and the sea clutter at 40 km are calculated and simulation report is given below:

```
After Pulse Compression Target and Interference Powers:
Target Echo Power: -75.53 dBm
Sea Clutter Power: -86.97 dBm
Rain Clutter Power: -75.30 dBm
Receiver Noise Power: -111.42 dBm
Sea Clutter to Noise Ratio: 24.45 dB
Rain Clutter to Noise Ratio: 36.11 dB
Sea Clutter Parameters:
Shape Parameter: 1.38
Mean Doppler Frequency: 30.48 Hz
Doppler Spread (sigma) due to Internal Clutter Motion: 10.75 Hz
Doppler Spread (sigma) due to Antenna Scanning Modulation: 8.64 Hz
Overall Doppler Spread (sigma): 13.80 Hz
Normalized Values:
Mean Doppler Frequency: 0.030 (normalized freq.)
Doppler Spread (sigma) due to Internal Clutter Motion: 0.011
(normalized freq.)
Doppler Spread (sigma) due to Antenna Scanning Modulation: 0.0086
(normalized freq.)
Overall Doppler Spread (sigma): 0.0138 (normalized freq.)

Rain Clutter Parameters:
Mean Doppler Frequency: 143.38 Hz
Doppler Spread (sigma) due to Internal Clutter Motion: 57.83 Hz
Doppler Spread (sigma, wind sheer component): 54.73 Hz
Doppler Spread (sigma, turbulence component): 18.67 Hz
Doppler Spread (sigma, beam broadening component): 0.00 Hz
Doppler Spread (sigma, fall velocity distribution component): 0.00 Hz
Doppler Spread (sigma) due to Antenna Scanning Modulation: 8.64 Hz
Overall Doppler Spread (sigma): 58.47 Hz
Normalized Values:
Mean Doppler Frequency: 0.143 (normalized freq.)
Doppler Spread (sigma) due to Internal Clutter Motion: 0.058
(normalized freq.)
Doppler Spread (sigma) due to Antenna Scanning Modulation: 0.0086
(normalized freq.)
Overall Doppler Spread (sigma): 0.0585 (normalized freq.)
```

The improvement factors are calculated according to the clutter parameters and the radar receiver noise level in the simulation report and presented in Figure 5-1.

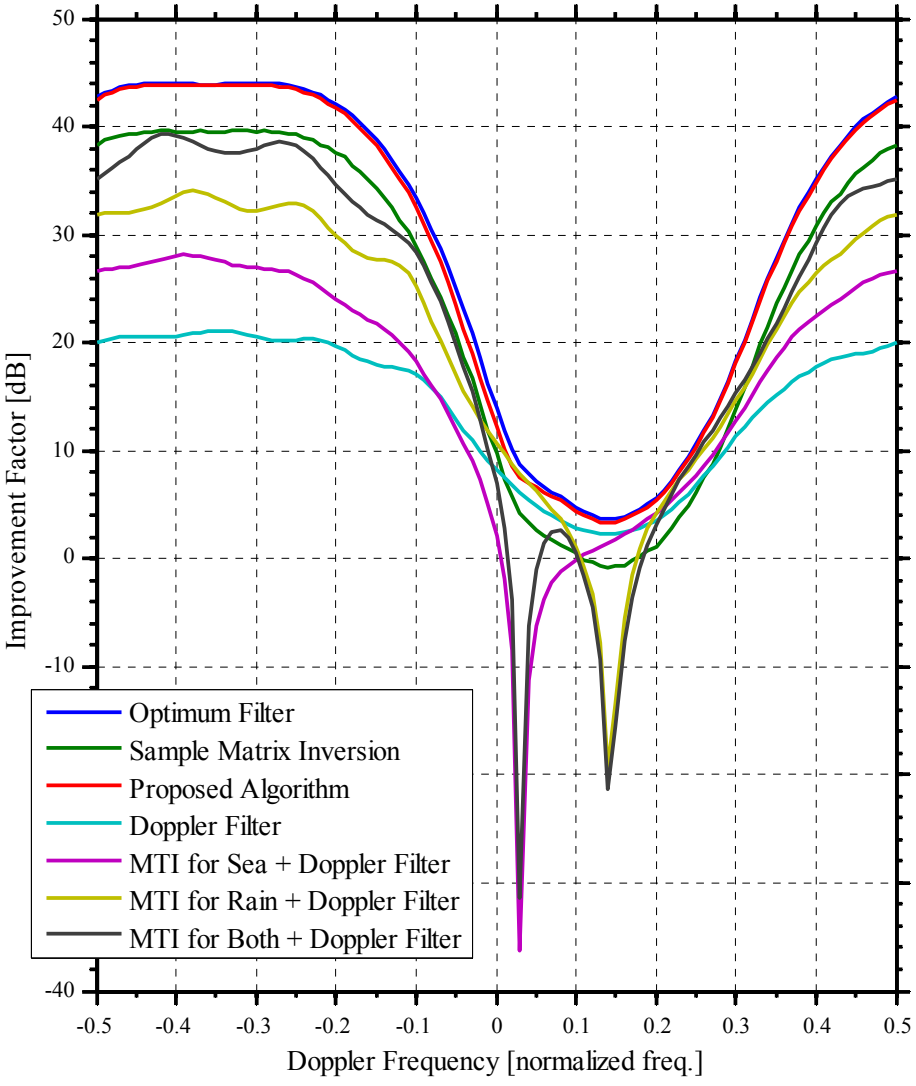

Figure 5-1: Improvement Factors for Scenario-1

According to Figure 5-1, we can observe that the improvement factor of the algebraic spectral moments based clutter parameter estimation method nearly fits the improvement factor of the optimum filter. Maximum 1.4 dB secession occurs around zero Doppler frequency.

The improvement factors of both the spectral moment estimation method and the optimum filter drop in the area of ±0.25 Doppler frequency around 0.15 Doppler frequency. This result is caused by the sea and the rain clutter Doppler spreads which are approximately 0.0828 (6 sigma) and 0.351 (6 sigma), respectively.

The methods using the steered MTI have deep nulls at the mean Doppler frequencies of clutters and in these areas, the improvement factor drops below 0. The Doppler filter is better around at the mean Doppler frequencies of clutters; however, its performance is worse than the methods using the steered MTI in exoclutter regions. This results from the fact that the clutters at the Doppler sidelobes have a negative effect on the improvement factor.

The SMI method has a better improvement factor than the other methods except for the optimum filter and the spectral moment estimation method. This shows that knowing apriori information about the spectral shapes of clutters and estimating the parameters that describe them result in a better improvement factor.

5.3.2 Scenario-2 (Only Sea Clutter Exists.)

In this scenario, ASR-11 is located 100 m above mean sea level and its beam is directed parallel to the earth surface. A target having 1 m^2 RCS is placed at 40 km range from the radar. There is **no rain** and the wind speed is 7.7 m/s towards the radar (corresponds to Sea State 3 according to the TSC model).

The number of coherent pulses and the number of independent range bins used in the spectral moment estimator are 8 and 10, respectively. It is assumed that the clutter spectrum can be expressed by 14 spectral moments. **The spectral moment**

estimator is using the assumption that there is both the rain and the sea clutter exist in the radar echoes, in fact only the sea clutter exists.

The power and the Doppler Characteristics of the target, the rain clutter and the sea clutter at 40 km are calculated and simulation report is given below:

```
After Pulse Compression Target and Interference Powers:
Target Echo Power: -75.53 dBm
Sea Clutter Power: -86.97 dBm
Rain Clutter Power: -Inf dBm
Receiver Noise Power: -111.42 dBm
Sea Clutter to Noise Ratio: 24.45 dB
Rain Clutter to Noise Ratio: -Inf dB

Sea Clutter Parameters:
Shape Parameter: 1.38
Mean Doppler Frequency: 30.48 Hz
Doppler Spread (sigma) due to Internal Clutter Motion: 10.75 Hz
Doppler Spread (sigma) due to Antenna Scanning Modulation: 8.64 Hz
Overall Doppler Spread (sigma): 13.80 Hz
Normalized Values:
Mean Doppler Frequency: 0.030 (normalized freq.)
Doppler Spread (sigma) due to Internal Clutter Motion: 0.011
(normalized freq.)
Doppler Spread (sigma) due to Antenna Scanning Modulation: 0.0086
(normalized freq.)
Overall Doppler Spread (sigma): 0.0138 (normalized freq.)
```

The improvement factors are calculated according to the clutter parameters and the radar receiver noise level in the simulation report and presented in Figure 5-2.

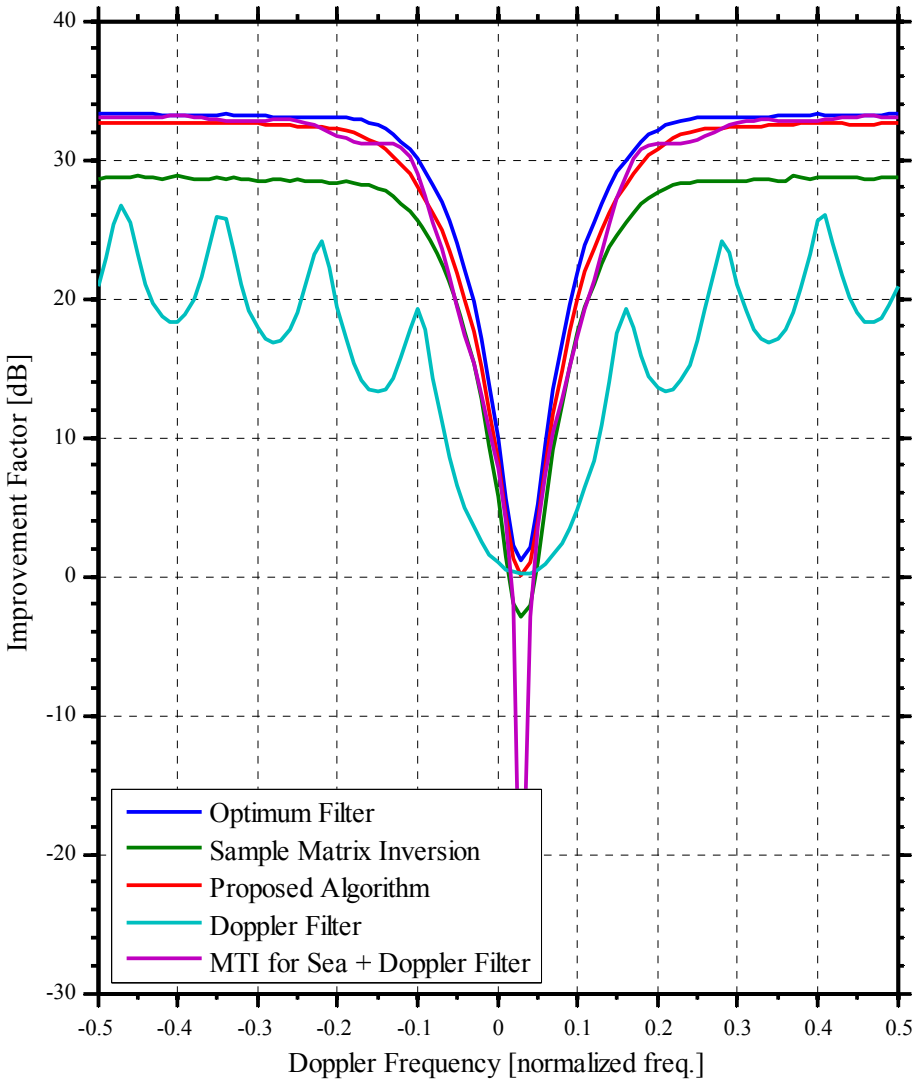

Figure 5-2: Improvement Factors for Scenario-2

According to Figure 5-2, we can observe that the improvement factor of the algebraic spectral moment based clutter parameter estimation and the steered MTI filter nearly fit the improvement factor of the optimum filter for exoclutter regions. In endoclutter

regions a maximum of 2 dB secession occurs for the spectral moment estimation method. The improvement factor of the spectral moment estimation is worse than scenario-1 since in this scenario, this method assumes that the rain and the sea clutter coexist in the environment, in fact, only the sea clutter exists. This results in that the spectral moment estimation tries to find two clutters and estimates their parameters as closely spaced clutters around the mean Doppler frequency of the sea clutter. Thus, the estimated clutter powers are half of the sea clutter power.

The improvement factors of both the spectral moment estimation method and the optimum filter drop in the area of ±0.1 Doppler frequency around 0.03 Doppler frequency. This result is caused by the sea clutter Doppler spread which is approximately 0.0828 (6 sigma).

The steered MTI filter has a deep null at the mean Doppler frequency of the sea clutter and in this area, the improvement factor drops below 0. The Doppler filter is better around the mean Doppler frequency of the sea clutter, however, its performance is worse than the steered MTI filter in exoclutter regions. This results from the fact that the sea clutter at Doppler sidelobes has a negative effect on the improvement factor.

The SMI method has a better improvement factor than the other methods except for the optimum filter and the spectral moment estimation method. This shows that knowing apriori information about the spectral shape of the clutter and estimating the parameters that describe it result in a better improvement factor.

5.3.3 Scenario-3 (Only Rain Clutter Exists.)

In this scenario, ASR-11 is located 100 m above mean sea level and its beam is directed towards the air, thus, the radar **echoes do not contain sea clutter**. A target having 1 m^2 RCS is placed at 40 km range from the radar. The rainfall rate is 4 mm/hr (moderate rain) and the wind speed is 7.7 m/s towards the radar.

The number of coherent pulses and the number of independent range bins used in the spectral moment estimator are 8 and 10, respectively. It is assumed that the clutter spectrum can be expressed by 14 spectral moments. **The spectral moment estimator is using the assumption that there is both the rain and the sea clutter exist in the radar echoes, in fact only the rain clutter exists.**

The power and the Doppler Characteristics of the target, the rain clutter and the sea clutter at 40 km are calculated and simulation report is given below:

```
After Pulse Compression Target and Interference Powers:
Target Echo Power: -75.53 dBm
Sea Clutter Power: -Inf dBm
Rain Clutter Power: -75.30 dBm
Receiver Noise Power: -111.42 dBm
Sea Clutter to Noise Ratio: -Inf dB
Rain Clutter to Noise Ratio: 36.11 dB

Rain Clutter Parameters:
Mean Doppler Frequency: 143.38 Hz
Doppler Spread (sigma) due to Internal Clutter Motion: 57.83 Hz
Doppler Spread (sigma, wind sheer component): 54.73 Hz
Doppler Spread (sigma, turbulence component): 18.67 Hz
Doppler Spread (sigma, beam broadening component): 0.00 Hz
Doppler Spread (sigma, fall velocity distribution component): 0.00 Hz
Doppler Spread (sigma) due to Antenna Scanning Modulation: 8.64 Hz
Overall Doppler Spread (sigma): 58.47 Hz
Normalized Values:
Mean Doppler Frequency: 0.143 (normalized freq.)
Doppler Spread (sigma) due to Internal Clutter Motion: 0.058
(normalized freq.)
Doppler Spread (sigma) due to Antenna Scanning Modulation: 0.0086
(normalized freq.)
Overall Doppler Spread (sigma): 0.0585 (normalized freq.)
```

The improvement factors are calculated according to the clutter parameters and the radar receiver noise level in the simulation report and presented in Figure 5-3.

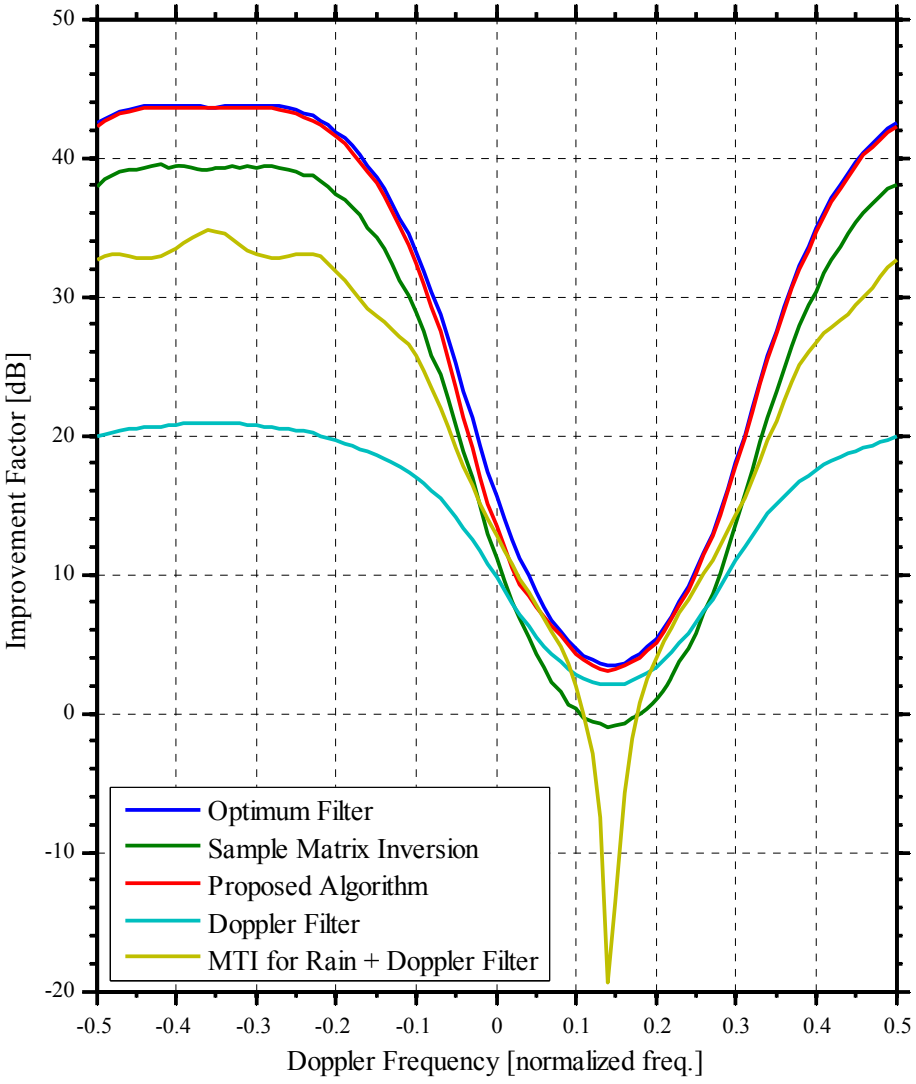

Figure 5-3: Improvement Factors for Scenario-3

According to Figure 5-3, we can observe that the improvement factor of algebraic spectral moment based clutter parameter estimation fits the improvement factor of the optimum filter for the whole range in spite of the fact that, in this scenario, this

method assumes the rain and the sea clutter coexist in the environment. The reason is that in Scenario-2, the sea clutter has a narrow Doppler spread while in Scenario-3, the rain clutter has a wider Doppler spread. The sum of the covariance matrices of the clutters found by the spectral moment estimation method is close to the covariance matrix of the rain since it has a wider Doppler spread. In other words, the spectral moment estimation method can describe the covariance matrix of the rain clutter in terms of two different closely spaced clutters since the rain clutter has a wider Doppler spread.

When compared to Scenario -2, the performance of the steered MTI drops in Scenario-3 since the rain clutter has a much larger Doppler spread.

The improvement factors of both the spectral moment estimation method and the optimum filter drop in the area of ±0.3 Doppler frequency around 0.15 Doppler frequency. This result is caused by the rain clutter Doppler spread which is approximately 0.351 (6 sigma).

The steered MTI filter has a deep null at the mean Doppler frequency of the rain clutter and in this area, the improvement factor drops below 0. The Doppler filter has a better performance around the mean Doppler frequency of rain clutter; however, its performance is worse than the steered MTI filter in exo-clutter regions. This results from the fact that the rain clutter at Doppler sidelobes has negative effect on improvement factor.

The SMI method has a better improvement factor than the other methods except for the optimum filter and the spectral moment estimation method. This shows that knowing apriori information about the spectral shapes of clutter and estimating parameters that describe it results in a better improvement factor.

5.3.4 Scenario-4 (Only Sea Clutter Exists.)

In this scenario, ASR-11 is located 100 m above mean sea level and its beam is directed parallel to the earth surface. A target having 1 m^2 RCS is placed at 40 km range from the radar. There is **no rain** and the wind speed is 7.7 m/s towards the radar (corresponds to Sea State 3 according to the TSC model).

The number of coherent pulses and the number of independent range bins used in the spectral moment estimator are 8 and 10, respectively. It is assumed that the clutter spectrum can be expressed by 14 spectral moments. **The spectral moment estimator is using the assumption that there is only the sea clutter in the environment**.

The power and the Doppler Characteristics of the target, the rain clutter and the sea clutter at 40 km are calculated and simulation report is given below:

```
After Pulse Compression Target and Interference Powers:
Target Echo Power: -75.53 dBm
Sea Clutter Power: -86.97 dBm
Rain Clutter Power: -Inf dBm
Receiver Noise Power: -111.42 dBm
Sea Clutter to Noise Ratio: 24.45 dB
Rain Clutter to Noise Ratio: -Inf dB

Sea Clutter Parameters:
Shape Parameter: 1.38
Mean Doppler Frequency: 30.48 Hz
Doppler Spread (sigma) due to Internal Clutter Motion: 10.75 Hz
Doppler Spread (sigma) due to Antenna Scanning Modulation: 8.64 Hz
Overall Doppler Spread (sigma): 13.80 Hz
Normalized Values:
Mean Doppler Frequency: 0.030 (normalized freq.)
Doppler Spread (sigma) due to Internal Clutter Motion: 0.011
(normalized freq.)
Doppler Spread (sigma) due to Antenna Scanning Modulation: 0.0086
(normalized freq.)
Overall Doppler Spread (sigma): 0.0138 (normalized freq.)
```

The improvement factors are calculated according to the clutter parameters and the radar receiver noise level in the simulation report and presented in Figure 5-4.

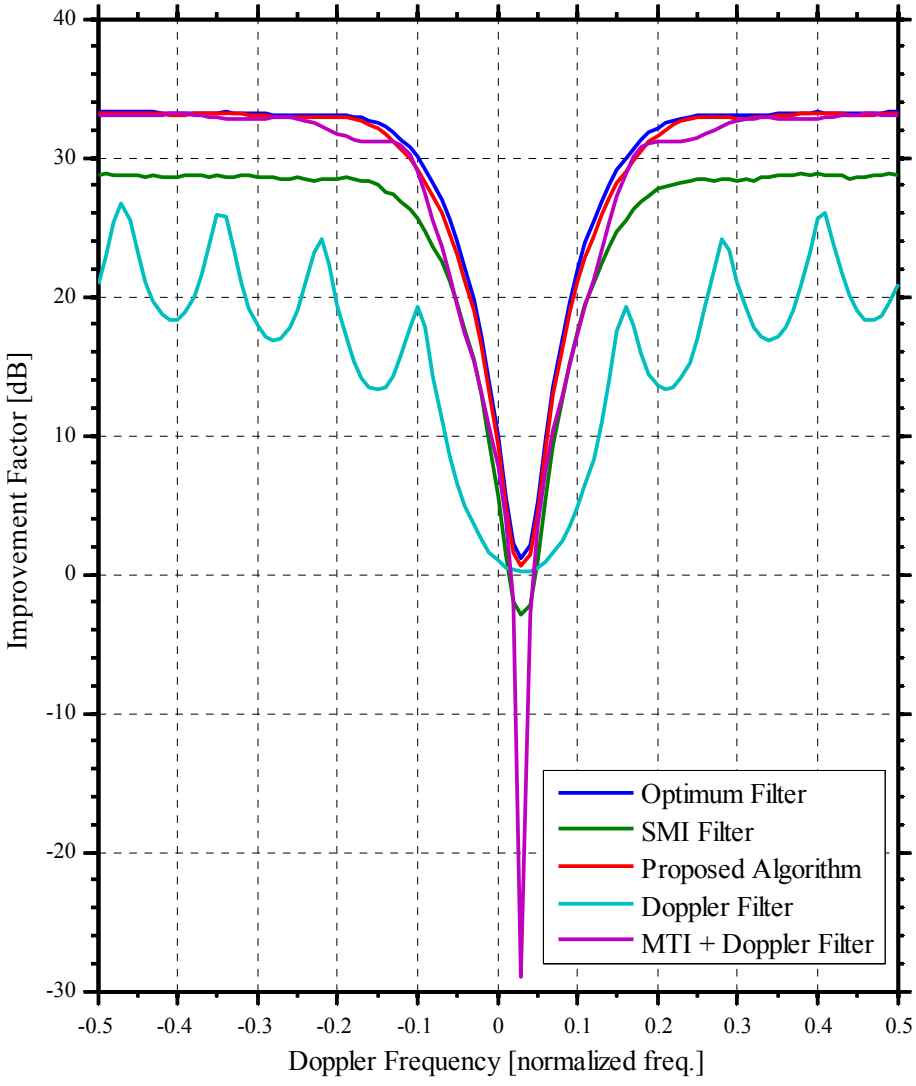

Figure 5-4: Improvement Factors for Scenario-4

According to Figure 5-4, we can observe that the improvement factor of the algebraic spectral moment based clutter parameter estimation fits the improvement factor of the optimum filter for both endo-clutter and exo-clutter clutter regions. The improvement factor of the spectral moment estimation method is better than scenario-2 since this method assumes only the sea clutter exists in the environment.

The improvement factors of both the spectral moment estimation method and the optimum filter drop in the area of ±0.1 Doppler frequency around 0.03 Doppler frequency. This result is caused by the sea clutter Doppler spread which is approximately 0.0828 (6 sigma).

The Steered MTI filter has a deep null at the mean Doppler frequency of the sea clutter and in this area the improvement factor drops below 0. The Doppler filter is better around the mean Doppler frequency of the sea clutter, however, its performance is worse than the steered MTI filter in exo-clutter regions. This results from the fact that the sea clutter at Doppler sidelobes has negative effect on improvement factor.

The SMI method has a better improvement factor than the other methods except for the optimum filter and the spectral moment estimation method. This shows that knowing apriori information about the spectral shape of clutter and estimating parameters that describes it results in a better improvement factor.

5.3.5 Scenario-5 (Only Sea Clutter with Exponential Autocorrelation Function Exists.)

The mean power and the mean Doppler frequency for the sea clutter in this scenario are the same as Scenario-4. The spectral moment estimator is using the assumption that there is only the sea clutter in the environment. However, in this scenario, the exponential autocorrelation function model for the sea clutter is used. The proposed

method still uses the assumption that the sea clutter obeys the Gaussian autocorrelation function model.

The improvement factors are calculated and presented in Figure 5-5.

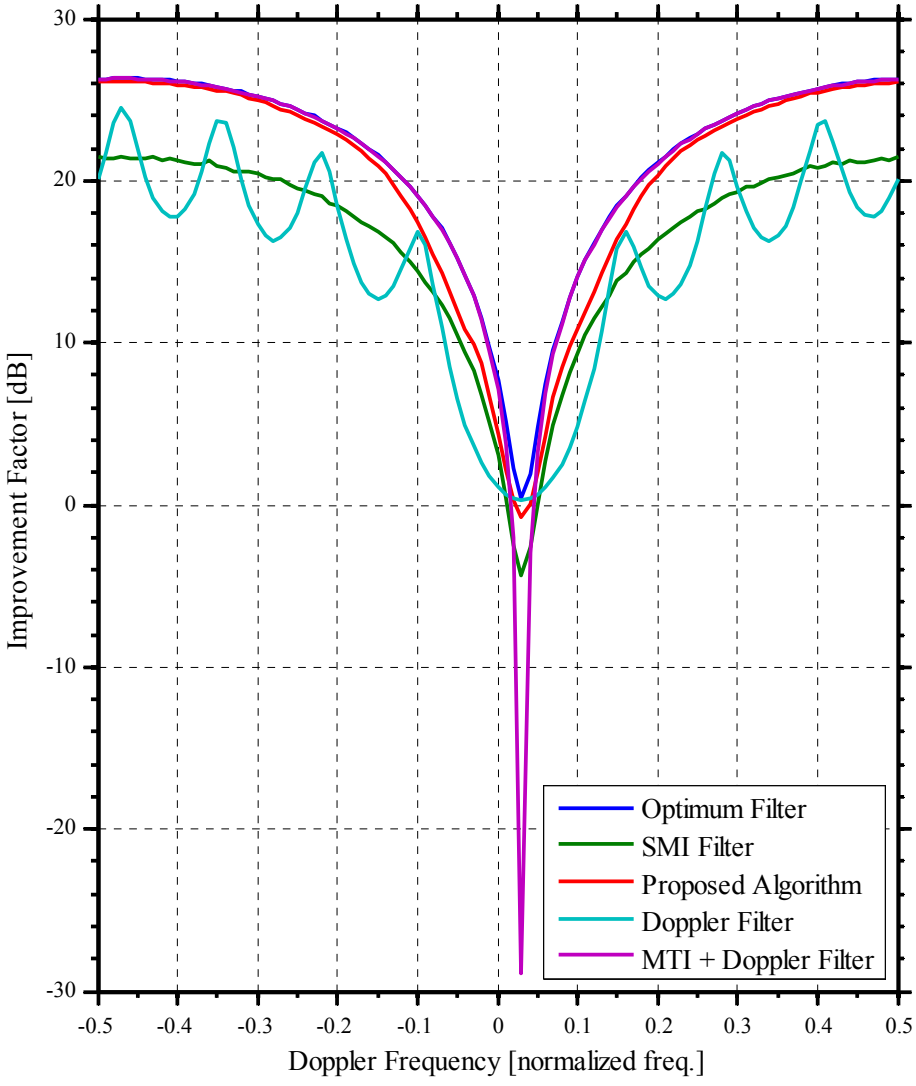

Figure 5-5: Improvement Factors for Scenario-5

According to Figure 5-5, we can observe some degradation in the performance of the proposed algorithm when compared to Scenario 4. Degradation amount can be observed from Figure 5-6. Degradation in the clutter suppression performance of the proposed method is due to the false assumption that the sea clutter obeys the exponential autocorrelation function model. Moreover, we can observe from Figure 5-5 that the improvement factors in Scenario-5 are less than Scenario-4. The reason is that in the exponential autocorrelation function model, the clutter correlation decays faster as the time between the clutter samples increases. This leads to increase in clutter spread and decrease in the improvement factors.

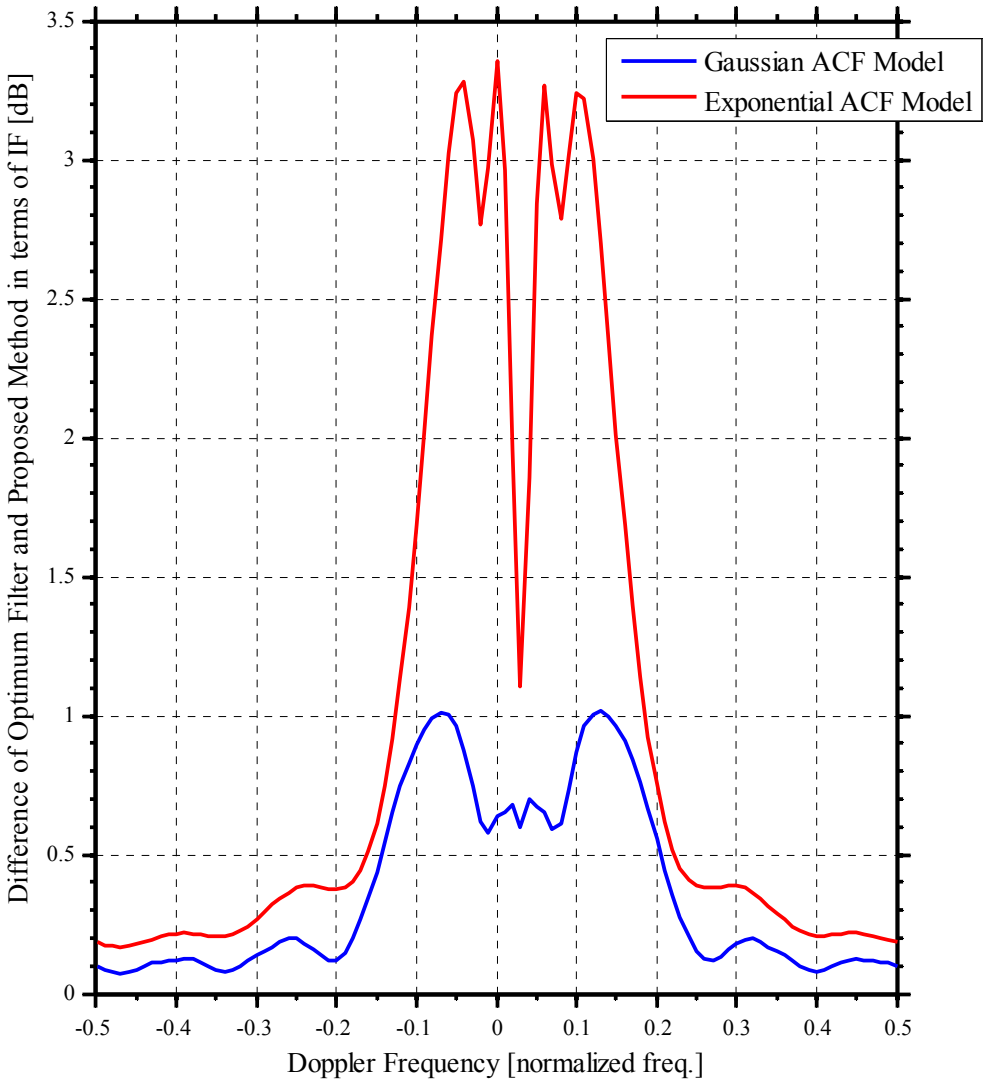

Figure 5-6: Degradation in the Performance of the Proposed Method in Scenario 5

5.3.6 Scenario-6 (Only Rain Clutter with Exponential Autocorrelation Function Exists.)

The mean power and the mean Doppler frequency for the rain clutter in this scenario are the same as Scenario-3. The spectral moment estimator is using the assumption that there is only the rain clutter in the environment. However, in this scenario, the exponential autocorrelation function model for the rain clutter is used. The proposed method still uses the assumption that the rain clutter obeys the Gaussian autocorrelation function model.

The improvement factors are calculated and presented in Figure 5-7.

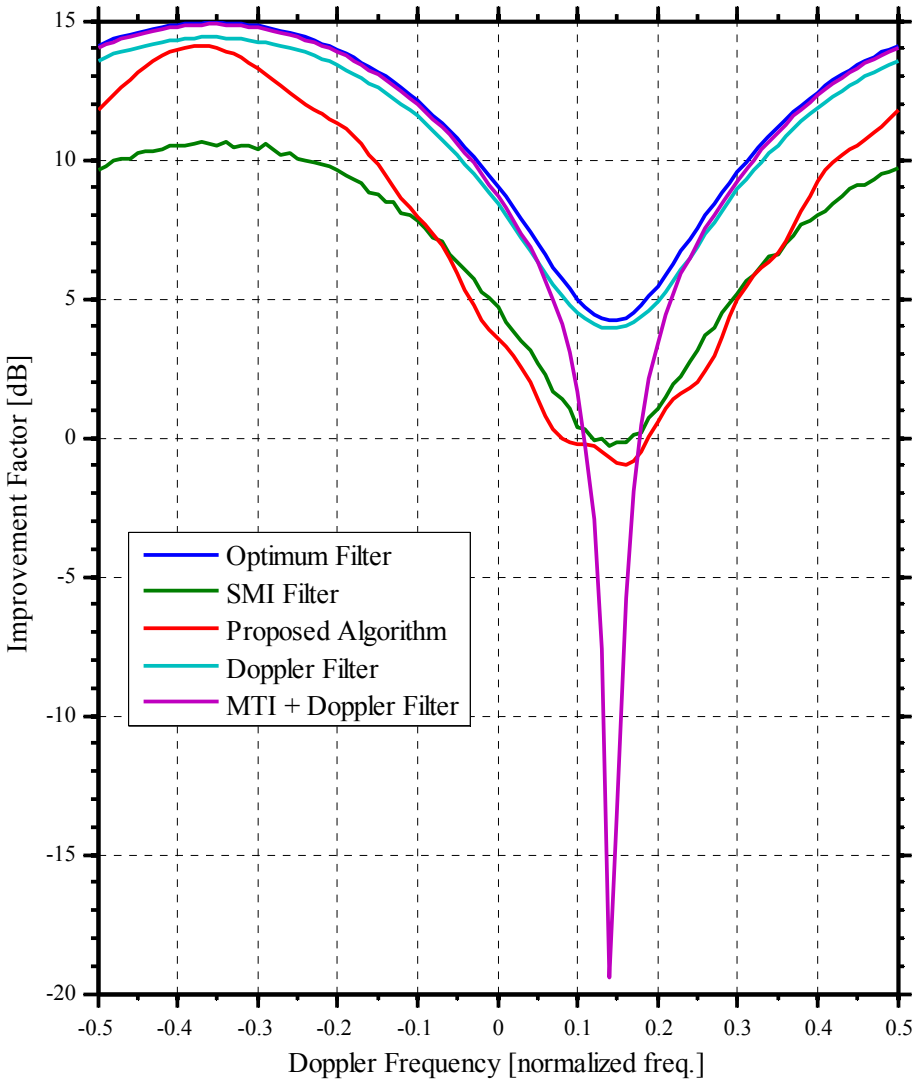

Figure 5-7: Improvement Factors for Scenario-6

According to Figure 5-7, we can observe some degradation in the performance of the proposed algorithm when compared to Scenario 3. Degradation amount can be observed from Figure 5-8. Degradation in the clutter suppression performance of the

proposed method is due to the false assumption that the rain clutter obeys the exponential autocorrelation function model. Moreover, we can observe from Figure 5-7 that the improvement factors in Scenario-6 are less than Scenario-3. The reason is that in the exponential autocorrelation function model, the clutter correlation decays faster as the time between the clutter samples increases. This leads to increase in clutter spread and decrease in the improvement factors.

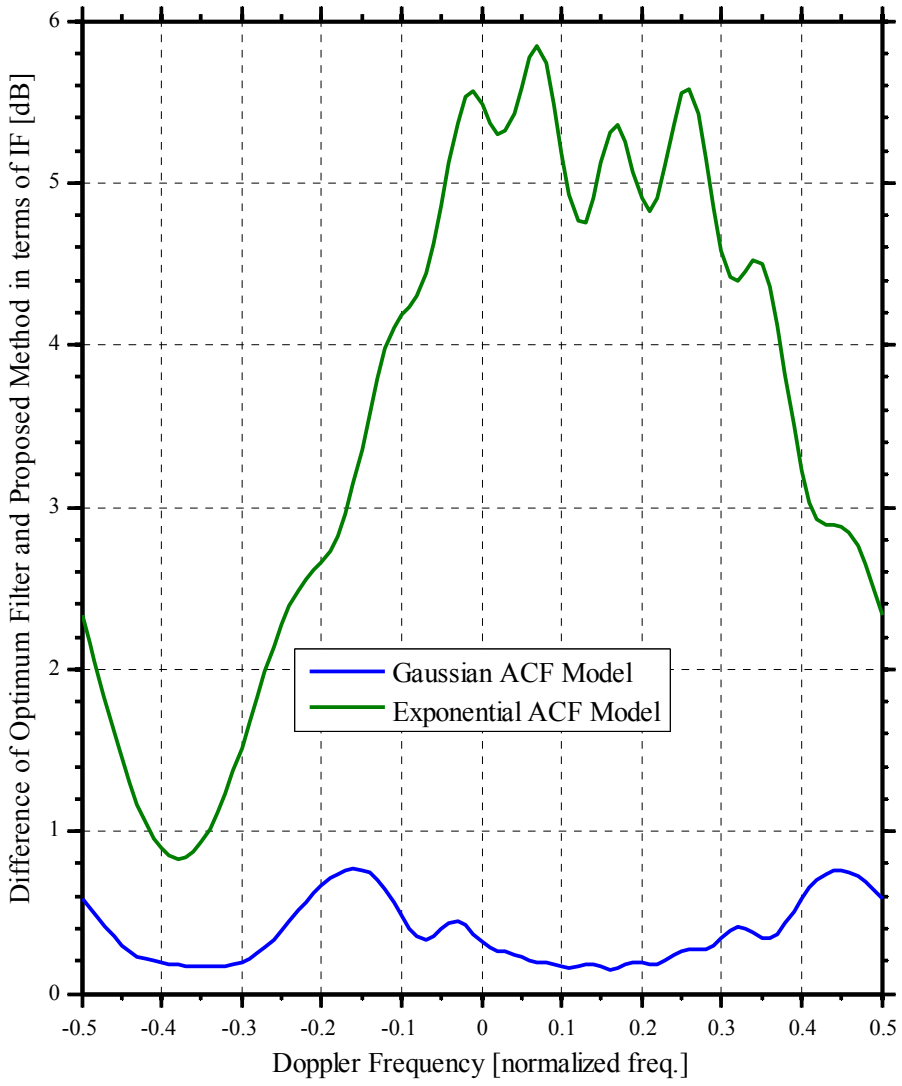

Figure 5-8: Degradation in the Performance of the Proposed Method in Scenario 6

5.3.7 Scenario-7 (Both The Sea Clutter and The Rain Clutter with Exponential Autocorrelation Function Coexist.)

The mean powers and the mean Doppler frequencies for the sea clutter and the rain clutter in this scenario are the same as Scenario-1. The spectral moment estimator is using the assumption that there are both the sea clutter and the rain clutter in the environment. However, in this scenario, the exponential autocorrelation function model for the sea clutter and the rain clutter is used. The proposed method still uses the assumption that the sea clutter and the rain clutter obey the Gaussian autocorrelation function model.

The improvement factors are calculated and presented in Figure 5-9.

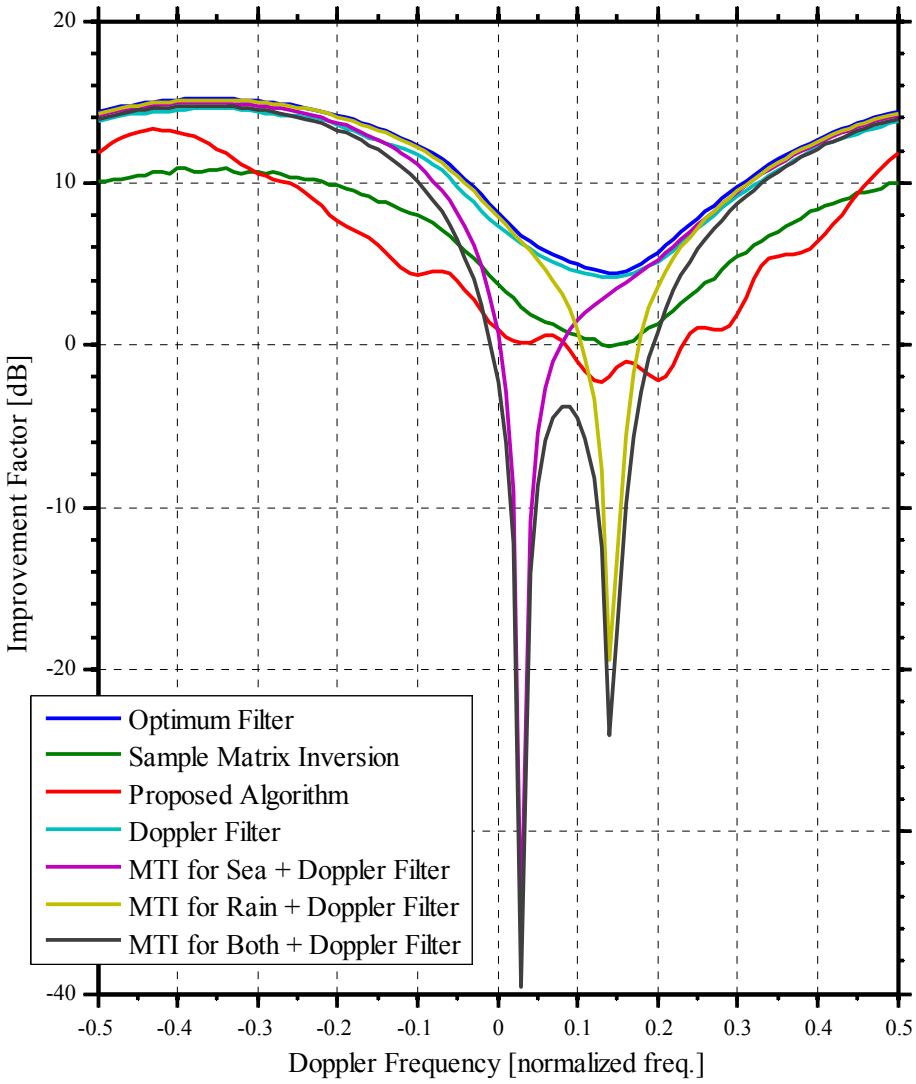

Figure 5-9: Improvement Factors for Scenario-7

According to Figure 5-9, we can observe some degradation in the performance of the proposed algorithm when compared to Scenario 1. Degradation amount can be observed from Figure 5-10. Degradation in the clutter suppression performance of

the proposed method is due to the false assumption that the sea clutter and the rain clutter obey the exponential autocorrelation function model. Moreover, we can observe from Figure 5-9 that the improvement factors in Scenario-7 are less than Scenario-1. The reason is that in the exponential autocorrelation function model, the clutter correlation decays faster as the time between the clutter samples increases. This leads to increase in clutter spread and decrease in the improvement factors.

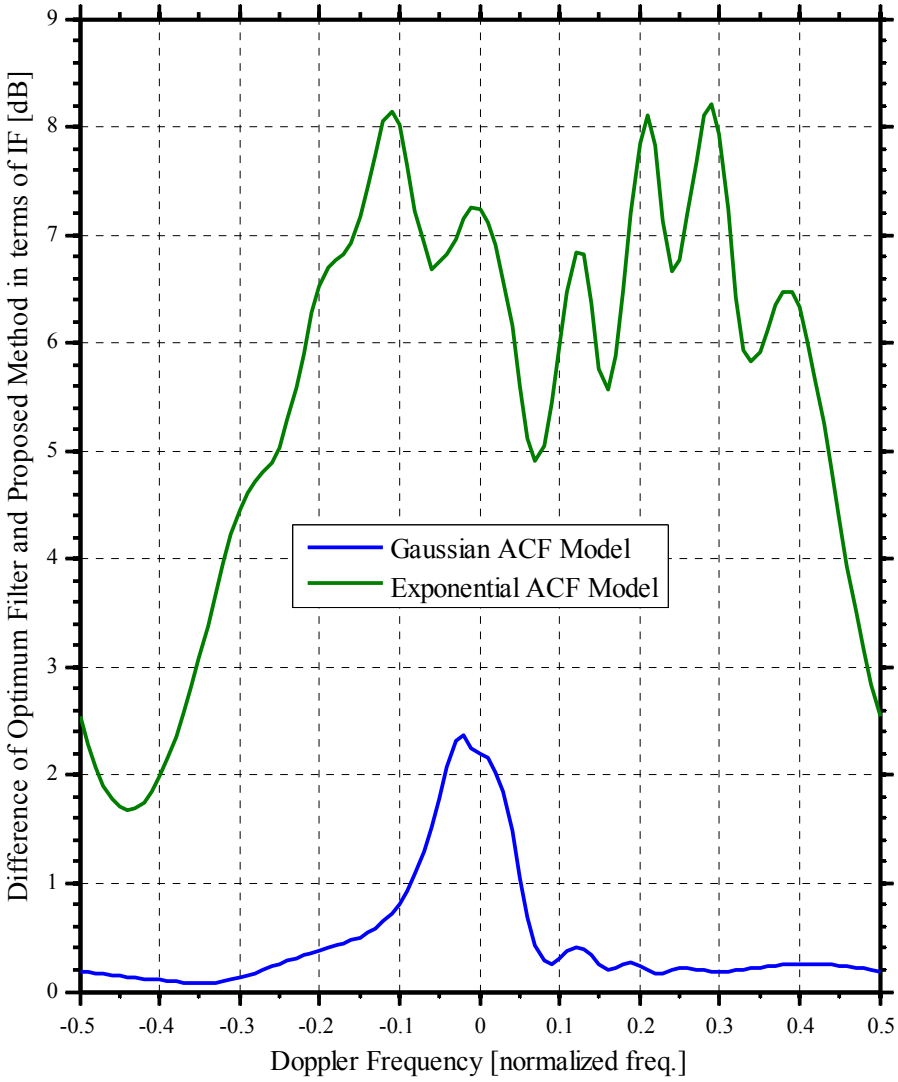

Figure 5-10: Degradation in the Performance of the Proposed Method in Scenario 7

CHAPTER 6

CONCLUSION

6.1 Summary

The main motivation of this thesis work was to investigate the performances of recently proposed clutter spectral parameter estimation techniques in an environment that includes both the sea and the rain clutter.

For this purpose, firstly, the definitions of the interference and the optimum interference suppression filtering were stated. Then, the MTI and the MTD algorithms, which are widely used algorithms in present radars to suppress the interference, are reviewed and their deficiencies which differentiate them from the optimum interference suppression filtering were stated.

Since the parametric methods which can effectively suppress the interference that includes both the rain and the sea clutter were investigated in this thesis, the characteristics of the rain clutter and the sea clutter were reviewed. In this context, the amplitude characteristics, the mean clutter reflectivity behaviours, the Doppler characteristics of both clutters were summarized. Moreover, the models and the methods that can be used to simulate synthetic sea and rain clutter that have specific amplitude distribution and specific time correlation properties were reviewed.

The parametric maximum-likelihood estimator, the WPSF (weighted pseudosubspace fitting) algorithm and the algebraic spectral moment estimation method were listed as the methods which can solve the moving clutter parameter estimation problem and their clutter parameter estimation performances were investigated in this thesis. It was noted that the clutter parameter estimation performance of the parametric maximum-likelihood estimator perfectly fits the Cramér-Rao bound. However, solving the minimization problem in this estimator requires high computational power. When compared to the parametric maximum-likelihood estimator, it was noted that the WPSF (weighted pseudosubspace fitting) algorithm has less computational power. However it is well shown in the literature that it fails when compared to the performance of the parametric maximum likelihood estimator.

On the other hand, the algebraic spectral moment estimation method is recently proposed to solve direction of arrival (DOA) problem of more than one interference signals. Original algorithm is developed to find the mean powers and the directions of more than one signal sources. In this thesis, this algorithm is used to find the mean powers and the mean Doppler shifts of more than one moving clutters. Since it provides the mean powers and the mean Doppler frequencies of the clutters only, it is combined with the parametric maximum-likelihood estimator to find additionally Doppler spreads of the clutters and it is proposed as a two step method to achieve full clutter characterization: In the first step, the mean powers and the mean Doppler frequencies of clutters are estimated using the algebraic spectral moments based estimation technique and in the second step, using the clutter parameters estimated in first step, minimization of the negative log-likelihood function is done by fixing the mean powers and the mean Doppler frequencies and changing the Doppler spreads.

To investigate the performance of the proposed clutter parameters estimation method, the sea and the rain clutter were simulated and the Monte-Carlo analysis were done to determine its RMS and bias performance. Then, the performance of the

proposed method was compared with the Cramér-Rao bounds for different mean clutter powers, the Doppler separations, the mean Doppler frequencies and the shape parameters. From the results, it was observed that, for above 10 dB CNR, 0.15 normalized Doppler separation value and above shape parameter value 3, its performance fits the Cramér-Rao bound. Moreover, the sufficiency of number of Monte Carlo runs was presented in terms of confidence interval of 95% together with the estimation performance of the proposed method.

To investigate the clutter suppression performance, the proposed method and conventional methods (the steering MTI followed by the Doppler filter, the optimum filter, the Doppler filter, the sample matrix inversion method) were compared in terms of the improvement factor for realistic radar parameters. In these comparisons, the technical parameters of next generation airport surveillance radar (ASR-11) were used.

For clutter environment in which both the rain clutter and the sea clutter coexists, it was observed that the improvement factor of the proposed method is very close to the optimum filter and its performance surpasses the more conventional methods.

For the clutter environments in which only the rain clutter exists and only the sea clutter exists, it was observed that the improvement factor of the proposed method is slightly decreased by 2 dB since it searches for two clutters in the radar echoes. In spite of this false assumption, it is observed from the improvement factor comparison results that the performance of the proposed method is closest to optimum filter when compared to the conventional methods.

After calibrating the proposed method in such a way that it searches only one clutter in the radar echoes, the improvement factor again becomes very close to optimum filter (less than 1 dB).

To investigate the robustness of the proposed algorithm, its clutter suppression performance under the exponential autocorrelation function model assumption is

calculated. Since it uses the assumption that the rain clutter and the sea clutter obey the Gaussian autocorrelation function model, it is observed that its clutter suppression performance degrades up to 6 dB due to the false assumption mentioned above.

6.2 Future Work

There are some topics regarding the clutter suppression subject to further develop the proposed parametric method. These topics are as follows:

- Investigating the performance of the proposed method for an environment which includes both the ground and the rain clutter,
- Comparing the performance of the proposed method with the subspace methods for different clutter powers, mean Doppler frequencies, Doppler spreads and shape parameters,
- Extending the covariance matrix estimation method used in the proposed method for different amplitude distributions as in the case of sea clutter and investigating the performance results,
- To reduce computation load, develop a method to find the transversal filter coefficients as a function of clutter parameters. (In this thesis, we accomplish this by calculating the interference covariance matrix from the clutter parameters and taking the inverse of the estimated clutter covariance matrix.)

REFERENCES

[1] Mahafza, B.R., Radar Systems Analysis and Design Using Matlab, Third Edition, CRC Press, Taylor & Francis Group, 2013

[2] Cartledge, L., O'Donnell R.M., "Description and Performance Evaluation of the Moving Target Detector", Lincoln Laboratory, Massachusetts Institute of Technology, Report No: FAA-RD-76-190, March 1977.

[3] Richards, M.A., Fundamentals of Radar Signal Processing,1st Ed. McGraw-Hill, New York, 2005.

[4] Skolnik, M.I., Introduction to Radar Systems, 3th edition, McGraw-Hill, New York, 2003.

[5] Raynal, A.M., Doerry, A.W, "Doppler Characteristics of Sea Clutter", Sandia National Laboratories, SAND2010-3828, June 2010.

[6] Antipov I., "Simulation of Sea Clutter Returns", Tactical Surveillance System Division, Electronic and Surveillance Research Laboratory, DSTO-TR-0679, June 1998.

[7] Watts, S., Ward, K., Tough, R., "Modelling the shape parameter of sea clutter", Radar Conference - Surveillance for a Safer World, October 2009.

[8] Chan, H.C., 'Radar Sea Clutter at Low Grazing Angles', IEE Proc., Vol. 137, Pt. F, No 2, Apr. 1990, pp. 102-112.

[9] Skolnik, M. I., Radar Handbook, McGraw-Hill, New York, 1970.

[10] Conte, E. Longo, M., and Lops, M., "Modelling and Simulation of non-Rayleigh Radar Clutter", IEE Proc. Vol. 138, Pt. F, No 2, Apr. 1991, pp. 121-130.

[11] Richards, M.A., Scheer, J.A., Holm, W.A., Principles of Modern Radar: Basic Principles, SciTech Publishing, Raleigh, NC, 2010

[12] Doviak, R.J., Zrnić, D.S., "Doppler Radar and Weather Observations", Academic Press, Inc., Orlando, FL, 1984.

[13] Barlow, E.J., "Doppler Radar", Proc. IRE, Vol. 37, no. 4, pp. 340-355, Apr. 1949.

[14] Nathanson, F.E., Reilly, J.P., Cohen, M.N., Radar Design Principles: Signal Processing and Environment, 2nd Ed. McGraw-Hill, 1990.

[15] Skolnik, M. I., Radar Handbook, Second Edition, McGraw-Hill, New York, 1970.

[16] Boyer, E., Larzabal, P., Adnet, C., Petitdidier, M., Parametric Spectral Moments Estimation for Wind Profiling Radar, IEEE Transactions on Geoscience And Remote Sensing, Vol. 41, No. 8, August 2003

[17] Stoica, P., and Nehorai, A., "Performances study of conditionnal and unconditionnal direction of arrival estimation," IEEE Trans. Acoust., Speech, Signal Processing, vol. 38, pp. 1783–1795, Oct. 1990.

[18] S. Valaee, B. Champagne, and P. Kabal, "Parametric localization of distributed sources," IEEE Trans. Signal Processing, vol. 43, pp. 2144–2153, Sept. 1995.

[19] Y. Meng, P. Stoica, and K.Wong, "Estimation of the directions of arrival of spatially dispersed signals in array processing," in Proc. Inst. Elect. Eng.—Radar. Sonar. Navigat., vol. 143, Feb. 1996, pp. 1–9.

[20] M. Bengtsson and B. Ottersten, “A generalization of weighted subspace fitting to full-rank models,” IEEE Trans. Signal Processing, vol. 49, pp. 1002–1012, May 2001.

[21] Monakov, A.A., Blagoveshchensky, D.V., “A Method of Spectral Moment Estimation” IEEE Tans. on Geoscience and Remote Sensing, Vol. 37, No. 2, March 1999.

[22] Monakov, A., “Spectral Moment Estimation of an Extended Target in ULA,” IEEE Transactions on Aerospace and Electronic Systems, Vol. 44, No. 1, January 2008.

[23] Monakov, A.A., Varfolomeev, G.A., “Resolution of Signal Sources via Spectral Moment Estimation”, IEEE Tans. on Aerospace and Electronic Systems, Vol. 42, No. 3, July 2006.

[24] Gini, F., Greco, M.V., Diani, M., Verrazani, L., “Performance Analysis of Two Adaptive Radar Detector Against Non-Gaussian Real Sea Clutter Data,” IEEE Transactions on Aerospace and Electronic Systems, Vol. 36, No. 4, October 2000.

[25] Sanders, F.H., Sole, R.L., Carroll, J.E., Secrest, G.S., Allmon, T.L., “Analysis and Resolution of RF Interference to Radars Operating in the Band 2700–2900 MHz from Broadband Communication Transmitters”, U.S. Department of Commerce, NTIA Report 13-490, October 2012.

[26] Porat, B., Friedlander, B., “Computation of the Exact Information Matrix of Gaussian Time Series with Stationary Random Components,” IEEE Tans. on Acoustics, Speech and Signal Processing, Vol. ASSP-34, No. 1, February 1986.

APPENDIX A

CRAMÉR-RAO BOUND CALCULATIONS

It will be useful to calculate the Cramér-Rao bounds for the clutter parameters since they permit to evaluate ultimate estimation performance and to know if an improvement for a practical algorithm is possible.

A.1 Cramér-Rao Bounds for Spectral Moments and Clutter Parameters of Simplified Narrow Band Interference Signals

We can model the sea and rain clutter returns as zero mean multivariate Gaussian random vectors with covariance matrices $\boldsymbol{R}_1$ and $\boldsymbol{R}_2$. Forms of $\boldsymbol{R}_1$ and $\boldsymbol{R}_2$ are the same as (3.15), however, for the purpose of making the covariance matrices independent of the radar PRF, we shall use normalized mean Doppler frequency for the Cramér-Rao bound derivations. Assuming that M observations are made in the CPI, MxM matrices $\boldsymbol{R}_1$ and $\boldsymbol{R}_2$ can be written as

$$\boldsymbol{R}_1(m,n) = P_1 \exp\left(j2\pi u_1 (m-n)\right),\ m,n = \overline{1,M}\ , \tag{A.1}$$

$$\boldsymbol{R}_2(m,n) = P_2 \exp\left(j2\pi u_2 (m-n)\right),\ m,n = \overline{1,M} \tag{A.2}$$

where P_1 and P_2 are the clutter powers and u_1 and u_2 are the normalized frequencies which corresponds to the mean radial velocities of the clutters.

Covariance matrix $\boldsymbol{R}$ of the radar return which contains the rain clutter, the sea clutter and the radar receiver noise can be expressed as following:

$$\boldsymbol{R} = \boldsymbol{R}_1 + \boldsymbol{R}_2 + P_n \boldsymbol{I} \tag{A.3}$$

where P_n stands for the power of receiver noise and $\boldsymbol{I}$ is the identity matrix.

We can express the covariance matrix $\boldsymbol{R}$ in terms of the spectral moments:

$$\boldsymbol{R} = \sum_{q=0}^{\infty} M_q \boldsymbol{A}_q + P_n \boldsymbol{I} \tag{A.4}$$

where $\boldsymbol{A}_q$ is an MxM matrix [21]

$$\boldsymbol{A}_q = \frac{1}{q!} \exp\left(-j2\pi(m-n)u_0\right)\left(-j2\pi(m-n)\right)^q . \tag{A.5}$$

When we define the unknown parameter vector as the first four spectral moments,

$$\theta = \begin{bmatrix} M_0 & M_1 & M_2 & M_3 \end{bmatrix}. \tag{A.6}$$

Fisher information matrix for N-variate normal distribution is obtained as [26]

$$\boldsymbol{I}(m,n) = \frac{\partial u^T}{\partial \theta_m} \boldsymbol{R}^{-1} \frac{\partial u}{\partial \theta_n} + \frac{1}{2} tr\left(\boldsymbol{R}^{-1} \frac{\partial \boldsymbol{R}}{\partial \theta_m} \boldsymbol{R}^{-1} \frac{\partial \boldsymbol{R}}{\partial \theta_n} \right), \; 1 \le m,n \le 4 \tag{A.7}$$

where u is the Nx1 column vector whose elements are the means of the complex clutter returns and $tr(\cdot)$ is the trace operator.

Since we model the clutters as zero mean multivariate Gaussian random vectors, the derivatives of the means with respect to the spectral moments are zero and the term $\frac{\partial u^T}{\partial \theta_m} \boldsymbol{R}^{-1} \frac{\partial u}{\partial \theta_n}$ drops. Furthermore, since our data is complex, the information contained in $\boldsymbol{R}$ doubles and the term $\frac{1}{2}$ drops also.

Hence, the Fisher information matrix for our case becomes

$$\boldsymbol{I}(m,n) = tr\left(\boldsymbol{R}^{-1} \frac{\partial \boldsymbol{R}}{\partial \theta_m} \boldsymbol{R}^{-1} \frac{\partial \boldsymbol{R}}{\partial \theta_n} \right),\ 1 \le m,n \le 4 . \tag{A.8}$$

Using (A.4), partial derivative of the covariance matrix with respect to the spectral moments is equal to

$$\frac{\partial \boldsymbol{R}}{\partial M_q} = \boldsymbol{A}_q ,\ 0 \le q < \infty . \tag{A.9}$$

Using (A.8) and (A.9), the Fisher information matrix can be expressed as

$$\boldsymbol{I}(m,n) = tr\left(\boldsymbol{R}^{-1} \boldsymbol{A}_m \boldsymbol{R}^{-1} \boldsymbol{A}_n \right),\ 1 \le m,n \le 4 . \tag{A.10}$$

Error covariances must satisfy the Cramér-Rao inequality

$$cov(\widehat{M_q}) \ge \boldsymbol{I}^{-1}(M_q) \tag{A.11}$$

where

$$\boldsymbol{I}^{-1}(M_q) = \boldsymbol{I}^{-1}(q,q), 1 \le q \le 4 . \tag{A.12}$$

To find the Cramér-Rao bounds for powers and mean frequencies of clutters, we need to change our unknown parameter set to

$$\theta = \begin{bmatrix} P_1 & P_2 & u_1 & u_2 \end{bmatrix} . \tag{A.13}$$

Then, partial derivatives of the covariance matrix with respect to unknown parameters in (A.13) become

$$\frac{\partial \boldsymbol{R}(m,n)}{\partial P_1} = \exp\left(j2\pi u_1 (m-n) \right),\ 1 \le m,n \le 4 , \tag{A.14}$$

$$\frac{\partial \boldsymbol{R}(m,n)}{\partial P_2} = \exp\left(j2\pi u_2 (m-n)\right),\ 1 \le m,n \le 4, \tag{A.15}$$

$$\frac{\partial \boldsymbol{R}(m,n)}{\partial u_1} = \begin{Bmatrix} P_1 \quad , \quad m=n \\ P_1 j2\pi (m-n)\exp\left(j2\pi u_1 (m-n)\right) \quad , \quad o.w. \end{Bmatrix},\ 1 \le m,n \le 4 \text{ and} \tag{A.16}$$

$$\frac{\partial \boldsymbol{R}(m,n)}{\partial u_2} = \begin{Bmatrix} P_2 \quad , \quad m=n \\ P_2 j2\pi (m-n)\exp\left(j2\pi u_2 (m-n)\right) \quad , \quad o.w. \end{Bmatrix},\ 1 \le m,n \le 4. \tag{A.17}$$

Error covariances must satisfy the Cramér-Rao bounds;

$$\begin{gathered} cov(\widehat{P_1}) \ge \boldsymbol{I}^{-1}(P_1), \\ cov(\widehat{P_2}) \ge \boldsymbol{I}^{-1}(P_2), \\ cov(\widehat{u_1}) \ge \boldsymbol{I}^{-1}(u_1) \text{ and} \\ cov(\widehat{u_2}) \ge \boldsymbol{I}^{-1}(u_2). \end{gathered} \tag{A.18}$$

A.2Cramér-Rao Bounds for Spectral Moments and Clutter Parameters of Wide Band Interference Signals

The Cramér-Rao bound derivations for the clutter signals that have Doppler spreads differ only in the form of the radar return covariance matrix $\boldsymbol{R}$ and the unknown parameter vector for the spectral moments and the clutter parameters.

In this case, the MxM matrices $\boldsymbol{R}_1$ and $\boldsymbol{R}_2$ take form of

$$\boldsymbol{R}_1(m,n) = P_1 \exp\left(-2\pi^2\sigma_1^2 (m-n)^2 + j2\pi u_1 (m-n)\right),\ 1 \le m,n \le 4 \text{ and} \tag{A.19}$$

$$\boldsymbol{R}_2(m,n) = P_2 \exp\left(-2\pi^2\sigma_2^2 (m-n)^2 + j2\pi u_2 (m-n)\right),\ 1 \le m,n \le 4 \tag{A.20}$$

where σ_1^2 and σ_2^2 represent the Doppler spreads of clutters.

The unknown parameter vector for the spectral moments becomes

$$\theta = \begin{bmatrix} M_0 & M_1 & M_2 & M_3 & M_4 & M_5 \end{bmatrix}, \tag{A.21}$$

and the rest of the derivation for the Cramér-Rao bounds is the same as the simplified signal model.

To find the Cramér-Rao bounds for the powers, the mean frequencies and the Doppler spreads of the clutters, the unknown parameter vector changes to

$$\theta = \begin{bmatrix} P_1 & P_2 & u_1 & u_2 & \sigma_1^2 & \sigma_2^2 \end{bmatrix} \tag{A.22}$$

and so the partial derivatives.

Then, the partial derivatives of the covariance matrix with respect to the unknown parameters in (A.22) become

$$\frac{\partial \boldsymbol{R}(m,n)}{\partial P_1} = \exp\left(-2\pi^2\sigma_1^2(m-n)^2 + j2\pi u_1(m-n)\right),\ 1 \le m,n \le 4, \tag{A.23}$$

$$\frac{\partial \boldsymbol{R}(m,n)}{\partial P_2} = \exp\left(-2\pi^2\sigma_2^2(m-n)^2 + j2\pi u_2(m-n)\right),\ 1 \le m,n \le 4, \tag{A.24}$$

$$\frac{\partial \boldsymbol{R}(m,n)}{\partial u_1} = \begin{cases} P_1 & , \quad m = n \\ P_1 j2\pi(m-n)\exp\left(-2\pi^2\sigma_1^2(m-n)^2 + j2\pi u_1(m-n)\right) & , \quad o.w. \end{cases}, \quad 1 \le m,n \le 4, \tag{A.25}$$

$$\frac{\partial \boldsymbol{R}(m,n)}{\partial u_2} = \begin{cases} P_2 & , \quad m = n \\ P_2 j2\pi(m-n)\exp\left(-2\pi^2\sigma_2^2(m-n)^2 + j2\pi u_2(m-n)\right) & , \quad o.w. \end{cases}, \quad 1 \le m,n \le 4, \tag{A.26}$$

$$\frac{\partial \boldsymbol{R}(m,n)}{\partial \sigma_1^2} = \begin{cases} P_1 & , \quad m = n \\ P_1\left(-2\pi^2(m-n)^2\right)\exp\left(-2\pi^2\sigma_1^2(m-n)^2 + j2\pi u_1(m-n)\right) & , \quad o.w. \end{cases}, \quad 1 \le m,n \le 4 \tag{A.27}$$

$$\frac{\partial \boldsymbol{R}(m,n)}{\partial \sigma_2^2} = \left\{ \begin{array}{ll} P_2 & , \quad m = n \\ P_2\left(-2\pi^2 (m-n)^2\right)\exp\left(-2\pi^2\sigma_2^2 (m-n)^2 + j2\pi u_2 (m-n)\right) & , \quad o.w. \end{array} \right\}, \qquad 1 \le m,n \le 4 \tag{A.28}$$